

**STRUCTURAL BEHAVIOUR OF THIN-WALLED DOUBLY-CORRUGATED
K-SPAN STRUCTURES WITH PINNED AND FIXED BASE SUPPORT
CONDITIONS**

**COMPORTEMENT STRUCTURAL DE PANNEAUX K-SPAN EN ACIER À
PAROIS MINCE DOUBLEMENT ONDULÉES AVEC APPUIS ARTICULÉS ET
ENCASTRÉS**

A Thesis Submitted to the Division of Graduate Studies of the Royal Military College of
Canada by

Denis Séguin, Captain

In partial Fulfillment of the Requirement for the Degree of Master of Applied Science in
Civil Engineering

13 October 2022

© This thesis may be used within the Department of National Defence but copyright for
open publication remains the property of the author.

*À mon fils Matthieu -
je te souhaite du bonheur et une passion qui enrichit ta vie.*

ACKNOWLEDGEMENT

I would like to start by thanking my thesis supervisors, Dr. Gordon Wight and Dr. Marc-André Dagenais for their guidance throughout my two years in the program. Despite the ever-changing pandemic regulations, their efforts and creativity in supporting this project at the early stages permitted its success, timely completion and encouraged potential future research projects.

Capt Guillaume Lépine's efforts, knowledge and initial research in this project has permitted a great understanding and ability to perform full-scale testing of specimens. Without the preliminary review, understanding behaviour and lessons learned, the research project ideas and logistics might not have been achievable within the time constraints given.

I wish to show my appreciation to the Royal Military College of Canada (RMC) Civil Engineering Laboratory Technicians, Mr. Dexter Gaskin, Mr. Steve Vanvolkingburgh, Mr. Louis Saulnier and Mr. John Shaw. They have contributed greatly to the success of this project. Their knowledge of the instrumentation, handling of industrial testing equipment and experience with the unique financial and procurement processes of RMC not only facilitated the efforts and streamlined the timeline expectations, but also provided me with great experience and appreciation for the work and details required in evaluating and testing materials and infrastructure. Officer Cadet (OCdt) A. Ramos and Officer Cadet (OCdt) H. Robinson were also of great assistance in the labour and construction of specimens throughout the project.

I wish to extend my gratitude to all members of 14 Construction Engineering Squadron (CES) for enabling the project, and for Sergeant (Sgt) H.T. Collins and Master Corporal (MCpl) P.F. Schulek that assisted in the initial construction the K-Span buildings, the usage of the Automatic Bending Machine (ABM) machine and the historical background of the construction of these buildings within the Department of National Defence (DND).

This research project was made possible with the funding and support of A4 Construction Engineering (A4CE) and Directorate of Architecture and Engineering Services (DAES). The possibilities and applications for K-Spans could provide great capabilities to the Canadian Armed Forces (CAF) and Canada's industrial sector.

I would like to thank my colleague, Major (Maj) Roy (Yung) Kang, who has worked with me to surmount all the challenges and changes throughout the research. May our efforts help you pursue further studies and possibilities of research.

Finally, I wish to extend the utmost gratitude to my loving wife, Stéphanie, who has supported and encouraged me throughout my Masters program and thesis research. Her patience and commitment to my success, while upkeeping a busy career, home life, and raising our first child, motivated me to complete this research.

ABSTRACT

K-Spans are structures made of thin-walled cold-formed steel arch panels. All panels are manufactured on-site with the use of an automated building machine (ABM) and seamed together, giving the arch structure its unique self-supporting characteristics and arched shape. The ABM also allows for the ability to concurrently assemble the structure while the panels are formed, making its construction time-limited and cost-effective. K-Spans are versatile and can easily be built in a variety of settings. Their economical and rapid construction process has increased the production and number of K-Span structures found in industrial areas, and also within the Department of National Defence (DND) for storage of military equipment.

Recent K-Span failures have led to concerns regarding the structures' capacities and behaviours, including detailed construction methods and the system's ability to sustain heavy loads. Although K-Spans can be an ideal solution in some environments, they are not immune to the elements, especially with the Canadian climate and its heavy snowfalls. With regards to construction methods, despite the manufacturer's recommendation of cast-in-concrete foundations, many K-Span structures within DND's infrastructure portfolio were built using steel hinges as support conditions.

This research investigated the overall behaviour and displacements of four large-scale K-Span specimens subjected to simulated snow loads, each comprised of four seamed ABM-120 panels with a 7 m diameter. Balanced and unbalanced loading patterns were used to assess the behaviour difference between fixed and pinned base support connections, the two support conditions found in K-Spans in Canada. The investigation was complimented by simulations using finite element analysis to estimate theoretical deflections and structural capacities of the same sized K-Spans.

The experimental and numerical results demonstrated that 7 m-diameter K-Span structures with both types of supports could reach the ultimate snow loads for many cities in Canada, but the flexibility of the structure permitted the structure to undergo large displacements under severe loading conditions. These large displacements which are more pronounced in the specimens with pinned supports conditions can cause localized buckling of panels and are a concern for the serviceability of the structure, especially under unbalanced snow loading patterns, where snow is present on only half of the structure. The localized buckling patterns created instabilities within the structure and worsened the already large deformations experienced by the structure which led to the loss of structural capacity of the specimens.

The structures built using hinges showed a reduction in panel stiffness as well as ultimate load capacity, compared to their equivalent structures built using the manufacturer's recommendation of having the end panels embedded in concrete. The K-Span specimens resisted 24% to 40% higher loads when built using fixed base supports, and exhibited more stiffness, deflecting 41% to 49% less than the equivalent pinned base support K-Spans. The reduction in thickness to account for the lack of double corrugation within the numerical also demonstrated a percentage difference of 1% to 31% difference within the numerical and experimental results. The pinned base support structures may present a risk in areas of Canada that may have large snow accumulations. In general, fixed support conditions should be used for future construction and any exceptional deviation from this approach should only be pursued with careful and deliberate analysis and thorough design. Further monitoring and analysis of larger size K-Spans (15 m or larger) is recommended and would allow for a better understanding of behaviour and correlation of the data between different K-Span sizes, both small and large.

RÉSUMÉ

Les K-Spans sont des structures en forme de dôme qui sont formées de plusieurs panneaux arqués, en acier formé-à-froid à paroi mince, dont la fabrication des panneaux est faite sur place dans le chantier de construction à l'aide d'une machine spécialisée appelée Machine de Construction Automatique (ABM). L'ABM permet l'assemblage et la fabrication des panneaux de façon concurrente sur le site du chantier de construction. Ceci facilite le processus et aussi réduit les coûts de construction de façon exponentielle, puisque la construction de K-Spans requiert très peu de matériaux et de main d'œuvre. Nous trouvons surtout ces structures uniques dans les milieux industriels et sur des bases militaires du ministère de la Défense nationale pour l'entreposage d'équipement, grâce aux nombreuses options quant à la grandeur de la structure, mais aussi leur habileté d'avoir de grands espaces ouverts dans la structure.

Récemment, l'effondrement de plusieurs structures K-Span autour du monde a généré des questionnements quant à sa capacité à soutenir une accumulation importante de neige, et déclenché une investigation sur sa méthode de construction. Au Canada, il y a plusieurs instances où les instructions du fabricant, M.I.C. Industries, n'ont pas été suivies pour la construction du K-Span. Dans ces cas, les supports ont été bâtis avec des charnières d'acier contrairement à la recommandation d'avoir la structure coulée dans le béton, impactant la capacité de la structure.

Cette recherche a investigué la performance, le comportement et la déformation structurelle de 4 spécimens de 7 mètres, composé de 4 panneaux ABM-120, sous différents types de chargements (équilibré et non-équilibré) afin de comparer les différents types de supports utilisés au Canada. La recherche a été complémentée par une investigation numérique utilisant une analyse d'élément fini pour estimer et comparer les déformations théoriques et la capacité structurelles des K-Spans.

L'efficacité et la rentabilité du processus de construction pour les structures K-Spans apporte plusieurs avantages économiques et permet leur construction dans n'importe quel environnement, qu'il soit industriel ou militaire. Les résultats du programme expérimental et numérique des spécimens de la recherche démontrent que les structures K-Spans peuvent soutenir une accumulation de neige importante, respectant les normes et codes du code national du bâtiment, mais la présence d'imperfections liée à la fabrication des panneaux arqués à paroi mince, combiné avec la flexibilité globale de la structure, fait en sorte que la structure subit de grandes déformations. Non seulement l'état de limite de service de la structure est une préoccupation dû aux déformations, mais la possibilité de flambage localisé des panneaux à paroi mince peuvent causer une diminution significative de la capacité globale de la structure.

L'utilisation de supports avec charnières en acier a aussi un impact significatif sur la résistance des K-Spans. Ce type de support présente un risque significatif pour les régions du Canada qui reçoivent de larges accumulations de neige, surtout si l'accumulation de neige se retrouve sur seulement la moitié de la structure, formant une charge non-équilibrée. Construire ces structures de façon à ce que les panneaux soient coulés dans le béton, et suivre les recommandations du fabricant à la lettre, sont essentiels pour que la structure se comporte tel que prévu par le fabricant. L'analyse et la surveillance de K-Spans dont le diamètre s'étend pour plus de 15 mètres permettrait d'avoir une meilleure compréhension sur ces structures uniques.

CO-AUTHORSHIP STATEMENT

This thesis document was written in the manuscript format as laid out in the Royal Military College of Canada Thesis Preparation Guide, dated May 2015. The author of this thesis, Denis Séguin, is the main contributor and author for the manuscript. The co-authors provided feedback and guidance through the writing and analysis steps. As the author plans to submit the manuscript in this document for publication in peer-reviewed journals, the article will include both supervisors and a colleague as co-authors.

TABLE OF CONTENTS

ACKNOWLEDGEMENT	iii
ABSTRACT.....	iv
RÉSUMÉ	v
CO-AUTHORSHIP STATEMENT.....	vi
TABLE OF CONTENTS.....	vii
LIST OF TABLES	x
LIST OF FIGURES	xi
LIST OF SYMBOLS	xvii
LIST OF ACRONYMS & ABBREVIATIONS	xviii
CHAPTER 1: INTRODUCTION	1
1.1 Project Background.....	1
1.2 Aim	2
1.3 Scope.....	3
1.4 Thesis Organization	3
CHAPTER 2: LITERATURE REVIEW	4
2.1 General.....	4
2.2 Background.....	4
2.2.1 K-Span & ABM Description.....	4
2.2.2 Panel Description	7
2.2.3 Cold-Formed Steel Members	8
2.3 History of Failure & Factors Influencing Behaviour	9
2.4 Loading of Arched Structures and Roofs.....	11
2.4.1 Snow Loads.....	11
2.4.2 Loading Scenario Patterns	13
2.4.3 Support Conditions	14

2.5	Experimental Testing	16
2.5.1	Global versus Local Buckling	16
2.5.2	Effective Area of Members	17
2.5.3	Rise-to-Span Ratio	19
2.5.4	Large Scale Testing.....	20
2.5.5	Numerical Modelling - Finite Element Analysis	21
2.6	Summary	24
CHAPTER 3: EXPERIMENTAL PROGRAM		25
3.1	Introduction.....	25
3.2	Experimental Setup.....	25
3.3	Equipment and Instrumentation	29
3.4	Experimental Procedure.....	31
3.5	Limitations	34
3.6	Summary.....	34
CHAPTER 4: MANUSCRIPT – FULL SCALE EXPERIMENTAL BEHAVIOUR OF THIN-WALLED AND DOUBLY CORRUGATED COLD-FORMED STEEL ARCHED STRUCTURE (K-SPAN) WITH VARYING BASE SUPPORT CONDITIONS		35
4.1	Abstract.....	35
4.2	Introduction.....	35
4.2.1	Background of K-Span Structures	36
4.2.2	Factors Influencing Structural Behaviours & Failures.....	36
4.2.3	Large Scale Testing.....	37
4.2.4	Aim and Objectives.....	37
4.3	Experimental Program	38
4.3.1	Geometry Overview	38
4.3.2	Test Set-Up	39
4.3.3	Instrumentation	41

4.4	Experimental Results and Discussion	42
4.5	Numerical Modelling Program	50
4.5.1	Model Description.....	50
4.5.2	Material Properties.....	51
4.5.3	Model Geometry	51
4.5.4	Boundary and Loading Conditions	53
4.5.5	Analysis Solution Method.....	54
4.6	Numerical Model Results and Discussion	55
4.7	Summary and Conclusions.....	59
4.8	References.....	60
CHAPTER 5: CONCLUSIONS AND RECOMMENDATIONS		62
5.1	General.....	62
5.2	Summary and Conclusion	62
5.3	Recommendations.....	63
REFERENCES		65
APPENDIX A - GRAPHICAL LOAD AND DISPLACEMENTS RESULTS		68
APPENDIX B - LARGE SCALE K-SPAN SPECIMEN SCHEMATICS AND DIMENSIONS		79
APPENDIX C - EXPERIMENTAL EQUIPMENT, SET-UP & RESULT IMAGES		83

LIST OF TABLES

Table 2-1: Moment in kNm for 16 m Span at supports and quarter points [9].....	15
Table 2-2: Positive Bending Capacity Following CSA S136-16 Compared to Testing Capacity Away from Support in Literature [9].....	18
Table 2-3: Equivalent Section Characteristics of Arched Corrugated Steel Roof [23].....	19
Table 3-1: Experimental Specimens Descriptions	25
Table 3-2: Instrumentation Identifiers and Directional Measurements	29
Table 4-1: Experimental Test Specimens	38
Table 4-2: Instrumentation Identifiers	41
Table 4-3: Material Properties	51

LIST OF FIGURES

Figure 1-1: K-Span Warehouse [1].....	1
Figure 2-1: ABM Trailer Machine Components [5].....	4
Figure 2-2: ABM-120 Straight (A) and Curved (B) Panels [7]	5
Figure 2-3: Erection Process of K-Span [8].....	5
Figure 2-4: Cross Section of K-Span Fixed (A) and Pinned (B) Support Conditions [9].....	6
Figure 2-5: Job Site Example [10]	7
Figure 2-6: Cross Section and Dimensions of ABM-120 Panel [9].....	8
Figure 2-7: Cold-Formed Steel Manufacturing Process [11].....	8
Figure 2-8: ABM Rolling Elements.....	9
Figure 2-9: Cold-Formed Steel Buckling Modes [11]	9
Figure 2-10: Collapse of K-Span in CFB Petawawa	10
Figure 2-11: K-Span Collapse Gdansk, Poland [14] (Left) and Yuzhno-Sakhalinsk, Russia [15] (Right)	10
Figure 2-12: 3D Optical Scanning of Corrugated ABM-120 Panels [2].....	11
Figure 2-13: NBCC Clause 4.1.6.10 Accumulation Factors and Loading Patterns for Curved Roofs [3] .	12
Figure 2-14: Hingeless and Two-Hinge Load and Bending Moment Diagrams [18].....	14
Figure 2-15: CFB Kingston K-Span Steel Hinge Support Connection.....	15
Figure 2-16: MIC-120 Panel Failure-Envelope [12].....	17
Figure 2-17: Small Scale Compression Test [12]	17
Figure 2-18: Effective Area of Panel [2]	18
Figure 2-19: Rise-to-Span Ratio Versus Ultimate Bearing Capacity Diagram for 20 m Span Arched MMR-178 Panels [24]	20
Figure 2-20: Airumyan et al. [17] General View of Tests Set-Up and Loading Patterns	21
Figure 2-21: Test Set-Up from Piekarczyk et al. [21][25]	21
Figure 2-22: Bending Moment for 16 m Span Fixed (A) & Pinned (B) K-Span Structures with Unbalanced Loading Pattern [9]	22
Figure 2-23: MIC-120 Mesh Model [12].....	23

Figure 2-24: Numerical and Experimental Comparison from Lépine (2021) [12]	23
Figure 2-25: Example of Displacements Results for ABM-240 K-Span Panels Using DIC Scanning Technology [5].....	24
Figure 3-1: Experimental Set-Up for Balanced Loading Pattern on a Fixed Base Support Specimen (A) and Unbalanced Loading Pattern on a Pinned Base Support Specimen (B).....	26
Figure 3-2: Side View Loading Dimensions for Balanced (A) and Unbalanced (B) Loading Patterns	27
Figure 3-3: Schematics of Fixed Base Support (A) and Pinned Base Support (B) in Millimeters	28
Figure 3-5: Actuator and Concrete Slab Loading Set-up for Balanced Loading Pattern.....	30
Figure 3-6: Instrumentation Layout and Positioning	31
Figure 3-7: Turnbuckles Used for Adding Tension in Loading Assembly.....	32
Figure 3-8: Pinned and Balanced Specimen Experimental Assembly.....	33
Figure 3-9: Video Recording View Top of Specimens.....	33
Figure 4-1: K-Span Structure (Photographed by G. Lépine [16])	36
Figure 4-2: ABM120 Geometry (A) and Description (B) (Photographed by G. Lépine) [16]	39
Figure 4-3: Fixed Support (Photographed by Louis Saulnier).....	39
Figure 4-4: Pinned Support (Photographed by Louis Saulnier).....	40
Figure 4-5: Pinned Support Condition Specimen with Unbalanced Loading Pattern (A) and Fixed Support Condition Specimen with Balanced Loading Pattern Schematic (B)	41
Figure 4-6: Linear String Potentiometer Instrumentation Positioning.....	42
Figure 4-7: Vertical Displacements at SP locations S3, S4, S5, and S6	44
Figure 4-8: K-Span 3 Times Magnified Shape After Loading for Each Loading Pattern Specimen.....	45
Figure 4-9: Horizontal Displacements	46
Figure 4-10: Localized Buckling and Plastic Deformations of Specimens (Photographs taken by Louis Saulnier).....	49
Figure 4-11: Localized buckling Zones Along Specimens	50
Figure 4-12: Crimping of Lips [16] (A) (Photographed by G. Lépine) and Numerical Representation (B)	52
Figure 4-13: Numerical Model Geometry Split Diagram for Balanced Loading Pattern	52

Figure 4-14: Numerical Model Geometry Split Diagram for Unbalanced Loading Pattern.....	53
Figure 4-15: Hinge Numerical Representation	53
Figure 4-16: Meshing Sizing for K-Span Panels	54
Figure 4-17: Numerical and Experimental Displacement Results Comparison	56
Figure 4-18: Total Deformation Comparison for Fixed and Balanced Model (A), Fixed and Unbalanced Model (B), Pinned and Balanced Model (C) and Pinned and Unbalanced Model (D) once Yielding Limit is Reached.....	58
Figure A-1: Vertical Displacements for Row S1	69
Figure A-2: Vertical Displacements for Row S2.....	69
Figure A-3: Vertical Displacements for Row S3.....	70
Figure A-4: Vertical Displacements for Row S4.....	70
Figure A-5: Vertical Displacements for Row S5.....	71
Figure A-6: Vertical Displacements for Row S6.....	71
Figure A-7: Vertical Displacements for Row S7.....	72
Figure A-8: Horizontal Displacements for SB1H.....	72
Figure A-9: Horizontal Displacements for SB2H.....	73
Figure A-10: Horizontal Displacements for SB6H.....	73
Figure A-11: Horizontal Displacements for SB7H.....	74
Figure A-12: Longitudinal Displacements for SL4	74
Figure A-13: Vertical Displacement Comparison for Balanced Loading Pattern Specimens	75
Figure A-14: Vertical Displacement Comparison for Unbalanced Loading Pattern Specimens	75
Figure A-15: Horizontal Displacement Comparison for Balanced Loading Pattern Specimens	76
Figure A-16: Horizontal Displacements Comparison for Unbalanced Loading Pattern Specimens	76
Figure A-17: Loading Distribution per Row for Balanced Loading Pattern & Fixed Support Specimen ..	77
Figure A-18: Loading Distribution per Row for Balanced Loading Pattern & Pinned Support Specimen	77
Figure A-19: Loading Distribution per Row for Unbalanced Loading Pattern & Fixed Support Specimen	78

Figure A-20: Loading Distribution per Row for Unbalanced Loading Pattern & Pinned Support Specimen	78
Figure B-1: Fixed Concrete Support Side View	80
Figure B-2: Pinned Concrete Support Side View	80
Figure B-3: Experimental Instrumentation & Loading Pattern Overview	81
Figure B-4: Instrumentation Layout for Both Balanced and Unbalance Loading Pattern	81
Figure B-5: Side View Loading Dimensions for Balanced Loading Pattern	82
Figure B-6: Side View Dimensions for Unbalanced Loading Pattern	82
Figure C-1: M.I.C. ABM Trailer.....	84
Figure C-2: ABM Set-Up.....	84
Figure C-3: Steel Panel Forming Process	85
Figure C-4: Scale of 7m-Diameter Panels on Jobsite	85
Figure C-5: Seaming Machine	86
Figure C-6: Steel Rollers for Seaming Machine	86
Figure C-7: Beginning of Seaming Process	87
Figure C-8: Seaming Process.....	87
Figure C-9: Seamed K-Span	88
Figure C-10: 100 kN Actuator Set-up.....	88
Figure C-11: Pulleys and Actuator Connection Configuration.....	89
Figure C-12: Pulleys Anchored to Concrete Slab	89
Figure C-13: Turnbuckles Used for Controlling Load on Cables.....	90
Figure C-14: K-Span Connections Between Eyebolts and Steel Cable.....	90
Figure C-15: One Row of Loading Points	91
Figure C-16: Loading Point and Load Cell Assembly.....	91
Figure C-17: Vertical Linear String Potentiometers	92
Figure C-18: Horizontal Linear String Potentiometer and Camera Set-Up	92
Figure C-19: Fixed Base Support 1.....	93

Figure C-20: Fixed Base Support 2.....	93
Figure C-21: Pinned Base Support 1.....	94
Figure C-22: Pinned Base Support 2.....	94
Figure C-23: Balanced Loading & Fixed Support Specimen Prior to Loading	95
Figure C-24: Balanced Loading & Fixed Support Specimen at Loading	95
Figure C-25: Balanced Loading & Fixed Support Specimen Localized Buckling near Supports	96
Figure C-26: Balanced Loading & Fixed Support Specimen Localized Crimping under Web.....	96
Figure C-27: Balanced Loading & Fixed Support Specimen Localized Crimping of Web from Back Side	97
Figure C-28: Balanced Loading & Fixed Support Specimen Localized Buckling near Supports	97
Figure C-29: Balanced Loading & Fixed Support Specimen Top View	98
Figure C-30: Balanced Loading & Fixed Support Specimen Localized Buckling of Seamed Lips	98
Figure C-31: Balanced Loading & Fixed Support Specimen Post Loading	99
Figure C-32: Balanced Loading & Pinned Support Specimen Prior to Loading	99
Figure C-33: Balanced Loading & Pinned Support Specimen during Loading.....	100
Figure C-34: Balanced Loading & Pinned Support Specimen Deformation Caused by Hinge Rotation 1	100
Figure C-35: Balanced Loading & Pinned Support Specimen Deformation Caused by Hinge Rotation 2	101
Figure C-36: Balanced Loading & Pinned Support Specimen Crimping of Webs.....	101
Figure C-37: Balanced Loading & Pinned Support Specimen Crimping of Webs Back Side	102
Figure C-38: Balanced Loading & Pinned Support Specimen Localized Buckling of Seamed Lips	102
Figure C-39: Unbalanced Loading & Fixed Support Specimen Prior to Loading.....	103
Figure C-40: Unbalanced Loading & Fixed Support Specimen During Loading.....	103
Figure C-41: Unbalanced Loading & Fixed Support Specimen Localized Web Deformations 1	104
Figure C-42: Unbalanced Loading & Fixed Support Specimen Localized Web Deformations 2	104
Figure C-43: Unbalanced Loading & Fixed Support Specimen Buckling of the Seamed Lips.....	105
Figure C-44: Unbalanced Loading & Pinned Support Specimen Prior to Loading.....	105

Figure C-45: Unbalanced Loading & Pinned Support Specimen During Loading..... 106
Figure C-46: Unbalanced Loading & Pinned Support Specimen Hinge Rotation Deformations..... 106
Figure C-47: Unbalanced Loading & Pinned Support Specimen Localized Web Crimping..... 107
Figure C-48: Unbalanced Loading & Pinned Support Specimen Buckling of Seamed Lips..... 107

LIST OF SYMBOLS

A_{eq}	Equivalent section area
C_a	Accumulation factor
C_b	Basic roof snow load factor
C_s	Slope factor
C_w	Wind exposure factor
f	Design stress of tensile, compressive or bending strength of steel
ft	Feet
Hz	Hertz
I_s	Importance factor for snow load
kN	Kilonewton(s)
kPa	Kilopascal(s)
m	Metre(s)
mm	Millimetre(s)
MPa	Megapascal(s)
M_n	Second order bending moment
MTS	Material Testing System
N_1	First order axial force
r	Radius
S	Variable load due to snow, including ice and associated rain
S_r	1-in-50-year associated rain load
S_s	1-in-50-year ground snow load
W_{eq}	Equivalent section modulus
x	Horizontal distance from the roof peak
x_{30}	Value of x where the slope $\alpha = 30^\circ$
α	Roof slope
$^\circ$	Degree(s)
%	Percent

LIST OF ACRONYMS & ABBREVIATIONS

2D	Two-Dimensional
3D	Three-Dimensional
A4CE	A4 Construction Engineering
ABM	Automatic Bending Machine
ASTM	American Society for Testing and Materials
CAD	Computer Aided Design
CAF	Canadian Armed Forces
CES	Construction Engineering Squadron
CFB	Canadian Forces Base
CSA	Canadian Standards Association
DAES	Directorate of Architecture and Engineering Services
DIC	Digital Image Correlation
DND	Department of National Defense
FEA	Finite Element Analysis
FEM	Finite Element Method
FOS	Fibre Optic Sensors
LVDT	Linear Variable Differential Transformer
NBCC	National Building Code of Canada
NL	Newfoundland
NS	Nova Scotia
ON	Ontario
RMC	Royal Military College of Canada

CHAPTER 1: INTRODUCTION

1.1 Project Background

K-Spans are a lightweight, self-supporting arch-type structure built with the use of Automatic Building Machine (ABM) technology owned by M.I.C. Industries. The ABM technology permits the formation of the structure with the use of a roll-forming machine mounted on a trailer unit. Due to the economical and rapid construction process of K-Spans, they have been increasing in popularity over the last few decades and are commonly used for military purposes. Since these arch-type structures come in a wide variety of sizes and large floor plans with clear open spans, K-Spans are often used as storage buildings, as presented in Figure 1-1.



Figure 1-1: K-Span Warehouse [1]

All K-Span construction is done onsite by forming the thin-walled cold-formed steel elements and assembling the whole structure with minimal equipment and tools. The ability to have all the construction and supporting work onsite ensures the structures are built in shorter timelines than other storage structures using conventional approaches. This also reduces the overall cost and manpower required for the construction by having small skilled crews that operate the machinery and assemble all the components.

The Canadian Armed Forces (CAF) has the capability to rapidly build these structures either domestically or for overseas operations. The reliability and efficiency of these buildings has led to the construction of multiple structures all over Canada within the infrastructure portfolio of the Department of National Defence (DND) during the past three decades. Although DND's K-Span construction capability is currently held by 14 Construction Engineering Squadron (CES) in Bridgewater (NS), the ABM technology has also been used by other units within the CAF throughout the years, building many structures throughout the country.

The ownership of the ABM equipment permits the CAF to have their own construction and operator crew without relying on civilian or external capabilities to build these structures. This gives the CAF the flexibility and ability to design and build these structures when required. M.I.C. Industries now provides a software when selling updated versions of these machines to assist contractors and owners of the equipment in the design of the infrastructure. However, during the past few decades, personnel within DND relied on printed manuals instead of software to provide guidance in the design and construction process of these structures. Throughout the years, the design of these buildings on CAF property has diverged from the recommendations of the original manuals. Some of the structures have different types of base support connections between the base of the structure and the cold-formed steel panels, assumed to be integrated into the design of the structures for convenience and ease of construction. The arched structure is typically fixed and embedded in concrete, but there have been some occurrences in which K-Span structures have been built with the use of hinges acting as pinned base support connections. The commonly encountered hinged construction method has led to concerns for DND's infrastructure inventory, that having K-Span structures with pinned base support connections may reduce the overall load capacity and increase the overall deformations experienced by K-Spans when subjected to severe snowfalls.

In recent years, failures of these structures have occurred around the world, mainly under significant snow loads. One of these instances occurred in 2019 at CFB Petawawa (ON), in which the structure collapsed after a heavy snow fall. Other European countries such as Poland have also had multiple cases of K-Span structures that either failed under snow loads or demonstrated significant deformations [2]. Since snow fall in Canada can be more severe than in other countries, the structural integrity of multiple K-Span buildings on DND property is an area of concern. This is particularly an issue for the already-built structures that diverged from the original design recommendations in terms of base support fixity. Therefore, a thorough investigation and analysis of these arch-type K-Spans is required to fully understand the behaviour of these structures under all conditions and ensure that safety measures and precautions are taken when dealing with existing self-supporting arch-type structures or designing new ones.

1.2 Aim

The aim of this research project was to investigate the structural behaviour and deformations of full-scale K-Span specimens under severe simulated snow load patterns. The assessment of behaviour and capacity of both fixed and pin-connected K-Spans through large-scale experimental testing was supplemented by finite element analysis. The comparison between K-Spans built using hinges versus the manufacturer's recommended fixed support connections was conducted to clarify difference in behaviour as it may affect serviceability and safety when subjected to extreme snow loads. A better understanding of how these types of structures behave will provide clear guidance on the use of existing and the design of new K-Spans. The specific objectives of this research are to:

1. Compare K-Span structures with fixed and pinned base support conditions under simulated Canadian snow loading conditions for their:
 - a. relative stiffness - vertical and horizontal load-deflection behaviours; and
 - b. ultimate load capacity.
2. Assess localized deformation patterns which may lead to failure or affect structural resistance.
3. Utilize a reduction in effective thickness to simplify finite element numerical models to adequately replicate the load-deflection behaviour of the K-Span specimens and compare behaviour between fixed and pinned supports.

1.3 Scope

To meet the objectives of this research, a detailed literature review on all pertinent subjects related to K-Spans was performed. The design of an experimental program using full-scale specimens constructed from ABM-120 K-Span panels was developed. The experimental program was limited to the testing of specimens constructed with two types of base support conditions (pinned and fixed). The structures were subjected to an array of point loads, simulating two critical independent snow loading patterns. A total of four large-scale specimens were tested. The behaviour of the loaded specimens were studied and compared to assess the effect of the base support conditions on the behaviour and to provide recommendations for future K-Span construction.

The large-scale specimens were tested in a laboratory setting. Due to space constraints, the clear span of the K-Span panel specimens was limited to a 7 m diameter. Further the width of the specimens were limited to 1.245 m, consisting of four seamed panels. A single span profile (semi-circular) was used for all specimens. Over 39 instruments gathered data on displacements and loading. A comparison of vertical and horizontal displacements recorded during the loading of specimens were used to quantify the overall structural behaviour and relative stiffness. The ultimate tested capacity of all specimens was also observed, assessed, and compared.

Finite element modelling using simplified geometry was completed for the specimens, wherein the conditions of the test were replicated within the numerical models. The experimental displacements of the specimens were compared to the finite element results. The loading pattern configurations and rates, used in the experiments, were applied to the finite element models.

1.4 Thesis Organization

This thesis was written using the manuscript and article style-based format as detailed in the Royal Military College of Canada (RMCC) Thesis Preparation Guide [4]. The document consists of a total of five chapters. Chapter 1 includes the research introduction, objectives and scope of the experimental research. Chapter 2 consists of a literature review, providing a detailed summary and review of other research and published experiments that pertains to this project. Chapter 3 provides a description of the experimental program. Chapter 4 is a standalone manuscript which is intended to be submitted to an engineering journal for publication. Chapter 4 also presents the experimental and numerical findings for the K-Spans' structural behaviour under simulated snow loading patterns. Chapter 5 is a summary of the research project and discusses recommendations for future experimental testing. A series of appendices follow Chapter 5 which supplements the information presented in the thesis document. These include, in Appendix A, further information related to the numerical results, the schematics in Appendix B and figures of the experimental set-up in Appendix C.

Chapter 4 contains its own reference list and is numbered independently, as it is a standalone document. The references for Chapter 1, 2, 3 and 5 are listed at the end of the document.

CHAPTER 2: LITERATURE REVIEW

2.1 General

This section provides an in-depth review of past and current relevant topics and literature that pertain to the study of K-Span structures. It provides background knowledge on the specific K-Span construction as well as the engineering communities' current understanding of these types of structures. This literature review covers all topics and important information relevant as background to the manuscript and provides an overall situational awareness of the behaviours of K-Spans. The overall description and usage of K-Span structures, the factors that influence structural behaviour, the loading methods and experimental and numerical evaluations are discussed. The manuscript in Chapter 4 includes its own summary of this literature review to provide readers with the most pertinent information and knowledge that are directly related to the manuscript. References for the complete thesis and this chapter are found after Chapter 5.

2.2 Background

2.2.1 K-Span & ABM Description

K-Spans are arched structures that are self-supporting. They are commonly used in military and civilian industrial areas due to their ability to span a large open footprint while minimizing construction costs and timelines. The construction of these structures allows for the forming of the cold-formed steel elements on-site. With the use of ABM technology owned by M.I.C. Industries, the arched panels are constructed by feeding the steel coil rolls through the ABM trailer. Similar to cold-formed steel machines used for roofing, the ABM forms the steel sheets through the machine into steel panels and gives them their unique shape required for the assembly. The ABM trailer manufacturing components and key operating controls required for the construction of K-Spans are presented in Figure 2-1. Although there are different types and shapes of ABMs, this report will focus on the use of ABM-120 technology used by the CAF.

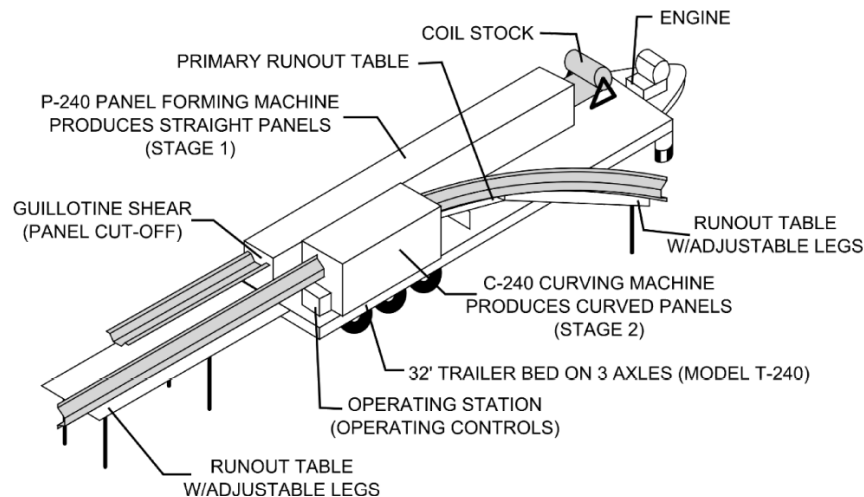


Figure 2-1: ABM Trailer Machine Components [5]

The construction of K-Span structures is a very efficient process which ensures low material and labour costs by having a quick construction and forming process of the panels. With a small trained crew

of 12 people, a 465 m² (5000 ft²) building can be constructed in less than 12 hours [6]. The construction process consists of cutting the steel coil to the desired length and passing the thin steel sheet through the ABM trailer rollers to form the straight panel into the desired cross-section. The newly formed straight panel is then passed through the ABM trailer a second time to bend the panel into the desired shape and curvature. At this stage of the process, the panels are given corrugation of different dimensions on the flanges and webs of the cross section to create the required design curvature for the span. The outcome is a thin-walled steel curved panel with double corrugation along the cross section. Both ends of the steel are bent, creating lips located at the end of each flange to facilitate the joining of adjacent panels during the erection and assembly of the structure, as seen in Figure 2-2.

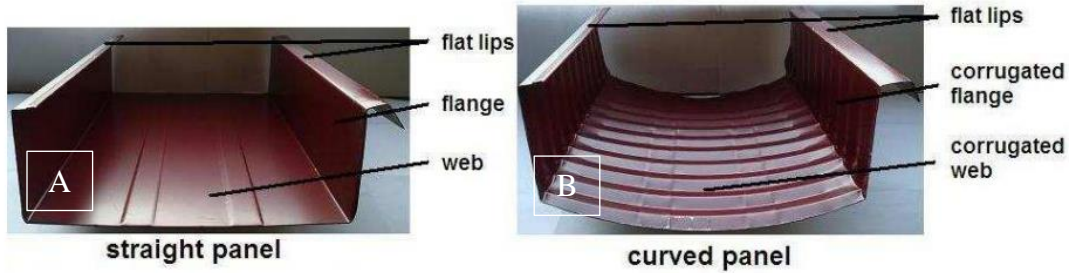


Figure 2-2: ABM-120 Straight (A) and Curved (B) Panels [7]

With the use of a seamer, the formed panels are assembled on the ground by cold-pressing the flat lips together along the length of the curvature. The lips are shaped specifically to permit one panel to fit into the opening of the next panel. The seaming of the lips along the curvature of the structure ensures a continuous connection on the exterior surface of the panels and allows the structure to be self-supporting. Once a set of four to six panels are seamed together, with the use of a crane, the panels are lifted into position for assembly and are seamed with the rest of the structure, as seen in Figure 2-3.



Figure 2-3: Erection Process of K-Span [8]

The arched structure is typically fixed and embedded in concrete, but there have been some occurrences in which K-Span structures have been built with the use of hinges acting as pinned base support connections, as seen in Figure 2-4.

K-Spans can also be open- or close-ended structures. End-wall panels are also formed through the ABM trailer and assembled through the seaming process similar to the rest of the structure. End-wall panels are cut near the top in a circular shape in order to be bolted to the last set of panels of the structure. The versatility of K-Span structures and their ability to meet different infrastructure requirements allows them to meet different needs such as the inclusion of garage doors, lighting systems, interior walls and more, depending on the requirements and needs of the customer. The final product is a quickly built and aesthetic open-space building, that has multiple applications in a civilian or military environment.

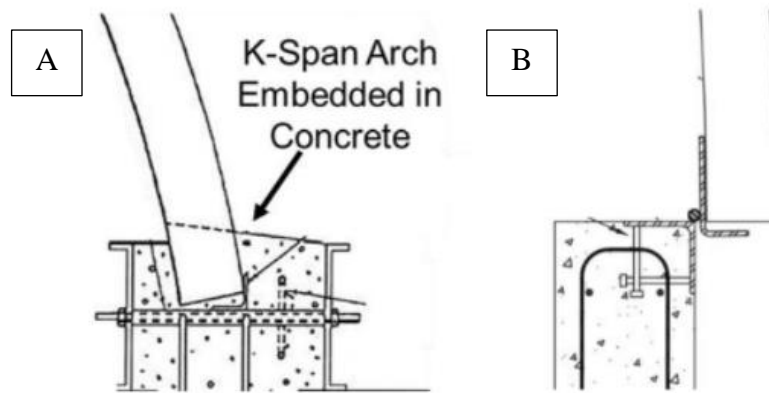
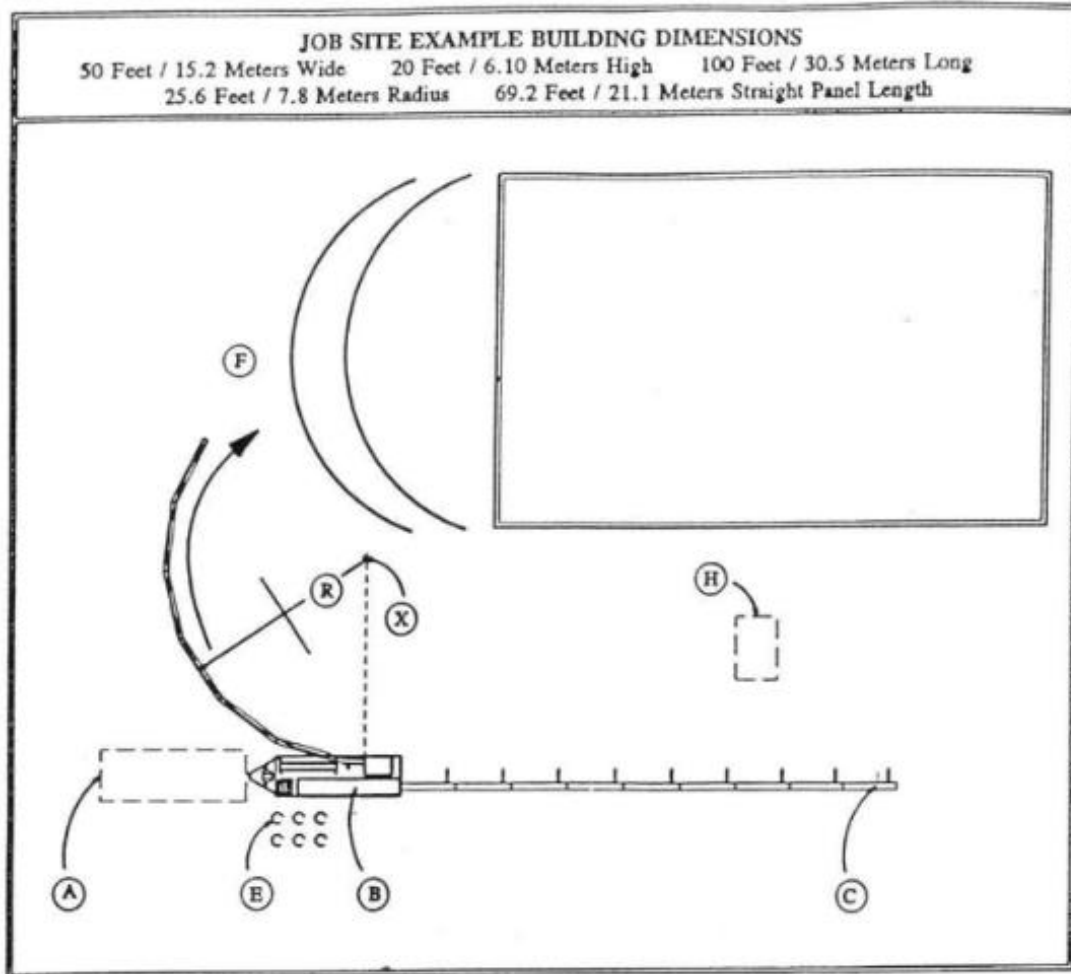


Figure 2-4: Cross Section of K-Span Fixed (A) and Pinned (B) Support Conditions [9]

K-Spans can be built in any type of environment with the mobile ABM trailer, as they are simple and quick to assemble. The ability to quickly build multiple structures within the same construction worksite provides great solutions for companies or military units in a deployed operational setting requiring multiple large structures side-by-side. The versatile K-Span has a variety of applications and is a great mid-to long-term solution for the construction of storage space in DND's inventory, especially when funding is not available to provide large and complex buildings in Canada or on deployed operations.

Many different spans and heights of structures can be achieved for K-Spans dependent on the need and requirements, but they do have limitations in the size and configurations that can be built. Although the operator has complete control of the on-site manufacturing of the panels through the ABM trailer, they are limited to spans ranging from 3.7m to 24m, with coil widths of 0.6m. For larger panels and structures, the placement of the ABM trailer is important, and a large job site is required to manoeuvre the seaming process to form a set of panels, as seen in Figure 2-5, for an effective construction and assembly process. The radius and the length of the panels are all controlled by the operator. The curvature is determined manually through an iterative process by measuring the length and radius of an existing panel and adjusting dials to have a more aggressive and larger radius as required. With the use of a sheet of plywood, a guide is built to assist in determining the proper curvature required for the size of structure determined. Runout tables and stands are used to assist in supporting the panels as they are produced and formed into the desired shape.

The ABM trailer is a self-powered unit that comes with all the necessary equipment to facilitate the process and minimize the need for other components to be brought to the job site. The only additional equipment and material required when building K-Spans are the steel coils for the panels, crane for lifting structural members, a seamer to assemble the panels together, fuel to power the equipment and a labour crew to operate and assemble the structure. All building processes, design guidelines and maintenance requirements are provided in the K-Span Automated Building Machine Training Manual produced by M.I.C. Industries [10].



Pre-plan job site layout to avoid set-up problems. All of the following must be considered:

LEVEL: If ground is uneven or sloped, align bed of trailer to correspond with general lay of the land. Avoid twisting of trailer bed as this can cause several operational problems. One or two hydraulic jacks under the rear of the trailer frame "I" beams may occasionally be necessary.

- A. Allow room to maneuver towing vehicle or plan to leave it attached to trailer.
- B. ABM System is 27' 8" long by 7' 4" wide (8.4 m long by 2.2 m wide).
- C. From rear of trailer, allow room for enough run-out stands to hold straight panel length. Stands have a net length of 9'6" each (2.9 m).
- D. Find point "X": From center of curver, measure distance equal to radius in line with front of curver frame. From point "X" scribe an arc equal to radius. This arc will define a path of the curved panels. Allow an additional two feet beyond this arc for run-out stands and legs.
- E. Need area to store coil stock and access for equipment to load it onto the ABM machine.
- F. Curved panels must be carried in this general direction after being formed.
- G. Must have level area to lay panels on ground for seaming horizontally stacked curved sections.
- H. Need space for crane operation.

Figure 2-5: Job Site Example [10]

2.2.2 Panel Description

The panels are formed with the use of galvanized steel sheets running through the ABM trailer. The typical grades of steel used for K-Spans, in accordance with ASTM Standards, are of grade C or D,

with yield strengths of 275 MPa and 345 MPa respectively [9]. The thickness of the steel sheets can vary from 0.731 mm to 1.14 mm [10]. Both the grade and thickness choice of steel are determined in the ABM-120 K-Span User Manual based on required K-Span size and the design determined. The typical geometry and dimensions of the formed panels are found in Figure 2-6. The galvanized steel coils can also be painted for aesthetics, to the requirement of the customer, adding up to 37 microns to the thickness [10].

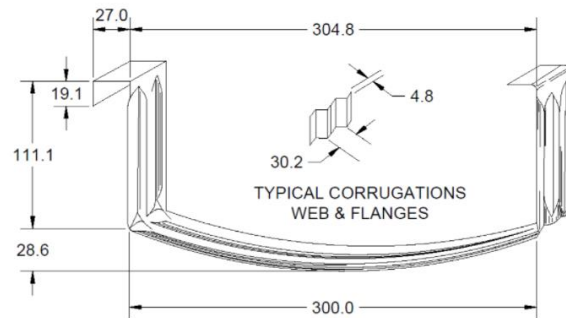


Figure 2-6: Cross Section and Dimensions of ABM-120 Panel [9]

2.2.3 Cold-Formed Steel Members

Cold forming steel gives the structural shape to a steel member through bending, press braking or roll-forming. Roll-forming machines shape the steel elements with the use of specific rollers that gradually give the required geometric properties to the member, as seen in Figure 2-7. K-Span structures use this form-rolling technique and technology by using the ABM trailer to roll the steel elements into their desired cross-section and final curvature shape, as presented in Figure 2-8. The advantage of having a mobile roll-forming machine goes beyond just the ability to have the structural members constructed on-site, but also that cold-formed steel can change its geometrical properties without having to go through a heating process or forming. The ABM trailer is also composed of curving rollers that give the panels their circular shape and transverse corrugation. The seaming process, in which the assembly of panels are attached together, is also based on cold-formed steel, since as the lips are folded and bent, the steel geometric properties of the panels change.

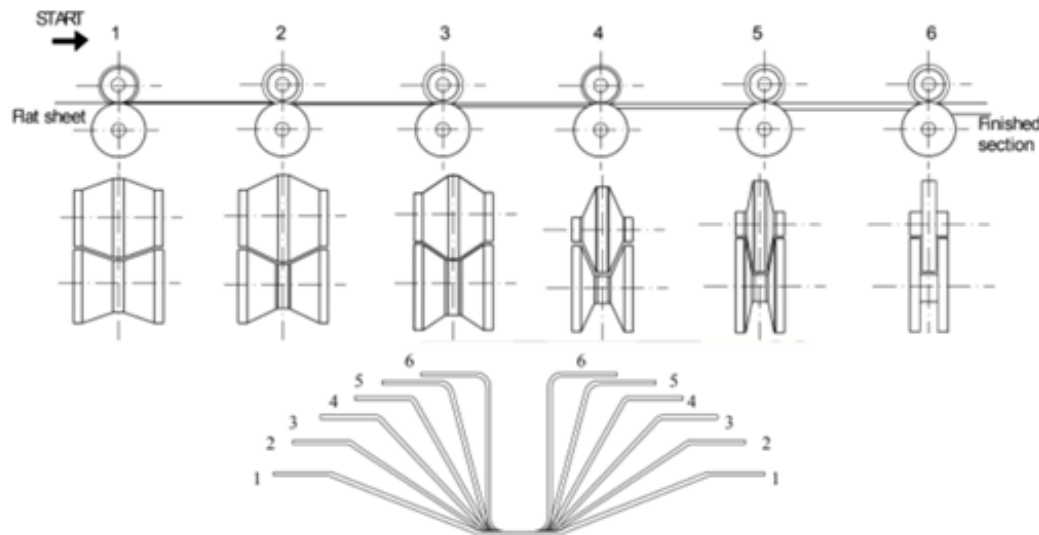


Figure 2-7: Cold-Formed Steel Manufacturing Process [11]



Figure 2-8: ABM Rolling Elements

Cold-formed steel structural members usually constitute thin-walled steel members due to the small thickness required to fold steel. They are valued for their lightness, easy production, fast installation and low cost [11]. But these thin-walled elements are subjected to possible modes of buckling before reaching the yield stress of the steel [12]. As seen in Figure 2-9, from left to right, the buckling modes are local, distortional, flexural, torsional, and flexural-torsional. Although the design of cold-formed steel structural members in Canada and North America are covered by the S136-16 North American Specification for design of cold-formed steel structural members [13], no current standard, within Europe or North America, provides guidelines to cover out of scope members or the subject of members that have double corrugation such as K-Spans [12]. The double corrugation found in structural members of K-Spans is due to the forming of the curved panels. The corrugation is required to give the steel members their circular shape but creates uncertainty in the behaviour and resistance of the members and in the overall behaviour of the structure under severe snow loads.

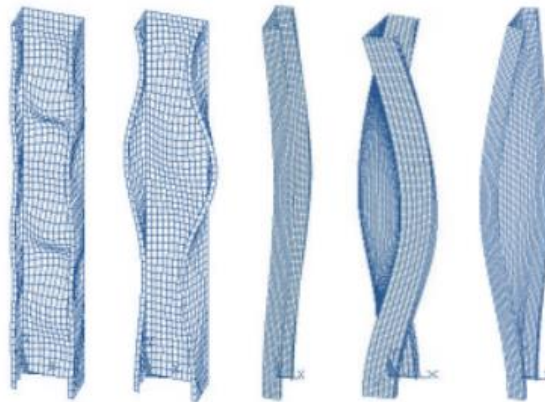


Figure 2-9: Cold-Formed Steel Buckling Modes [11]

2.3 History of Failure & Factors Influencing Behaviour

K-Spans are also susceptible to environmental conditions and deterioration. Multiple occurrences of K-Span failures have been noted in recent years all over the world, specifically in Poland, China and Canada. CFB Petawawa was the site of the failure of a K-Span in 2019 where the structure collapsed under significant snow accumulation [9] as presented in Figure 2-10. One of the major similarities noted from the literature is that the accumulation of snow may lead to catastrophic failure of the structure. This was the

case for the collapses in Gdansk (Poland) and Tuszyn (Poland) in 2009 [14], as well as Yuzhno-Sakhalinsk in Russia [15], seen in Figure 2-11.

The cases of K-Span collapses around the world have led multiple researchers and academic institutions to look further into the possible failure modes of these structures and investigate its design process and ultimate loading capacities. The common factor of significant snowfall leading to numerous collapses demonstrate many similarities in the buckling and plastic deformation patterns. The thin-walled cold-formed steel elements also undergo large deflections under significant loads. The members are susceptible to imperfections during the forming process which can highly influence the behaviour and resistance of the structure [14].



Figure 2-10: Collapse of K-Span in CFB Petawawa



Figure 2-11: K-Span Collapse Gdansk, Poland [14] (Left) and Yuzhno-Sakhalinsk, Russia [15] (Right)

The observation made by Walentynski et al. (2013) [16], is that there are no specific codes or guidelines in Europe to assist in reviewing or designing K-Span panel members to account for the double transversal corrugation that the panels receive during the forming process [16]. In Canada, there is also no current code specifying designs for doubly corrugated thin-walled members. This presence of imperfections causes unique structural behaviours, and the complex geometry of the panels influences the resistance and behaviours of K-Spans. Cybulski et al. (2014) used a 3D optical scanning camera to scan and capture the unique shape of the K-Span panels, as seen in Figure 2-12, and compile the geometry into FEM software in order to analyze its capacity and determine the strain patterns when loading these structures experimentally [2]. This appears to be an effective way to capture the imperfections included in ABM-120 steel panels which may not be readily seen or drawn by hand in FEM software.



Figure 2-12: 3D Optical Scanning of Corrugated ABM-120 Panels [2]

Multiple experimental tests have been conducted to determine the load capacity and buckling behaviour of the K-Span panels. Research demonstrates that although the global effect of loads is a deflection of the overall structure, local buckling is the lead cause of collapse due to the instability of the structure [17]. Mainly small-scale panels have been tested in laboratories to better understand the behaviour and attempt to account for the double corrugation of the panels and its effect on the overall reaction of the structure through numerical modelling. Studies done by Piekarczyk et al. (2015) have demonstrated that neglecting the transverse corrugation of the profiles in the design process of the panel geometry led to inaccurate estimates of the load capacity and stability of K-Span structures [15].

MacDonald (2021) has shown that for future K-Span construction, greater attention needs to be given to the snow load factors to ensure ABM-120 panels have the capacity to support snow loads characteristic of the region in which the K-Span will be built [9]. Other factors that affect the overall behaviour of K-Span structures, is the difference between pinned and fixed base supports, where having a pinned arched structure greatly reduces its capacity to support snow and rain loads [9]. The difference in balanced and unbalanced snow loading patterns also creates a negative effect on the behaviour of the structure. The unbalanced loading pattern is considered the worst-case scenario for K-Spans or arched structures [9]. Rusting, abnormalities, and local imperfections in the construction process also contributes negatively to the overall capacity and behaviour of the structure.

2.4 Loading of Arched Structures and Roofs

2.4.1 Snow Loads

Arched and curved structures are established practices in the engineering community. The analysis of effects for snow loads and loading mechanisms for these types of structures are established by standards such as the National Building Code of Canada (NBCC) [3] and can be used to determine critical loading patterns and factors according to the regions' historical data in Canada. The NBCC developed its factors and loading equations through research and standard engineering practices. The NBCC uses historical snow loading factors and provides a 1-in-50-year worst snowfall conditions snow load factor based on the Canadian cities.

The curved K-Span structures are different from the typical flat or slope shaped roof elements, in that the building surface is part of the structural members. The self-supporting curved panels, which are considered to be roofs, have two conditions which need to be verified as per the NBCC: a snow loading pattern on the full curved surface of the structure, as well as a loading pattern on only one half of the curved

surface, as presented in Figure 2-13. Since the K-Span panels that form the shell of the structure, are self-supporting and are the only structural component of the structure, an extra consideration needs to be taken for K-Spans to meet the snow load conditions for each region in which they are built. Since most K-Span structural failures occurred under severe snow loads around the world, it is also important to include the snow sliding effects on the surface of the curvature when estimating snow loads. The snow load equation from the NBCC Clause 4.1.6.2 for estimating the ultimate snow load conditions is represented by equation (1).

$$S = I_s [S_s (C_b C_w C_s C_a) + S_r] \quad (1)$$

All factors in the equation can be found and estimated in section 4.1.6.2 of the NBCC [3] depending on the type of structure, its importance factor and region within Canada. The only unique factor that influences the snow loads for K-Span structures compared to regular storage buildings is the accumulation of snow factor (C_a) for curved roofs, because K-Spans are mainly built with large rise-to-span ratios. Due to the nature of their design and semicircle curvature, snow accumulation on the edge of the structure has a high chance of slipping off the structure, creating a loading pattern where the majority of the load is found near the top surface of the structure. The curved elements cause K-Spans to have different slopes along the span of the structure. As the curvature becomes steeper through the building, the chances of having snow slip off the structure are greater. The factor for snow accumulation is directly linked to the slope of the arch and the rise-to-span ratio.

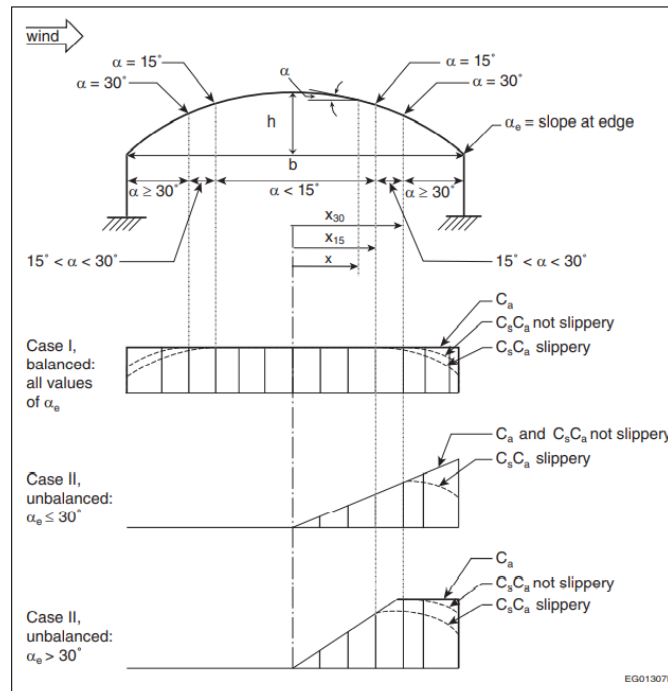


Figure 2-13: NBCC Clause 4.1.6.10 Accumulation Factors and Loading Patterns for Curved Roofs [3]

Two equations are necessary to find the accumulation factor for curved roofs such as K-Spans. The snow accumulation factor is based on the slope of the roof, where from the peak of the structure to a distance in the X axis where the slope is 30°, represented in the equations as x_{30} , snow accumulates as a normal flat roof, and past that distance where the slope increases above 30°, snow slippage occurs. The accumulation and basic roof snow load factors are represented by C_a and C_b , and the roof slope is represented by α . The rise-to-span ratio for K-Spans can differ dependant on the size and utility of the structure, but it is normally

found as 0.5, which means the following two equations are used and described in section 4.1.6.10.4 of NBCC [3]. With these equations, two major snow loading patterns are created. One where the snow is accumulated on one side of the structure, creating an unbalanced loading pattern caused by strong winds pushing the snow to one side of the structure, and a balanced loading pattern, where snow accumulates on the top portion of the K-Span.

$$C_a = \frac{2x}{c_b x_{30}} \text{ from peak to } \alpha = 30^\circ, \text{ and} \quad (2)$$

$$C_a = \frac{2}{c_b} \text{ for } \alpha > 30^\circ \quad (3)$$

The snow load equation (1) is also dependant on the 1-in-50-year ground snow load factor which differs by province and location of the structures. Since Canada has such a diverse and wide variety of climates, loading critical loading patterns may differ region to region, where an area prone to wind and heavy snowfalls such as Ottawa (ON) could potentially lead to both loading patterns, as opposed to an area such as Gander (NL), which would expect much more snow, and therefore a balanced loading pattern.

2.4.2 Loading Scenario Patterns

Leontovich [18], described that arched and curved structures have multiple usages in civil engineering. The interior forces, including, bending moments experienced by loading on these structures may be estimated by engineers by applying derived condensed solutions. In recent years, numerical modeling has gained popularity in the engineering community and has been a great tool used to estimate and simulate the structure's internal behaviour for increasingly complex geometry structures. However, the mathematical and pre-derived equations remain a quick and useful tool to estimate the values for moment, shear and axial force along the length of the spans. Approximation of axial forces and bending moment equations for large rise-to-span ratios are described in the Frames and Arches textbook from Leontovich [18]. The arches are represented as hingeless and two-hinge structures of lower rise-to-span ratios, and the reactions are represented in Figure 2-14, but provide a good approximation for the diagram of larger ratios.

For K-Span structures, where the structural members are self-supporting panels, it is important to consider that for all areas along the span, the positive and negative moments are crucial in the structural capacity of the structure. As the structure can undergo a multitude of loading patterns, the difference between point loads and distributed loading does impact the internal behaviours of arched structures. Although point loads can occur, the probability of having uniform loading on K-Spans are much greater due to snow accumulation.

When comparing the bending moment diagrams from Leontovich [18], the fixed base support arches experience bending moments near the supports, whereas the pinned base supports experiences no bending moments at the supports. Due to the slipping of the snow, the snow would never cover the full surface of the structure, which means that there would also never be a fully distributed loading pattern across the whole structure, as K-Spans are built as semi-circles with a rise-to-span ratio of 0.5. This means that the worst-case scenarios should consider snow accumulation over the centre of the span or over half of the structure. Although the pinned base support connections experience greater positive and negative bending moments across the structure, the maximum values are located within the same areas. As per the bending moment diagrams found in Figure 2-14, the areas of loading will create positive bending moments on those sections of K-Spans.

Hingeless Load and Bending Moment Diagram	Two-Hinge Load and Bending Moment Diagram
--	--

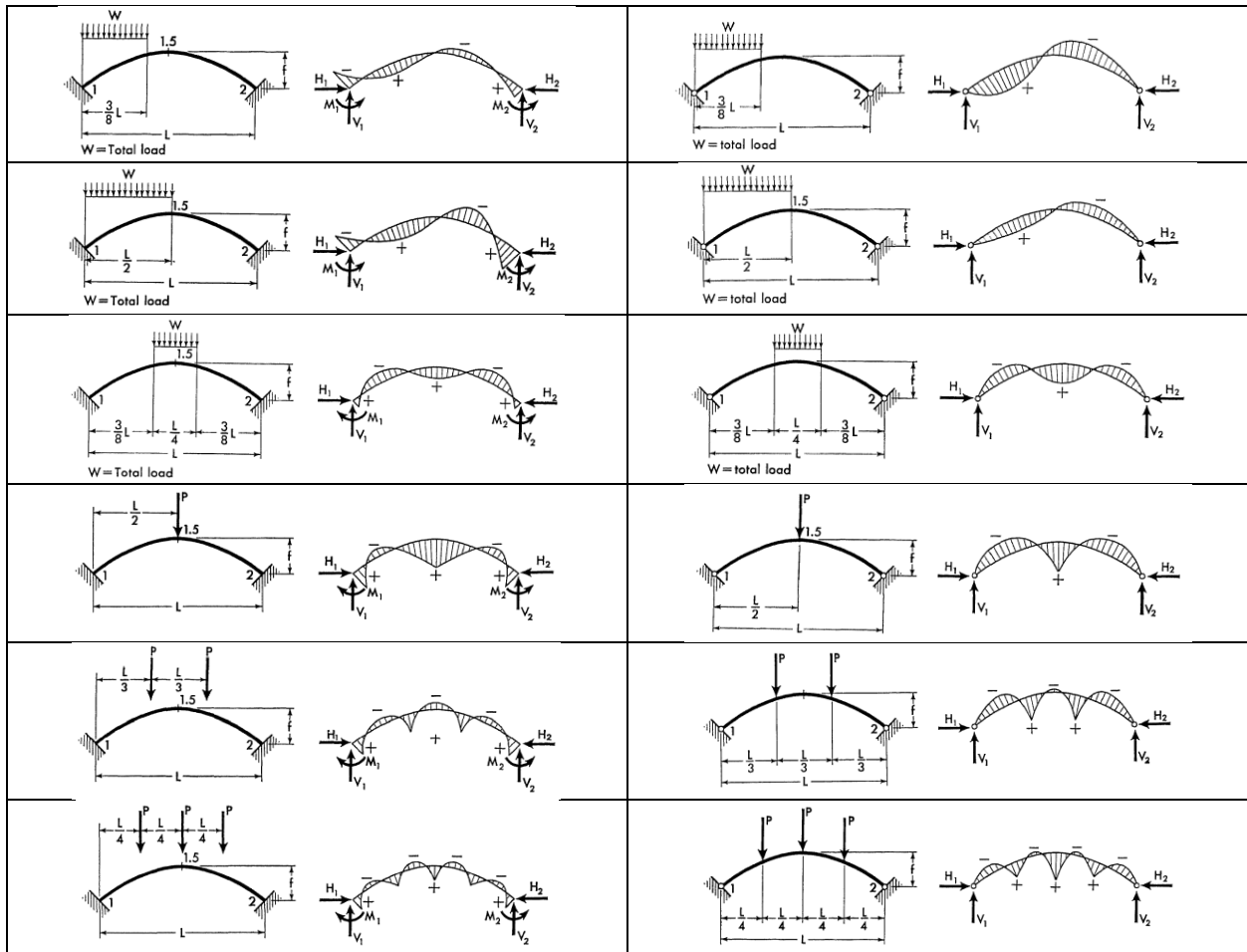


Figure 2-14: Hingeless and Two-Hinge Load and Bending Moment Diagrams [18]

2.4.3 Support Conditions

The support conditions greatly change the effects of the bending moments and reactions occurring during loading. In general, it is always preferred to have fixed base support connections for arched structures such as K-Spans, but both are capable structures that if appropriately designed and assessed, may be able to support significant snow loads [9]. Pinned base supported K-Span structures experience larger bending moments throughout the structure. The manufacturer of K-Spans, M.I.C. Industries, specifies that fixed base support connections that are embedded in concrete are required for the construction of K-Spans [10]. This allows for an efficient and effective distribution of bending moments. The use of steel hinges as pinned base supports for K-Spans under the same loading patterns creates greater positive bending moments, especially in a scenario where the structure is being loaded in an unbalanced loading pattern due to wind accumulating a greater snow depth over half of the structure [9]. Figure 2-15 provides an example of a pinned support K-Span found in CFB Kingston.



Figure 2-15: CFB Kingston K-Span Steel Hinge Support Connection

As per Table 2-1 from Macdonald [9], the largest bending moments occur near the supports, quarter length and centre of the structure. These areas and large bending moments will govern the structural capacity of the K-Spans for fixed supported structures, whereas K-Spans built with pinned support conditions will be governed by bending moments near the quarter length and centre of the structure only. This table represents the bending moments calculated using the equations found in textbook from Leontovich [18] with a distributed load of 1 kN/m. The regions of greatest concern are at the loading portions of the structure where large positive bending moments occur and in the areas that are experiencing negative bending moments a quarter length away from the supports.

The major difference between the two support connections is that large bending moments tend to be at the supports for the fixed supports, while for the pinned supports, the largest bending moments tend to occur near the quarter length points from the edges. As described earlier, no moments are occurring near the end supports and an increase of bending moments is distributed throughout the arched members. Although the fixed base support K-Spans experiences large moments near the end supports, the positive and negative bending moments near the loading patterns are significant, which could lead to failure of the pinned base support structures.

Table 2-1: Moment in kNm for 16 m Span at supports and quarter points [9]

Case	Arch Type	Load Condition of W	M_{0L}	$M_{0.25L}$	$M_{0.5L}$	$M_{0.75L}$	M_L
1	Hingeless		-4.39	1.64	-0.68	-1.85	2.64
	Two-Hinge		0	3.36	-0.91	-3.64	0
2	Hingeless		1.75	-2.04	1.37	-2.05	1.75
	Two-Hinge		0	-2.01	1.81	-2.01	0
3	Hingeless		-5.96	2.06	-0.72	-1.51	2.22
	Two-Hinge		0	4.07	-1.17	-3.58	0
4	Hingeless		-3.32	0.21	-1.40	0.13	-2.17
	Two-Hinge		0	0.43	-2.08	-0.23	0

2.5 Experimental Testing

2.5.1 Global versus Local Buckling

Local versus global buckling are discussed by Piekarczyk et al. and Lépine [21][22][12], which are the governing modes of failure for K-Span structures, and lead to structural failure or loss of capacity.

Marzouk et al. [19] explains that orthotropic cylindrical shell load-carrying capacities are governed by their overall buckling limits. Similarly, through large-scale testing, Xiliang et al. [20] studied large-scale models through an experimental program and concluded that local buckling and material strength are not the controlling factors of its load-carrying capacity. Through the analysis and usage of Digital Image Correlation (DIC) cameras, Piekarczyk et al. [21][22] noted that initial localized buckling imperfections created and lead to asymmetrical deformations in larger scale testing of K-Span panels, and that the impact of local instabilities and local buckling reduces the ultimate load-carrying capacity of K-Spans. This indicates that local buckling plays an important role in the behaviour of the structure under severe loading and that it may lead to overall instabilities and potential structural failure.

The evaluation of load-capacity on local buckling and deformations has been studied in smaller scale K-Span panels to develop a bending moment-axial load failure envelope to facilitate the design capacity for large scale K-Spans introduced by Piekarczyk et al. (2019) [22]. The study of short length panels subjected to axial compression loads as well as bending moments was used to evaluate the deformations and ultimate capacities of K-Span panels, as presented by Piekarczyk et al. (2019). This evaluation method was also used by Lépine (2021) [12], who studied the capacity of an 8 m radius K-Span, in length of 1-metre single and double-seamed panels to develop the failure envelope found in Figure 2-16 for the corresponding K-Span size. The panels were loaded through a system of steel plates and beams designed to obtain proper curvature angles, to be representative of the bending and compression forces experienced by an 8 m diameter K-Span structure. Following the numerical and small-scale experimental tests, as seen in Figure 2-17, the compression and bending tests of the K-Span panels helped develop the failure envelope, but also helped in evaluating the local buckling occurring through the thin-walled steel members.

The localized deformation patterns are crucial in determining the overall behaviour and effects of the transversal double corrugation of the K-Span panels. A few reoccurring patterns were noted by Lépine (2021) [12] where the compression of the webs would occur from the negative eccentric loads, the buckling of the flat seamed lips near the ends of the panels caused from positive eccentric loads, and the buckling of the flat seamed lips at the mid length of the short panels. Small-scale testing is necessary to analyse the effects of localized instabilities and understand the overall behaviour and capacity. It would allow the capture and more precise analysis of deformations experienced by the panels compared to the larger scale experimental tests, where other factors may come into play, or localized deformations may not be captured in the proper area.

Although small scale testing methods are an efficient and easy way to analyse the structures panel capacity, the global effects of the localized buckling patterns are also required to have a full understanding of its influence.

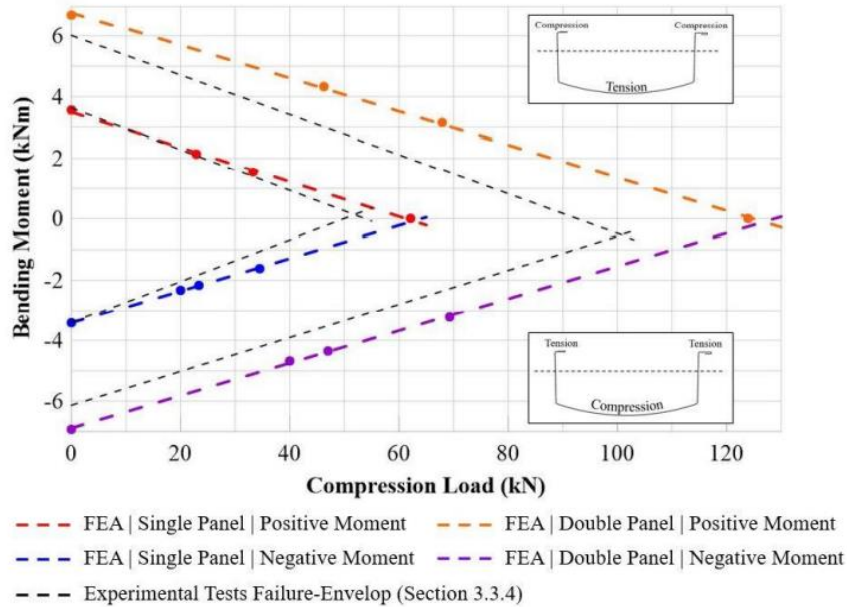


Figure 2-16: MIC-120 Panel Failure-Envelope [12]

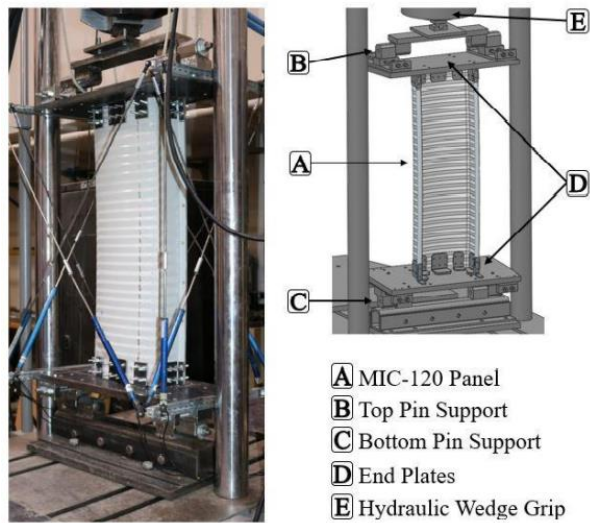


Figure 2-17: Small Scale Compression Test [12]

2.5.2 Effective Area of Members

The presence of double corrugation does contribute to the complexity of the design and evaluation of the ultimate strength of K-Spans structures. Many engineering codes provide analytical solutions to estimate ultimate capacities for straight or single-corrugated cross-sections of thin-walled steel structural members but provide little to no guidance on the inclusion of transversal double-corrugation, which is perpendicular to the cross-section of the panel. MacDonald [9] analyzed the ABM-120 panels following CSA S136-16, and provided an equivalent thickness to account for the transversal double-corrugation of the cross section. He compared his results to the experimental results described in literature from Sweeney et al. [6]. The paper determined that there was a difference ranging from 40% to 1% between the theoretical

results of the specified bending capacity away from supports following CSA S136-16, and the experimental results from Sweeny et al., as presented in Table 2-2.

Table 2-2: Positive Bending Capacity Following CSA S136-16 Compared to Testing Capacity Away from Support in Literature [9]

Steel Grade	Thickness	CSA-S136-16 Positive Bending Capacity, Specified	CSA-S136-16 Positive Bending Capacity, Factored	Literature Review Tested Capacity	Percent Difference Specified/Tested
275 MPa	0.85 mm	8.08 kNm	7.3 kNm	-	-
345 MPa	0.85 mm	9.2 kNm	8.3 kNm	6.4 kNm to 9.1 kNm	+40% to +1%
275 MPa	1.00 mm	10.4 kNm	9.3 kNm	10.4 kNm	0%
345 MPa	1.00 mm	11.8 kNm	10.6 kNm	-	

Other papers have analysed the K-Span’s unique features by looking at the cross-sectional area of ABM-120 panels. The presence of double corrugation requires a reduction of the effective area in order to reduce the resistance of the cross-section, as described by Cybulski et al. [2]. This paper proposes three different methods to calculate the ultimate compression load for K-Span members of ABM-120 profiles, which includes analytical, numerical, and experimental methods.

The analytical method used for calculating the ultimate capacity of the panels focused on accounting for only the effective widths of the ABM-120 cross-section. Although the analytical method can be used to calculate an effective area as per Figure 2-18, the determination of the strength of the panels through scanning them with 3D optical cameras and using finite element evaluation, confirmed through experimental testing, has proven to be a more effective and accurate method to estimate ultimate load capacity. The disadvantage of these methods is that it requires the use of advanced technological equipment which may not be easily available and may become more complex and cumbersome when analyzing and testing larger scale experimental specimens.

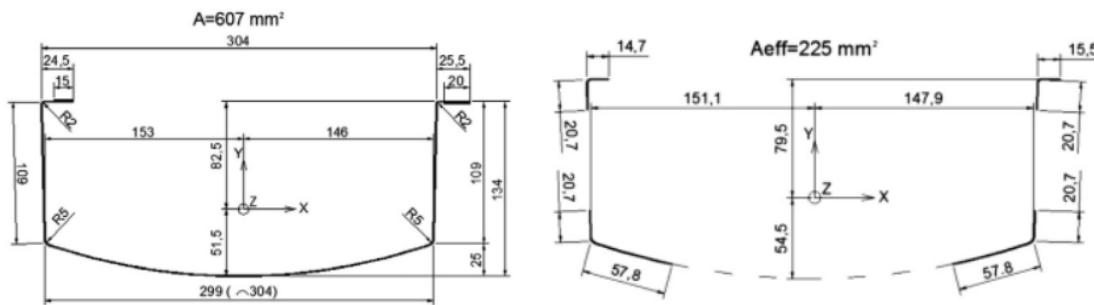


Figure 2-18: Effective Area of Panel [2]

The Association of Standard of the People’s Republic of China researched and produced technical papers providing technical specifications for the development of arched corrugated steel roofs, such as K-Spans that have less than a 30 m span [23]. Although this standard does not specifically cover the M.I.C. Industries ABM-120 and ABM-240 panels, the cross-sectional models, and the presence of double-corrugation within the thin-walled steel panels, are almost identical. This guidance provides empirical equations, as presented in Table 2-3, to find an equivalent area and moment of inertia dependent on curvature of the panels and thickness of the material, found through an extensive testing of several

specimens of different sizes, to estimate the structural capacity of arched corrugated roofs based on the radius in meters of the structure.

Using these simplified methods and equations, the structural capacity of the corrugated arched roofs is estimated following the equation (4) below, where the combination of axial forces (N_1) divided by the equivalent area (A_{eq}) and bending moments (M_n) divided by the equivalent section modulus (W_{eq}) should be lower than the design value of tensile, compressive or bending strength of steel (f).

$$\frac{N_1}{A_{eq}} + \frac{M_n}{W_{eq}} \leq f \quad (4)$$

Through multiple papers, the simplification of reducing the moment of inertia, thickness, and cross-sectional area to an effective or equivalent area of the panel has demonstrated to be a simplified and efficient method to estimate the ultimate capacity of K-Span panels. These methods of reduction could facilitate the design of numerical models of K-Span structures to replicate the structural behaviours in FEM analysis without accounting for designing the transversal double-corrugation. Although additional data and testing may be required to determine appropriate reductions dependent on curvature and size of K-Span structures, the possibility to simplify the analysis without the use of DIC cameras and inclusion of the complex K-Span geometry could facilitate efficient and reliable design of these structures in future.

Table 2-3: Equivalent Section Characteristics of Arched Corrugated Steel Roof [23]

Plate Thickness (mm)	A_{eq} (cm ²)	I_{eq} (cm ⁴)	$W_{eq}^{(1)}$ (cm ³)
0.9	$2.85387+0.19619r-0.00218r^2$	$70.79445+3.21631r-0.03679r^2$	$9.82775+0.40017r-0.00672r^2$
1.0	$3.48511+0.21613r-0.00218r^2$	$83.43775+3.61434r-0.03024r^2$	$11.92385+0.38327r-0.00481r^2$
1.1	$3.80873+0.29297r-0.00218r^2$	$88.45267+5.34056r-0.06855r^2$	$13.228333+0.49589r-0.00731r^2$

2.5.3 Rise-to-Span Ratio

The dimensions of arched structures are an important factor in the overall stability and strength capacity limits for K-Spans. The ratio between the height and diameter of the structure, called rise-to-span, greatly impacts the capacity of arched structures as described by Litong et al. [24], and as presented in Figure 2-19, comparing the ultimate capacity and rise-to-span ratio of MMR-178 arched structures. MMR-178 panels follow a similar design as ABM-120 panels. A ratio ranging between 0.2 to 0.3 leads to a stronger and more stable structure that can support higher loads, compared to a ratio of 0.5, which is equivalent to a perfect semicircular structure. Having the height of the arch only a quarter of the span of the structure greatly increases its capacity, but also creates potential need for higher end walls where the panels connect to the base supports.

This is also confirmed in the Technical Specification for Arched Corrugated Roofs standard produced by the Association of Standard of the People’s Republic of China [23], where it is recommended to have a rise-to-span ratio between 0.2 to 0.25 for corrugated arched structures. However, they also permit a ratio between 0.1 to 0.5, dependant on the functional requirements of the structure and loading conditions. Having a ratio of 0.5 permits a higher structure, essential for industrial areas that may require large loading vehicles accessing the interior of the structure. Considerations should be taken in the design process to

enlarge the footprint of the building without increasing the height, to prevent having unnecessarily high rise-span ratios.

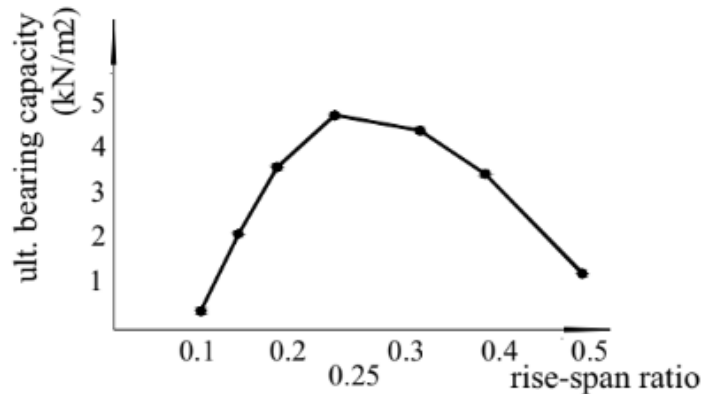


Figure 2-19: Rise-to-Span Ratio Versus Ultimate Bearing Capacity Diagram for 20 m Span Arched MMR-178 Panels [24]

2.5.4 Large Scale Testing

Many studies have been conducted to investigate K-Span panels on a small scale to focus on localized deformation patterns and analysing the effect of transversal double-corrugation on individual panel strength capacity. However, due to the difficulty of instrumentation, space constraints, construction and maintaining larger scale models, full-scale studies of K-Spans, including the whole structure and its base support connections, are scarce.

Studies such as Airumyan et al. [17] tested self-supporting arched roofs having 15 to 21 m spans using cold-formed steel shells of different thicknesses, similar to ABM-120 panels. The experimental program consisted of evaluating different loading conditions and various shaped arches of different height-to-width ratios. Using a suspended beam system for loading, as seen in Figure 2-20, the finding was that the decrease in capacity can be associated with localized buckling due to the inclusion of transverse corrugation in the flanges. Experimental deflections of specimens were provided and concluded that a concentrated load applied to one K-Span section made of steel thickness less than 1.0 mm should not exceed 2.0 kN in self-supporting arched members [17].

Recent research on K-Span structures, produced by Piekarczuck et al. [21][25], also studied K-Spans on a larger scale with the intent to use FEM analysis to link experimental and numerical models. Similar to Airumyan et al., the large-scale testing of K-Spans, as demonstrated in Figure 2-21, shows the use of steel beams to load the structure downwards. Using DIC cameras, these experimental tests of K-Spans helped the team of researchers determine that compression of the webs led to failure of the structure. The correlation between large-scale, small-scale and numerical work is important to comprehend and assess K-Spans in further detail.

One common research point to all the studies completed on large-scale K-Span structures is the flexibility of K-Span structural members. K-Spans deform greatly under loading, and the presence of localized deformations greatly affects the structural capacity of the structure. This has led some studies to be conducted to determine strengthening methods, which would reduce deformations, increase panels stiffness and prevent failures from occurring, such as Xiliang et al. [20], where tension chords were used to reinforce the structure.

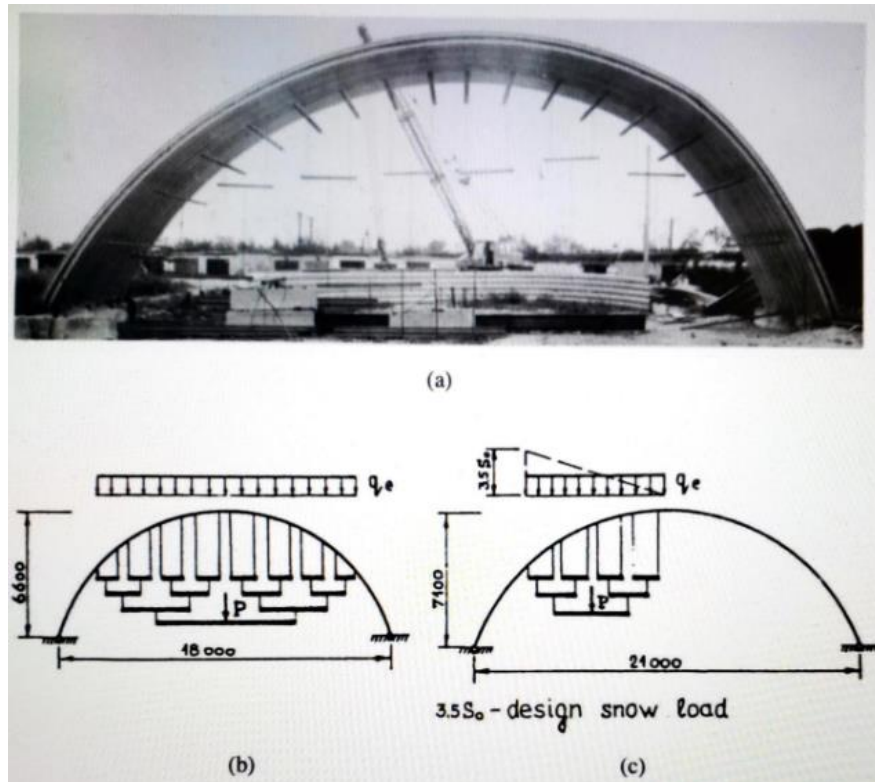


Figure 2-20: Airumyan et al. [17] General View of Tests Set-Up and Loading Patterns



Figure 2-21: Test Set-Up from Piekarczyk et al. [21][25]

2.5.5 Numerical Modelling - Finite Element Analysis

Due to the lack of guidance and design standards for the inclusion of transversal doubly-corrugation found in arched structures, appropriate methods to estimate strength capacities for K-Span structures are through numerical modelling and finite element analysis. The ability to include non-linearities in numerical models is a necessity when analysing structures with unique shapes and geometry such as K-Spans. Due to the panels' flexibility and deformations experienced under loading, finite element analysis is helpful in estimating large deflections and buckling behaviours. Although software is a great tool to analyze structures and estimate internal forces and stresses, a layer of complexity is added for the modelling of K-Spans, specifically due its complex geometry, and the inclusion of transversal double-corrugation in the panels

caused by the forming process. This often creates a challenge for numerical models to reduce computational times and reduce the number of nodes and elements, due to the level of detail required to model a perfect geometry with all geometric details included. Many different methods have been used in studies conducted on K-Spans, which often include shell elements, large deflections, and the inclusion of 3D optical scanning technology to assist in the development of the numerical model to capture the shape of corrugations.

K-Spans were evaluated by MacDonald (2021) [9] using the standard structural analysis program SAP2000 V21 in order to estimate cross-sectional properties and the flexural capacity of different K-Span sizes and thicknesses. Using a 2D FEM analysis with four panel frame elements, and the inclusion of P-Delta effects and large displacements, Macdonald was able to compare bending moments for both a pinned and fixed support connection K-Span, as seen in Figure 2-22. The positive bending moments experienced by the model shown in the figure are more severe than the negative bending moments. The numerical model also demonstrates a large difference in the bending moments felt throughout the structural members, where the pinned base support K-Span experiences larger bending moments. The study also included a conversion of the results into maximum snow loads in kPa for each size evaluated in the software, to associate levels of snowfall to potential risk of failures.

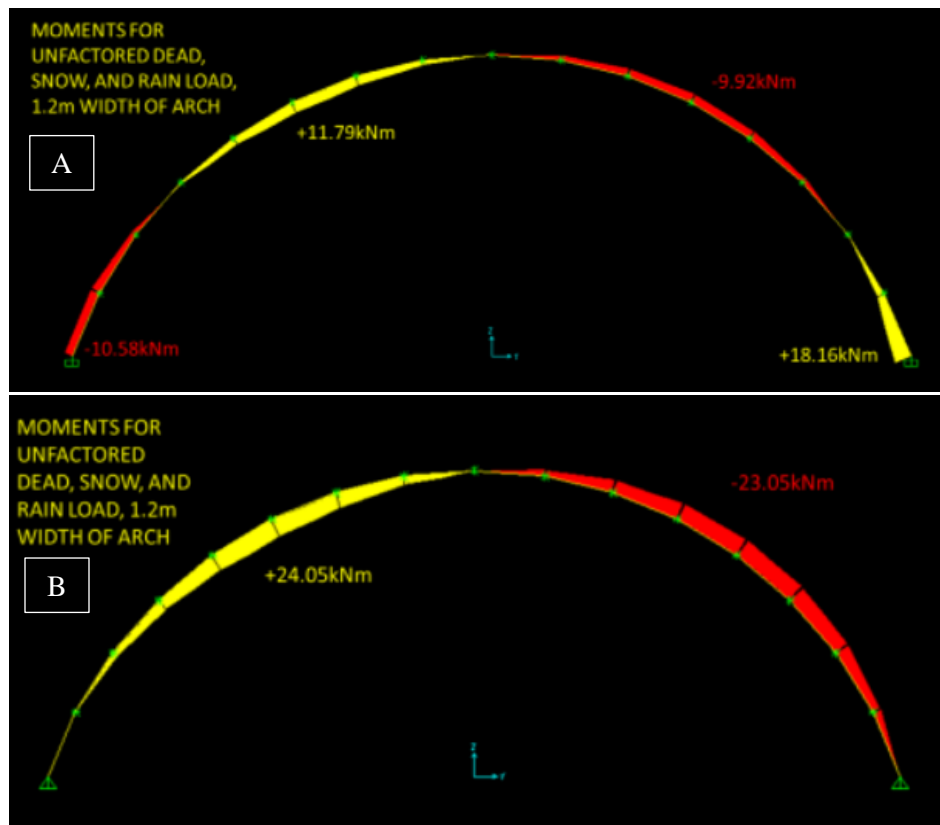


Figure 2-22: Bending Moment for 16 m Span Fixed (A) & Pinned (B) K-Span Structures with Unbalanced Loading Pattern [9]

Other studies produced by Piekarczyk et al. [5] and Lépine [12] focused their efforts on 3D modelling to gain a better understanding on the local instabilities of K-Span panels. Their numerical results were used to validate the experimental laboratory tests, as seen in Figure 2-24. The advantage of using numerical models is the ability to find small, localized deformations, but also include non-linear properties of material, large deflections and buckling behaviours experienced from loading of the panels [12]. Through

software such as ANSYS, detailed designs of K-Span panels can be reproduced and modelled to include all geometrical patterns, as the mesh is divided into small elements, with focus on corners and seamed lips, as presented in Figure 2-23.

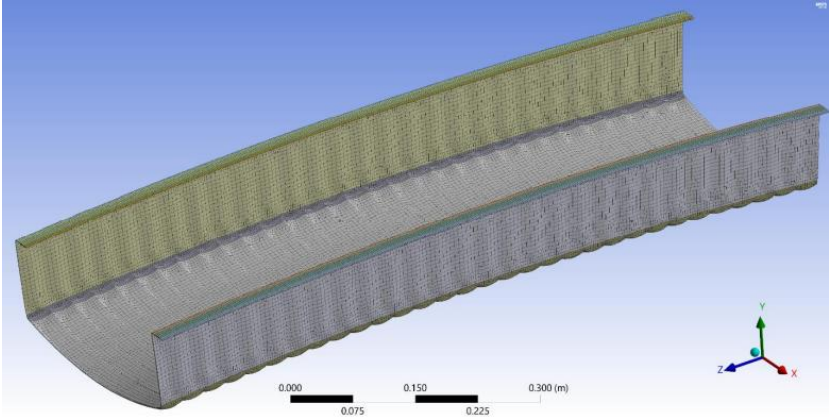


Figure 2-23: MIC-120 Mesh Model [12]

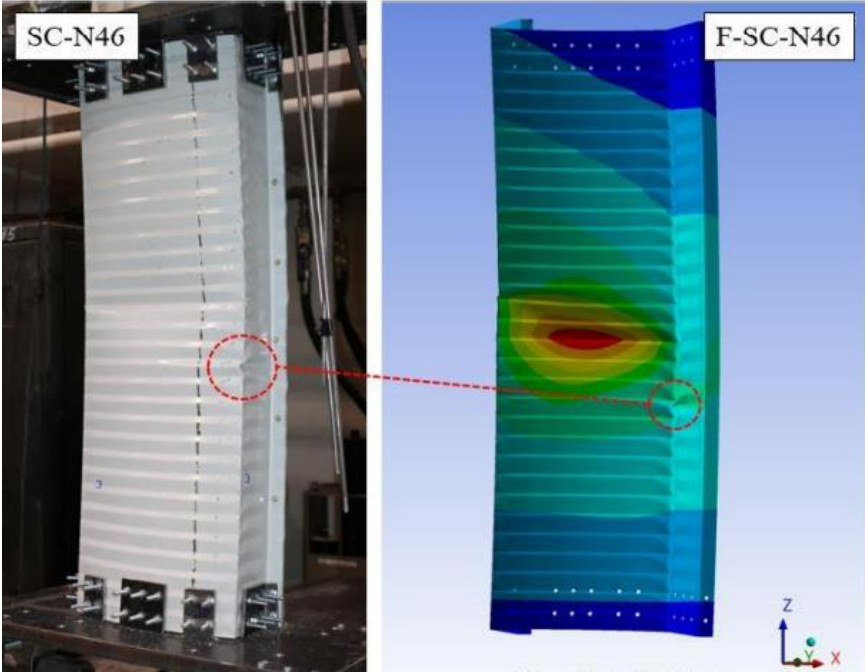


Figure 2-24: Numerical and Experimental Comparison from Lépine (2021) [12]

The unique geometry of the panel can be manually reproduced with CAD software, but this can be time-consuming to capture all the details of the corrugation. The geometry can also be reproduced using 3D optical scanning systems, a measurement instrument which converts the surface of the geometry into a cloud of high-density points with 3D coordinates [7]. This model and geometric data is then imported into CAD and FEM software to analyse. This facilitates the modelling process and can record even the smallest imperfection which might not have been noticeable initially or captured in a manually designed geometry.

Digital image correlation (DIC), which is optical scanning technology, is used for contactless displacement and strain measurements [15], can easily be compared to numerical models. This is helpful

when analysing K-Spans, as it provides accurate and efficient measurements that can easily correlate to FEM result models, as seen in Figure 2-25. DIC was used by Piekarczyk et al. (2021) [15] to measure strains on large scale specimens in areas where the structure was expected to experience large deformations and strains. The study also recorded data using displacement sensors and was able to confirm that the values extrapolated did not exceed an error difference larger than 2%. DIC technology, which has existed since the 1980's [15], has been subjected to major upgrades and advancements. When analysing specific areas that have a complex surface like the corrugated K-Span panels, DIC should be considered for the analysis of stress and displacement if available.

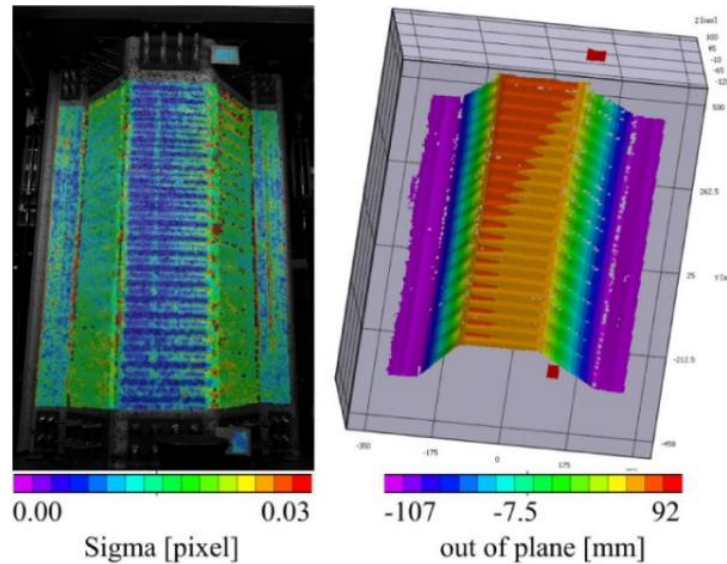


Figure 2-25: Example of Displacements Results for ABM-240 K-Span Panels Using DIC Scanning Technology [5]

2.6 Summary

This literature review intended to provide readers sufficient knowledge and information on the subjects and concepts studied in this research project. Although research related to ABM-120 panels is limited, K-Span literature is consistent with one another and could lead to future design best-practices when thin-walled self-supporting arch-type structures are built.

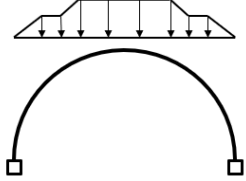
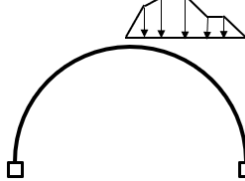
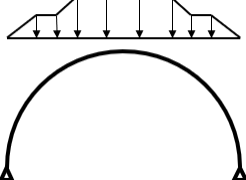
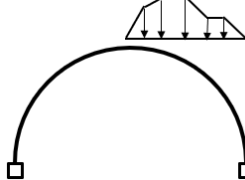
The presence of multiple factors mentioned in this literature review could lead to severe and unexpected collapses of K-Spans. With the unique and complex geometry of K-Span panels, future research is required to account for the inclusion of corrugation in the forming process and its effects on the structure's behaviour during loading. There is also a lack of research regarding structures that have been built using hinges versus the manufacturers' specification of fixed base supports, which this research aims to compare through the study of large-scale experimental specimens. Gaining a better understanding of the difference in behaviour of the structure based on its support conditions and determining how to account for the complex geometry of double corrugation and curvature, will lead to better design practices and guidelines for K-Spans and arched structures. It will also encourage the discovery of enhanced design or strengthening methods to ensure the structure resists expected loads and prevents any failures for future K-Span construction. The manuscript found within this research contains a summary of this literature review within its introduction, as it is a standalone document.

CHAPTER 3: EXPERIMENTAL PROGRAM

3.1 Introduction

This section contains a description of the specimens used, the experimental program set-up and procedures used for the research. The equipment used to study the structural behaviour of the specimens and the instrumentation plan is also summarized. The experimental program description provides information and includes schematics of the research test specimens which is relevant for the testing of the large-scale specimens reported in the manuscript. The large-scale experimental program consisted of four 7-meter diameter ABM120 arch specimens. The specimens were loaded using two different loading arrangements representing two independent critical snow loading patterns as well as using being constructed with two different types of base support conditions as described in Table 3-1.

Table 3-1: Experimental Specimens Descriptions

	Balanced Loading Pattern – Simulated Snow Load Where Accumulation is Present on the Whole Surface	Unbalanced Loading Pattern – Simulated Snow Load Where Accumulation is Present on Half of the Surface
Fixed End Support Condition – End of Panels are Embedded in Concrete		
Pinned End Support Condition – End of Panels are Bolted on Steel Hinge Assembly		

3.2 Experimental Setup

The experimental program involved the representation of an accumulated worst-case snow loading pattern as per the National Building Code of Canada (NBCC) [3], where two distinct loading patterns were used. The first pattern consisted of a balanced loading pattern, where a fully distributed snow load on the surface of the structure was transformed into four rows of loading points. The second pattern consisted of an unbalanced loading pattern, where a distributed snow load was applied to only half of the surface of the K-Span, which was transformed into two rows of loading points. The simulated snow loading pattern included the change in the accumulation factors caused by slippage of snow due to the slope increase near the base supports. Both loading patterns were considered critical loading conditions for arched structures as per the NBCC. Both loading patterns are represented in Figure 3-1. Both figures show the experimental set-up of the tested specimens with the loading points, concrete support conditions, sets of four seamed ABM-120 panels that created an individual specimen for testing and actuator placement along the side of the specimens. Figure 3-1 (A) represents the balanced loading pattern where 16 loading points are equally spaced on each side of the centre of the arched K-Span in sets of four rows. Figure 3-1 (B) represents the

experimental set-up for the unbalanced loading pattern, where a total of eight loading points are applied only on one half of the arched specimen. All loading points included in the Figure 3-1 for both A and B includes the pulleys and steel cables assembly for the loading points.

The loading points on the K-Span were positioned in areas where the total loading would be representative of the respective snow loading patterns. In order to determine the positioning of the loading points along the specimens, the distributed loads along the roof of the arch for the 7 m diameter specimens were transformed into 24 blocks of distributed loads. These small loading points were in turn converted into four larger loading points to facilitate the replication of loading in the laboratory.

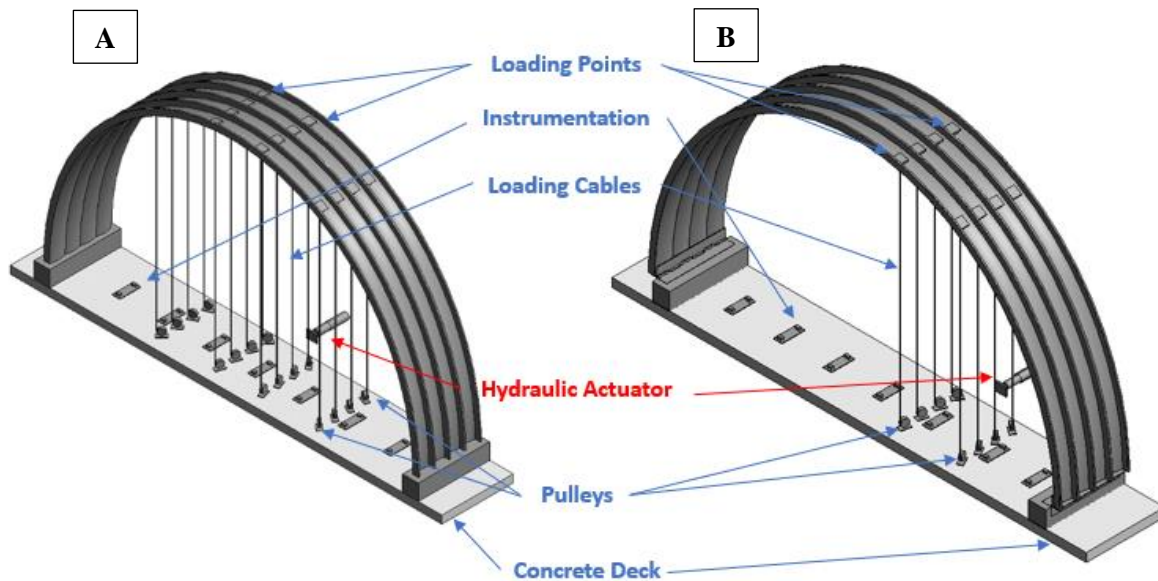


Figure 3-1: Experimental Set-Up for Balanced Loading Pattern on a Fixed Base Support Specimen (A) and Unbalanced Loading Pattern on a Pinned Base Support Specimen (B)

An elevated reinforced concrete deck provided a testing base. The concrete deck also allowed for the positioning of loading equipment and instrumentation. This facilitated the configuration of the loading system where the actuator and attached steel cable anchor block was mounted horizontally and with the assistance of pulleys anchored to the deck, the force in the steel aircraft cables was re-directed vertically to load the K-span downwards. The loading of the specimens was achieved using 27 kN (6100 pound-force) rated steel aircraft cable going through the high-capacity pulleys to redirect the cables towards the steel plate cable anchor block where all steel aircraft cables were joined and pulled under stroke control at a rate of 5 to 10 mm per minute by a 100 kN Material Testing System (MTS) hydraulic actuator. The movement of the actuator was controlled by an MTS Flextest 40 digital controller, an HBM MGCplus Data Acquisition system and a PC operating CATMAN AP software. The cable arrangement and positioning of loading points are presented in Figure 3-2 for both the balanced and unbalanced loading patterns. The cables were all separated by turnbuckles to control the loading on each steel aircraft cable, ensuring they had a similar level of distributed load during the initial stages of loading. Figure 3-2 (A) demonstrates the balanced loading pattern. It is characterized by equal spacing for the central loading rows of 0.442 m from the centre line of the specimen and 1.568 m for the exterior loading rows. As for the unbalanced loading pattern represented in Figure 3-2 (B), the loading rows are spaced 0.657 m and 1.715 m on one side of the specimen, away from the centre line. The loading points are attached along the top of the specimens and the steel

cables goes straight down through pulleys anchored to the concrete deck and all join a steel plate anchor block connected and pulled by an actuator.

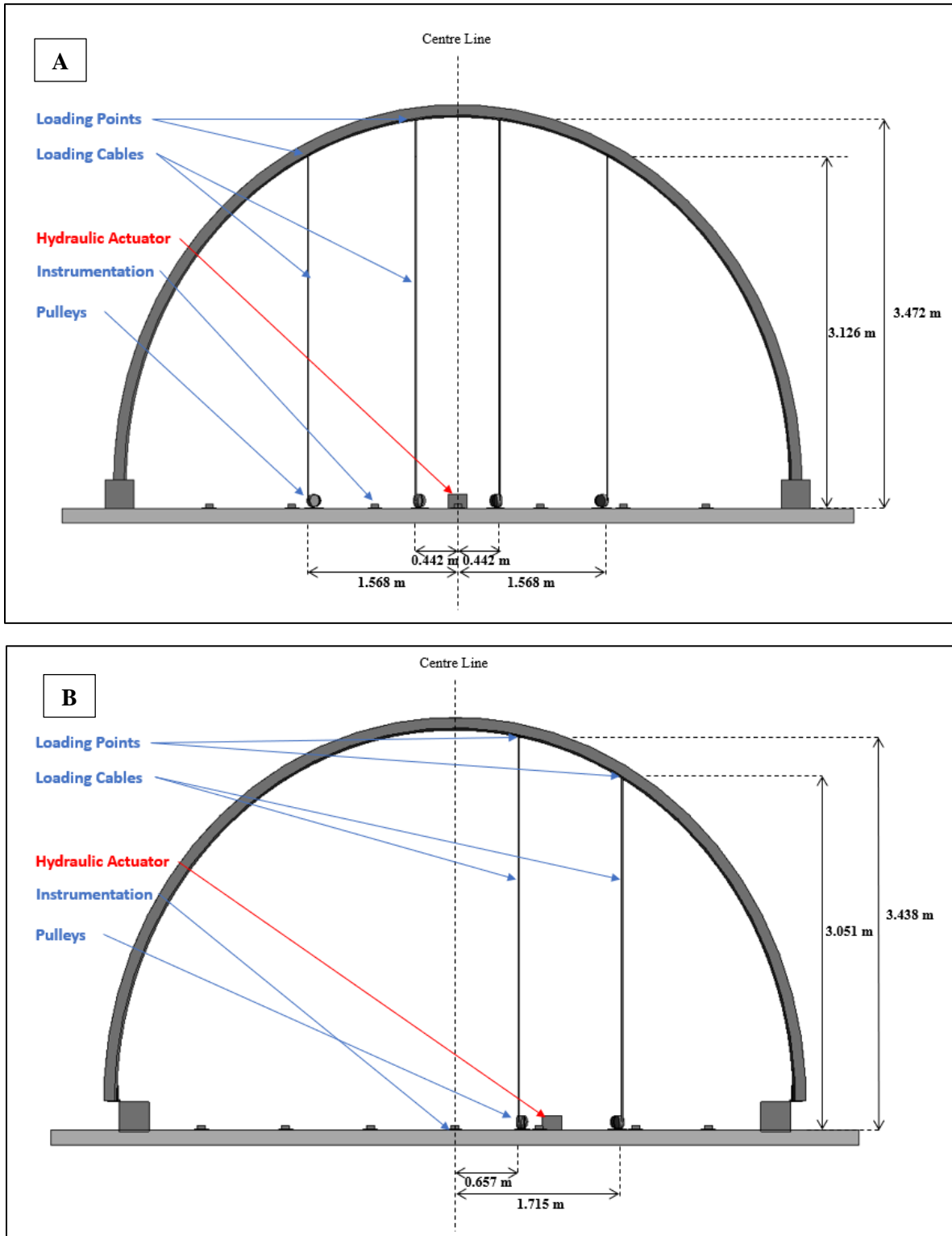


Figure 3-2: Side View Loading Dimensions for Balanced (A) and Unbalanced (B) Loading Patterns

A comparison of the base support connections was also done as two types are found across the DND infrastructure portfolio. The first type of base support was fixed, where the ends of the K-Span panels were embedded into reinforced concrete. The second type of base support was pinned, where the ends of the panels were bolted to steel hinges that were attached to the concrete bases. The dimensions of the concrete base blocks were 300 mm by 300 mm. The design of the reinforced concrete supports was based on existing plans of K-Span structures in order to fully represent the support conditions found within DND's infrastructure inventory. The dimensions of both support conditions are presented in Figure 3-3.

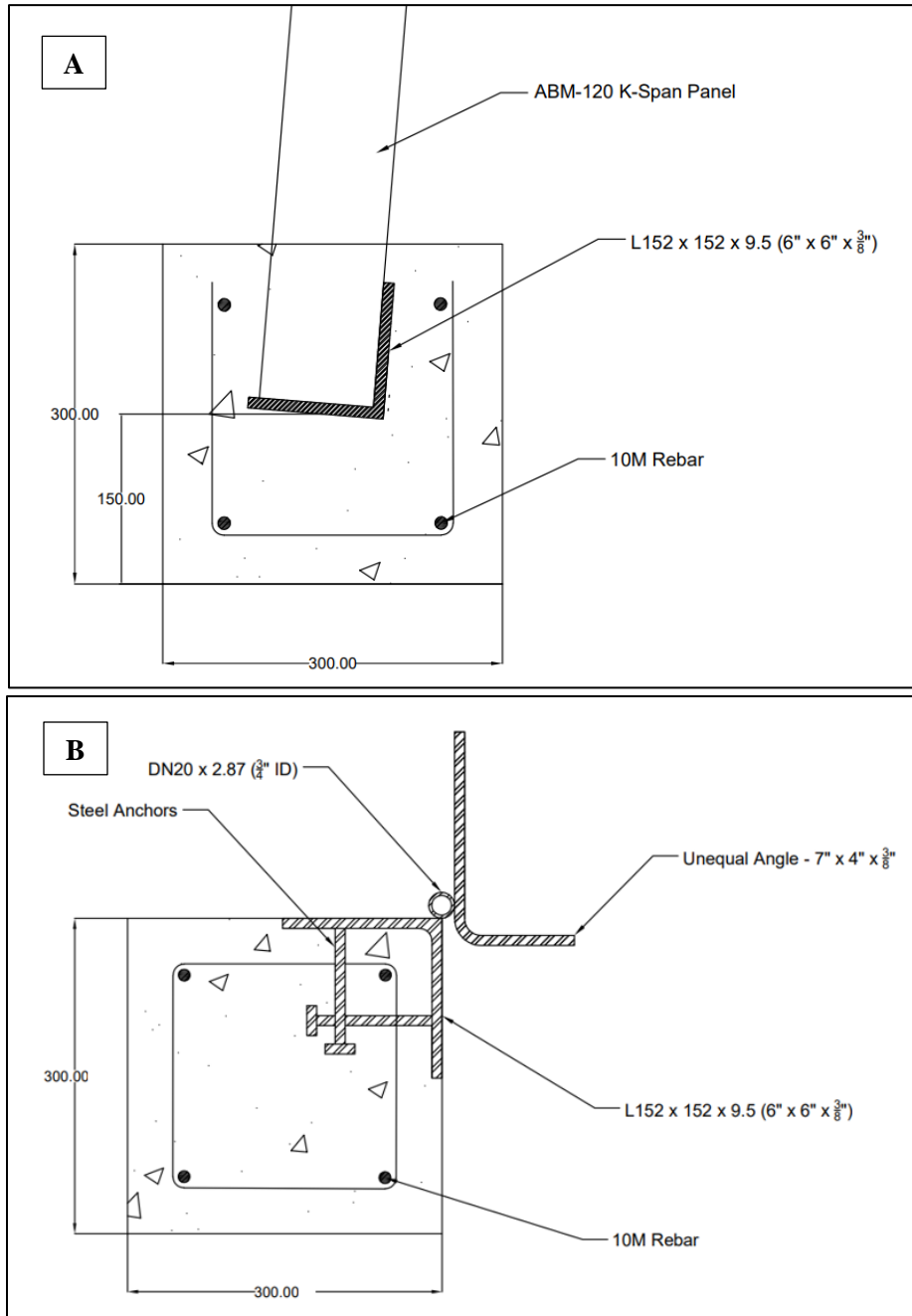


Figure 3-3: Schematics of Fixed Base Support (A) and Pinned Base Support (B) in Millimeters

Space within the structures laboratory was limited, which dictated the size of the possible specimens, ensuring that not only the panels once formed would be able to enter the laboratory but also able to vertically fit without impacting the crane movement within the laboratory. A span size of 7 m was determined to be the maximum allowable diameter so that the four-panel specimens could be positioned onto a concrete deck, and capable of including sufficient space for loading equipment, instrumentation and facilitating movement beside the large-scale specimens.

The base supports were bolted to the concrete deck to prevent their movement and rotation while structure was loaded, and this attachment method facilitated the replacement of base support blocks throughout the experimental program. Throughout the experimental program, the average concrete strength used for all support types was 19.8 MPa.

3.3 Equipment and Instrumentation

The experimental program required the use of multiple equipment and instrumentation in order to capture the structural behaviour of the 7 m span specimens. A total of 39 instruments were used to gather data on displacements and loading during the experimental program. These instruments consisted of load cells, string potentiometers and linear variable differential transducers (LVDTs). The load cells were used to measure the total load applied to the structure, while the string potentiometers and LVDTs were used to gather data on the vertical, horizontal and lateral displacements of the K-Span panels, the concrete slab and the pinned base support's rotation. All instrumentation was monitored at a sampling rate of one (1) Hz by an HBM MGCplus Data Acquisition system and a PC operating CATMAN AP software. The instrumentation identifiers and measuring direction are presented in Table 3-1.

Table 3-2: Instrumentation Identifiers and Directional Measurements

Instrument Name and Directional Measurement	Identifier	Total Numbers
Vertical Linear String Potentiometer	S	14
Horizontal Linear String Potentiometer	SH	4
Longitudinal Linear String Potentiometer	SL	1
Load Cell	LC	17
Linear Variable Differential Transducer	LVDT	3

The loading scheme on top of the K-Span is arranged of components to distribute the load and prevent the loading points from punching through the K-Span. It includes a sandwich of a steel plates, a load cell, an aluminum plate, a larger piece of wood and a foam at the bottom, as presented in Figure 3-4. A total of 17 load cells were part of the loading assembly to measure the load experienced on each loading point. The load cells present at the loading points were designed with sufficient sensitivity to read lower load levels throughout the K-Span. The whole loading arrangement was attached to an eyebolt connected to the aircraft cable pulled by the actuator. All loads are measured in kilonewtons (kN). The actuator load cell was used as the control, ensuring that the total load of the system was captured and compared to the loading points.

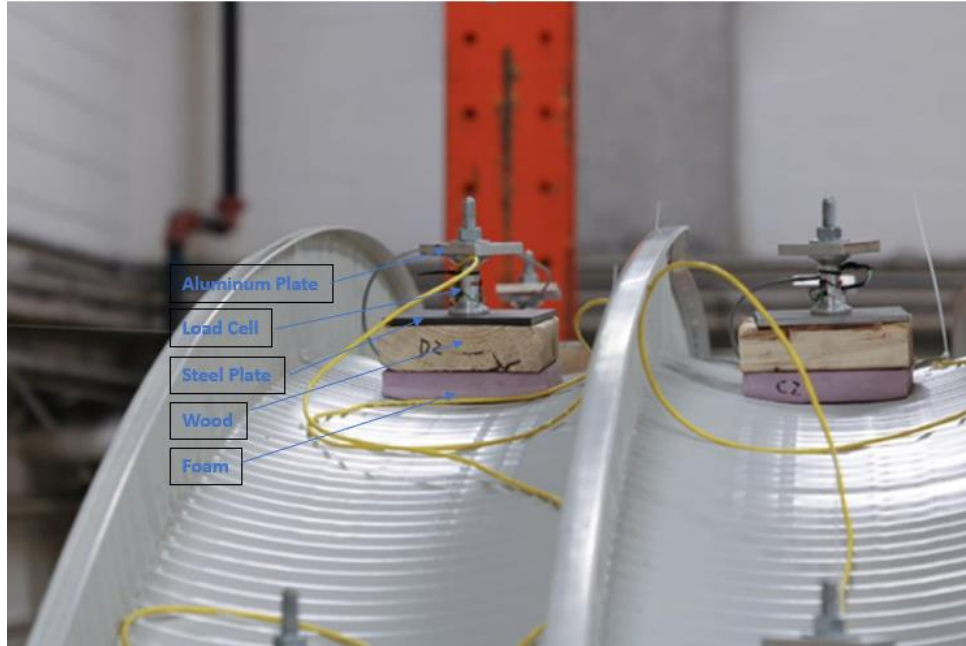


Figure 3-4: Loading Assembly and Loadcells Top of Specimens

The overall loading of the specimens was done by the actuator pulling the loading points through a system of steel aircraft cables all connected to a steel plate. The steel plate was connected to the actuator and positioned at the centre of the K-Span for the balanced scenario, and only one meter off the centre for the unbalanced scenario. The concrete deck assembly of the actuator, pulleys and steel aircraft cables is presented in Figure 3-5.

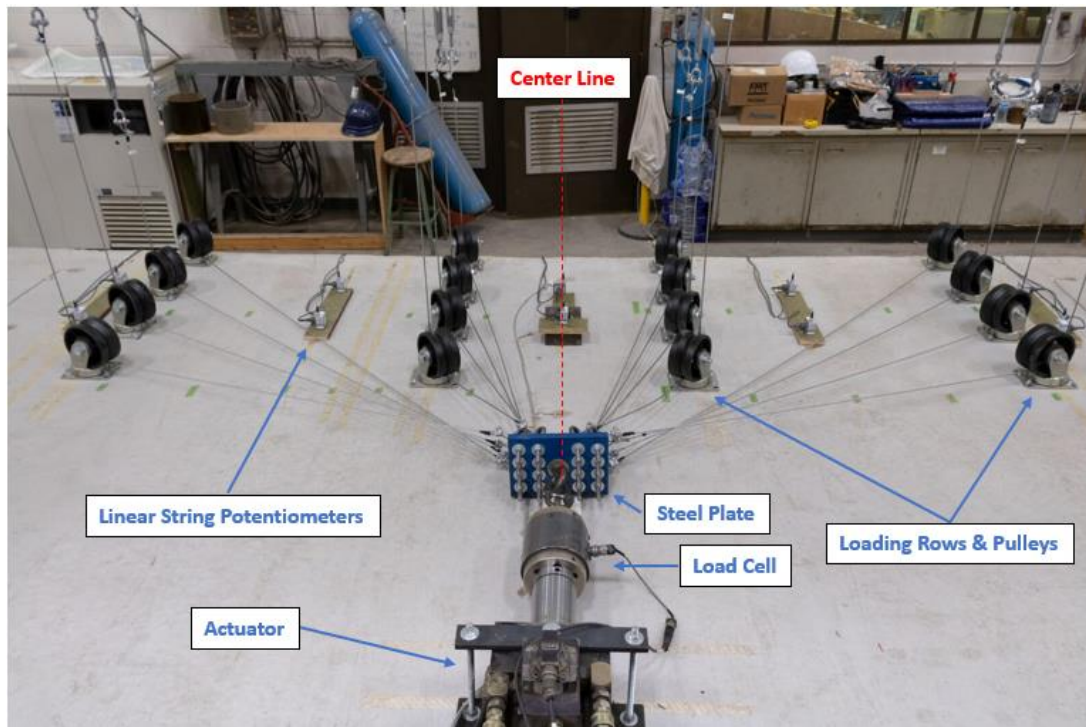


Figure 3-5: Actuator and Concrete Slab Loading Set-up for Balanced Loading Pattern

Linear string potentiometers were used to measure vertical, horizontal, and longitudinal displacements along the structure. All displacement measurements were done in millimeters (mm). A total of 14 potentiometers measured the middle two panels at every 1/8th diameter spacing at the base of the structure, four potentiometers measured the horizontal displacement, and finally, the last potentiometer measured the lateral displacements, for a total of 19 linear string potentiometers. Linear variable differential transducers (LVDT) were used on the hinges and concrete slab to monitor rotational deformations. The positions of the vertical and horizontal potentiometers are presented in Figure 3-6.

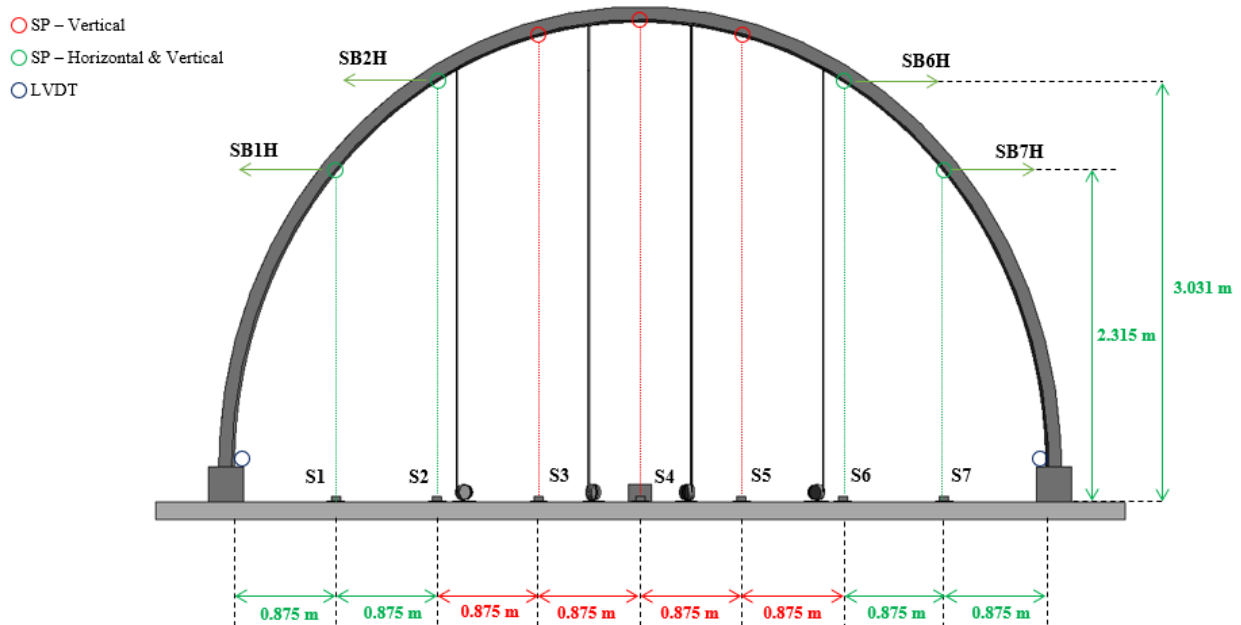


Figure 3-6: Instrumentation Layout and Positioning

3.4 Experimental Procedure

The experimental loading procedure consisted of pulling steel aircraft cables downwards on the set of panels, in areas where snow accumulation would normally apply and create large internal loads and deformations in the structure. The whole structure was erected on top of a concrete slab, which was used as an anchor point for supports and the loading equipment. The positioning of the loading equipment and instrumentation were intended to force the specimens downwards until failure occurs.

With the actuator bolted onto the concrete deck, the steel aircraft cables were all pulled at the same rate as they were re-directed from horizontal to a vertical direction through pulleys before reaching the top of the structure. At the beginning of the experimental testing, all loading points and steel aircraft cables were balanced to similar levels of load (0.2 kN +/- 0.02 kN) prior to slowly applying the full test load with the actuator. The steel aircraft cables all included turnbuckles in order to match the loading at all points as presented for one cable in Figure 3-7.



Figure 3-7: Turnbuckles Used for Adding Tension in Loading Assembly

Once equal tension was present throughout all loading points, the actuator pulled all steel aircraft cables through displacement-controlled measures. Loading of the specimens continued past ultimate capacity of the 7 m K-Spans, until either deformations were so significant that the linear string potentiometers were no longer capable of providing accurate results, or the severity of the failure of the specimens during the loading process ensured that the structure had very little residual strength capacity.

The experimental test for each specimen is characterized by three phases: The first phase being the loading of the specimens prior to ultimate load, the second phase being the loading of the specimen post ultimate load and the last phase being the unloading process of the experimental specimens.

The initial phase was the loading of the specimens until ultimate load was reached. Detailed observations were made during this first step, such as the displacements directions and overall movement of the structure, as well as any localized buckling occurring prior to reaching ultimate load. Behaviour of the specimens along the interior and exterior portion of the panels were observed.

The second phase was post-ultimate or post-buckling behaviour, where once the ultimate capacity was reached for the specimens, loading continued to assess the residual strength of the specimens. The localized buckling areas during this step was also important to observe as they could increase the displacements of the specimens and dramatically reduce the residual strength of the arch. The behaviour of the specimens post-ultimate is significant in that it provides valuable information on the potential of a completed K-Span structure to re-distribute loads along the length of the K-Span.

Finally, the last phase was the unloading of the specimens, where once the instrumentation was no longer recording accurate data, the structure was unloaded in the same displacement-controlled measure as the loading of the structure. The structures' ability to recover or permanently deform was also noted. The total assembly of the equipment and instrumentation is represented in Figure 3-8.



Figure 3-8: Pinned and Balanced Specimen Experimental Assembly

Photography and a video recording program of the experimental testing included three different ways to record the behaviour of the specimens. The first method was maintaining a photographic record of the overall specimens' profiles during testing seen from a side view located where the actuator was positioned. The perspective of these images is as shown in Figure 3-8. Pictures were taken every 30 seconds to capture overall deformations along the whole specimen. The second location was a video recording from the top portion of the specimen. The view of the loading points and behaviour of the exterior seamed lips of the specimens were recorded throughout all testing stages as seen from the perspective shown in Figure 3-9. Finally, localized deformation, buckling or equipment-related events were photographed using movable individual cameras as testing proceeded or significant events occurred. The recordings and photographs were used to substantiate and assist in the analysis of the overall behaviour of the test specimens.

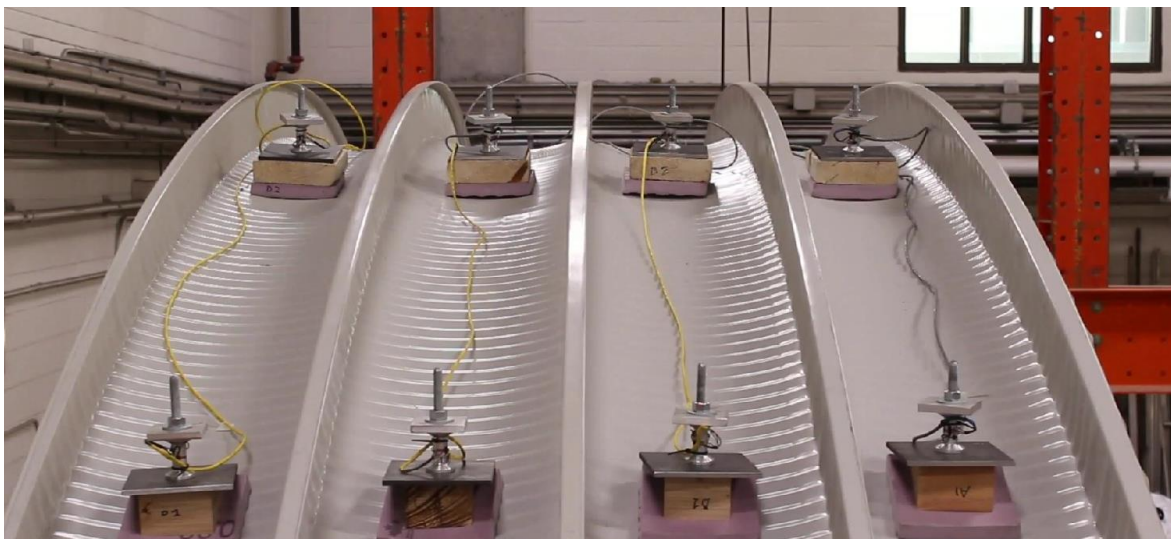


Figure 3-9: Video Recording View Top of Specimens

3.5 Limitations

K-Span structures can routinely be built with spans exceeding 15 m, but given the limitations of space in the laboratory, the K-Span specimens for this research were constructed as a set of four seamed ABM-120 panels with a semi-circular profile, a diameter of 7 m and steel thickness of 1.016 mm. The same dimensions were used for all four test specimens of this research. The height of the laboratory also did not allow for the loading downwards with an actuator, which required to have pulleys installed on the concrete deck to permit the actuator to pull the steel aircraft cables sideways. This change in the loading direction complicated efforts to balance loads in the cables.

Although the scale of these specimens were smaller than K-Spans seen in industrial areas, the construction, forming and assembly still required a similar construction effort and time as for larger structures. This only allowed for a limited number of experimental tests, as the time required for removing the specimens and building new ones at the testing location did not facilitate the concurrent construction or testing of multiple specimens.

3.6 Summary

The experimental program outlined in this chapter was designed to provide information regarding the behaviour of K-Span structures when subjected to a high level of loading exceeding the ultimate capacity of the specimens. The methodology and processes were used for the evaluation and testing of the four large-scale test specimens studied in this research project. The presence of multiple instrumentation and equipment used during the experimental program allowed the study of the unique and complex geometry of K-Span panels, using different support conditions and loading scenarios. All data collected and obtained from the experimental program was used to compare relative stiffness of the fixed and pinned based structures by considering the vertical and horizontal displacements as well as the ultimate capacities. The experimental results were also used to validate a simplified finite element model applying a reduced shell element thickness approach. The results of the experimental program as well as the comparison of these to the experimental results are in presented in the manuscript included as Chapter 4.

CHAPTER 4: MANUSCRIPT – FULL SCALE EXPERIMENTAL BEHAVIOUR OF THIN-WALLED AND DOUBLY CORRUGATED COLD-FORMED STEEL ARCHED STRUCTURE (K-SPAN) WITH VARYING BASE SUPPORT CONDITIONS

4.1 Abstract

K-Span buildings are low-cost rapidly-erected arch-type structures that have been growing in popularity all over the world in recent years. They allow for large open floor plans with their self-supporting panels. These structures are well-suited for industrial developments requiring large open storage areas and have the advantage that they can be built on-site with little requirement for heavy equipment. There have been instances of K-Span failures, precipitated by large snow loads, and therefore, a review of construction practices used in Canada was initiated, focusing primarily on base support conditions. This paper focuses on evaluating and observing the overall behavior and displacement of large-scale K-Spans with either fixed or hinged base support conditions when subjected to heavy loads.

Loads arranged to simulate snow-loading conditions were applied on 7 m diameter full-scale K-Span specimens in balanced and unbalanced loading patterns. The structural behaviour of specimens built using fixed base support conditions, which were embedded in concrete, and pinned base supports conditions, which used steel hinges, were compared when loaded up to and beyond their ultimate capacities. Regardless of the loading patterns, the behaviour of K-Span structures was influenced by the presence of double corrugations, seamed connections between panels and flexible panels which permitted large displacements under extreme loading conditions. The base support conditions significantly impacted the structural behaviours of K-Spans. The K-Span specimens demonstrated that they could resist 24% to 40% higher loads when built using fixed base supports, and exhibited more stiffness, deflecting 41% to 49% less than the equivalent pinned base support K-Spans. The use of hinges in pinned base supports therefore presents an additional risk in areas of Canada that typically expect large snow accumulations. The experimental results were used to validate a simplified finite element analysis which applied a reduced thickness approach to adequately represent the structural behaviour of the specimens.

4.2 Introduction

K-Spans are a type of thin-walled cold-formed steel structure formed through the use of an Automatic Bending Machine (ABM) to create self-supporting elements that form an arched structure. With the use of ABM machines, K-Spans are manufactured and erected on site, making them a very economical and efficient solution for rapid construction in both the industrial and military sectors [1]. These structures are created using a unique construction approach, as they do not require manufacturing in advance, neither are they assembled using nuts and bolts. K-Span sections are fully self-supporting, as the individually formed panels are seamed together to form an assembled arched structure. The unique geometrical characteristics of the transversal corrugation of K-Spans panels and overall structural shape influences the structure's behaviour under loading and has led to structural failures. Full-scale testing of K-Span specimens has been conducted to better understand these characteristic behaviours.

4.2.1 Background of K-Span Structures

K-Spans and the ABM construction machinery are designed by M.I.C. Industries. Two different sets of arched structures can be formed depending on the type of ABM machine used, either the ABM-120 (or MIC-120) or ABM-240 (or MIC-240). The 120 model has a rectangular shape, and the 240 has a trapezoidal shaped cross-section. The two-step process in which the panels are formed facilitates the forming and construction of K-Spans fully on-site. The flat steel coil is passed through the ABM's first set of rolls to form the panel lips and flanges, and each section is cut to the desired design length. This section is then bent into an arched shape through a second set of rolls, forming its transverse corrugation.

The panels are then seamed together at the lips in sets of 3 to 5 panels and lifted into position with the use of a crane to form and connect the structure. There is no defined limit to the length of a K-Span structure, but the individual panels may be formed with spans that range between a minimum of 3.7 m to a maximum of 24.0 m [2]. The bases of the K-Spans are typically fixed in concrete, as per the manufacturer's recommendations, but there have been several instances in Canada where K-Spans have been built using pin-connected supports with hinges, as presented in Figure 4-1. Since the distribution of moments for fixed and pinned arched structures is different, this has led to concerns in the reduction of loading capacity associated with the pin-supported K-Spans.



Figure 4-1: K-Span Structure (Photographed by G. Lépine [16])

4.2.2 Factors Influencing Structural Behaviours & Failures

Multiple occurrences of K-Span failures have been noted all over the world, including Czechia, Poland, China and Canada [3][4][5][6]. These failures are often associated with large accumulations of snow that cause large deflections. The behaviour and resistance of the structure is influenced by the thin-walled, doubly-corrugated, cold-formed steel panels forming the structure [3]. As studied by A. MacDonald [4], the different loading scenarios can create a change in behaviours. In particular, unbalanced snow conditions with pinned K-Spans may create significantly higher bending moments in the structure compared to those built using fixed support conditions.

There are no current design clauses in the governing North American Specification for the Design of Cold-formed Steel Structural Members [7], that account for strength or stiffness reductions in the panels that may be caused by transverse corrugations created in the panels through the forming of the panel

curvature. This may have led to simplified and inaccurate estimations of the capacity of these structures, which may have played a role in the past collapses of K-Spans.

Many studies have been conducted during recent years to investigate global and local instabilities [9][10] as well as the influence of panel geometry [11] on panel stability and collapse. Studies have shown, through small-scale experimental tests, that the local instability of the double corrugation lowers the overall capacity of the panels [11]. Although the maximum load for the straight panels before the corrugation can be estimated using European codes, the inclusion of the double corrugation imposes a significant difference between the predicted and experimental results. Walentynski et al. (2013) note that the curved panels undergo a “squashing” effect in the webs where corrugation is located, referred to as “accordion behavior” when buckling is observed [11]. Using ABM240 panels, an overall capacity decrease of 20% to 39% has been recorded between the straight panels versus the equivalent corrugated panels, as noted by Xu et al. [12], demonstrating that the inclusion of double corrugation affects the strength of the panels.

4.2.3 Large Scale Testing

Other studies have investigated K-Span structures on a larger scale [13][14]. However, due to difficult instrumentation control and maintenance in outdoor settings, and the space constraints in a laboratory setting, these large-scale studies are scarce.

Research conducted has been mainly focused on the modes of failure, such as distortional and lateral-torsional buckling for large-scale models. Although it is known through numerical modeling and engineering concepts that arch structures with hinge supports have less capacity than those that are fixed and encased in concrete [4], no large-scale testing for ABM120 panels has been conducted in a laboratory setting to compare the deformation behaviours between fixed and pin-connected panels.

The presence of corrugation requires a reduction in the effective area as described in Cybulski et al. [6], in order to reduce the resistance of the cross-section caused by the effects of local buckling. This method is also presented in a Chinese design manual [15] specifically related to panels which very closely resemble K-Span panels, where “equivalent” characteristics of the panel geometry are determined from coefficients based on the thickness and curvature of the structure.

Representative K-Span panel strength capacities have been determined by researchers by testing small strips of panels such as the research completed by G. Lépine [16]. This study evaluated and studied local deformations but also helped produce a failure envelope diagram by experimental testing and finite element modelling of panel sections under bending, axial and combined loadings. This envelope, with the corresponding full-scale evaluations, could lead to better understanding the effects of local instabilities on the overall structure and prediction of the ultimate strengths of K-Span structures.

4.2.4 Aim and Objectives

This research aims to assess the behavior and capacity of both fixed and pin-connected K-Spans through large-scale experimental testing, complimented by finite element numerical analysis. The analysis of the overall capacity of K-Spans built using pinned support conditions versus the fixed support conditions from the manufacturing specifications will determine if having K-Spans built using steel hinges should be a source of concern for areas within Canada expecting to receive large accumulations of snow. The specific objectives of this research are to:

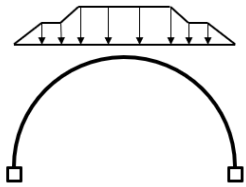
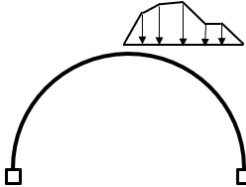
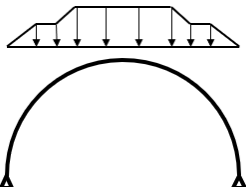
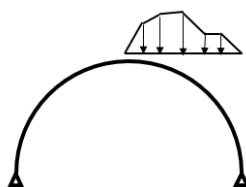
1. Compare vertical and horizontal load-deflection behaviours including ultimate capacities of full-scale 7 m diameter K-Span specimens with fixed and pinned base support conditions subjected to simulated balanced and unbalanced Canadian snow loading conditions.

2. Observe localized deformation patterns of large-scale specimens that impact structural resistance.
3. Utilize a reduction in effective thickness to simplify finite element numerical models to adequately replicate the load-deflection behaviour of the K-Span specimens and compare behaviour between pinned and fixed support conditions.

4.3 Experimental Program

This section contains a description of the specimens used, experimental program set-up and discussion of experimental results. An overview of the instrumentation plan is also provided to indicate key locations of interest. The large-scale experimental program consisted of four 7 m diameter ABM-120 arch specimens with a semi-circular profile. Each K-Span specimen, comprised of four seamed panels, which were loaded using two different loading conditions, representative of snow loading patterns, namely balanced and unbalanced. Two different types of base support conditions were used, namely fixed and pinned. The experimental program consisted of a total of four experimental test specimens which are presented in Table 4-1.

Table 4-1: Experimental Test Specimens

		Loading Pattern	
		Balanced	Unbalanced
End Support Condition	Fixed		
	Pinned		

4.3.1 Geometry Overview

The geometry of a single steel panel is presented in Figure 4-2. The steel panels had a thickness of 1.016 mm. The specimen panels were shaped by the ABM trailer to give it its unique corrugation pattern and remained maneuverable and flexible after the forming process. K-Span panels were assembled with the use of a crimper that pressed the top lips of the right side of the panel to the left side of the next, making it thicker at the seam. Once the panels were assembled, they were lifted into position with the use of a crane and connected to pinned or fixed base supports. Vertical and horizontal panels displacements were observed and recorded for the behavioral analysis.

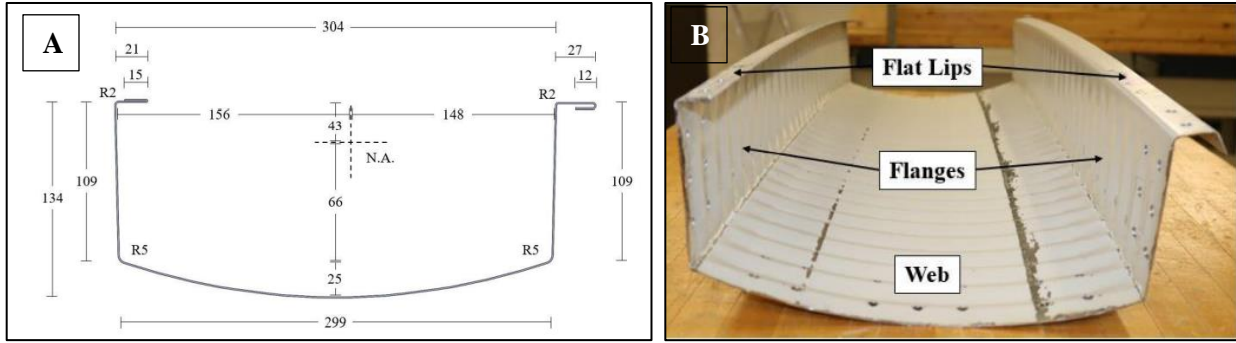


Figure 4-2: ABM120 Geometry (A) and Description (B) (Photographed by G. Lépine) [16]

4.3.2 Test Set-Up

The experimental test set-up comprised of a system of steel aircraft cables, pulleys and actuator that facilitated the overall loading of the specimens. It also included different types of base support conditions, a loading arrangement at the top of the specimen to apply two different loading patterns, and instrumentation along the span of the specimens. The two different types of support conditions, fixed and pinned, are presented in Figure 4-3 and Figure 4-4. The fixed-support specimens consisted of 7 m-span panels encased in reinforced concrete. For construction, the ends of the panels were inserted inside the concrete formwork, onto a steel angle which rested 150 mm from the bottom of the form. Following concrete placement, a 150 mm length of the K-Span was embedded into the concrete. The pinned support condition consisted of two steel angles connected by a 17.5 mm-diameter (11/16 inch) bar going through a 19 mm-diameter (3/4 inch) pipe welded to the angles and forming a hinge, of which one steel angle is embedded in concrete with the use of steel anchors. The panels were tightly bolted to the hinges on the concrete formwork with 2 bolts per panel. The specimens bolted to the pinned support had the ability to rotate. The 300 mm X 300 mm X 1372 mm concrete blocks forming the main component of the support were fixed to the reinforced concrete base slab to prevent lateral movement and rotation. The schematics of the support conditions are also represented in Figure 4-3 and Figure 4-4.

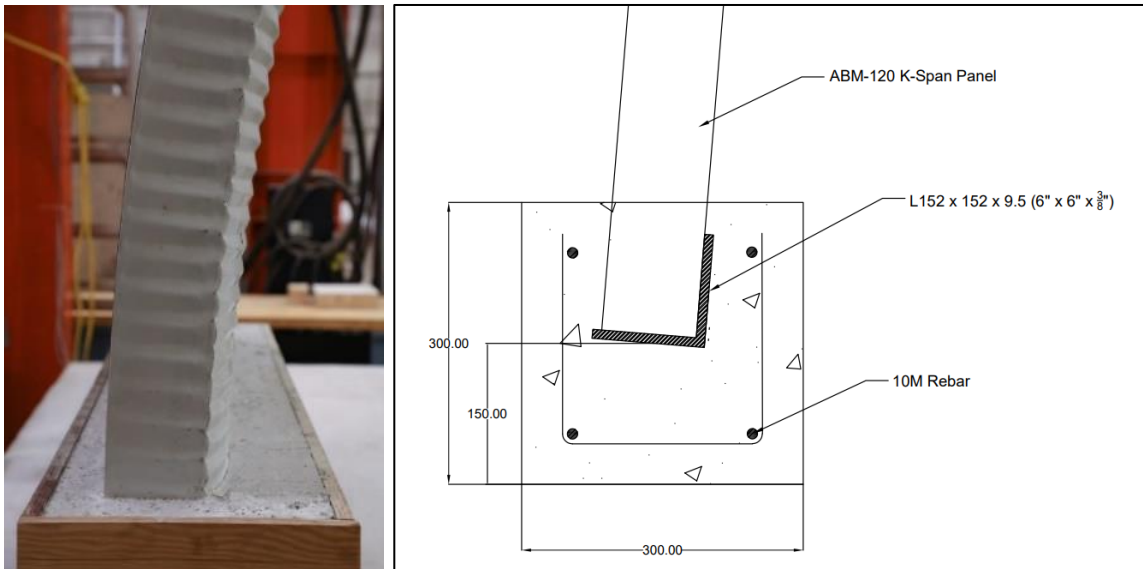


Figure 4-3: Fixed Support (Photographed by Louis Saulnier)

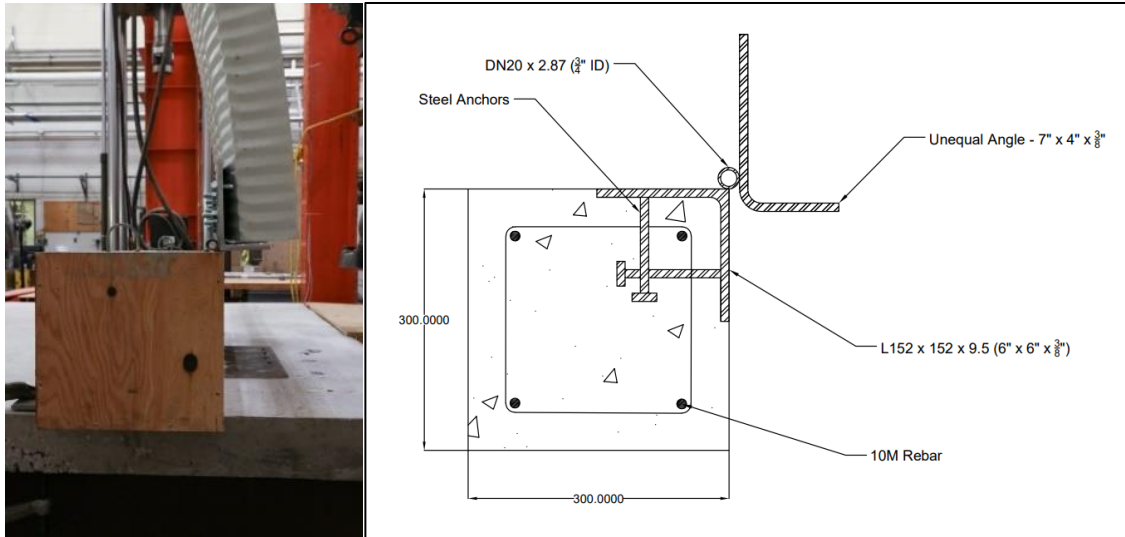


Figure 4-4: Pinned Support (Photographed by Louis Saulnier)

The specimens were loaded through the use of 27 kN (6100 pound-force) rated steel aircraft cable and pulleys attached to the concrete slab. A system of eyebolts and turnbuckles were used to add or remove tension in the steel aircraft cables to ensure distributed and equal loads at each point. The steel aircraft cables were connected to a displacement-controlled hydraulic actuator. The aircraft cables were attached to a steel plate, which permitted the actuator joint connection to freely rotate, and to evenly distribute load at the main loading point. At the top of the K-Span specimens, the steel aircraft cables were attached to a loading assembly composed of multiple elements to distribute the load evenly over the bottom web surface of the panel. This assembly included steel plates, load cells, and foam to reduce localized deformations around the surface of the loading points. The test specimens were loaded past ultimate load until instrumentation stroke would no longer provide relevant data.

The balanced loading pattern comprised of four rows of four loading points for a total of 16 loading points, whereas the unbalanced loading patterns used two rows of four loading points for a total of eight points. The loading points were positioned in a specific pattern to simulate various snow load conditions of uniformly distributed loads over the entire surface area as described in NBCC Clause 4.1.6.3 [8]. Figure 4-5 demonstrates the four rows of loading points that represent a balanced distributed loading pattern. The simulated snow loading pattern included the change in the accumulation factors caused by slippage of snow due to the slope increase near the base supports. Both loading patterns were considered critical loading conditions for arched structures as per the NBCC. The balanced and unbalanced loading patterns differ by the symmetrical accumulation of snow over the whole structure or the accumulation of snow covering only half of the structure accounting for snow drifting, as well as accounting for snow slipping off the surface of the roof when the degree of angle is larger than 30°. The different combinations of loading patterns and type of base supports applied for the four different K-Span specimens are shown in Table 4-1. All specimens were subjected to loads gradually applied up to and beyond their ultimate capacities to compare behaviours and deformations.

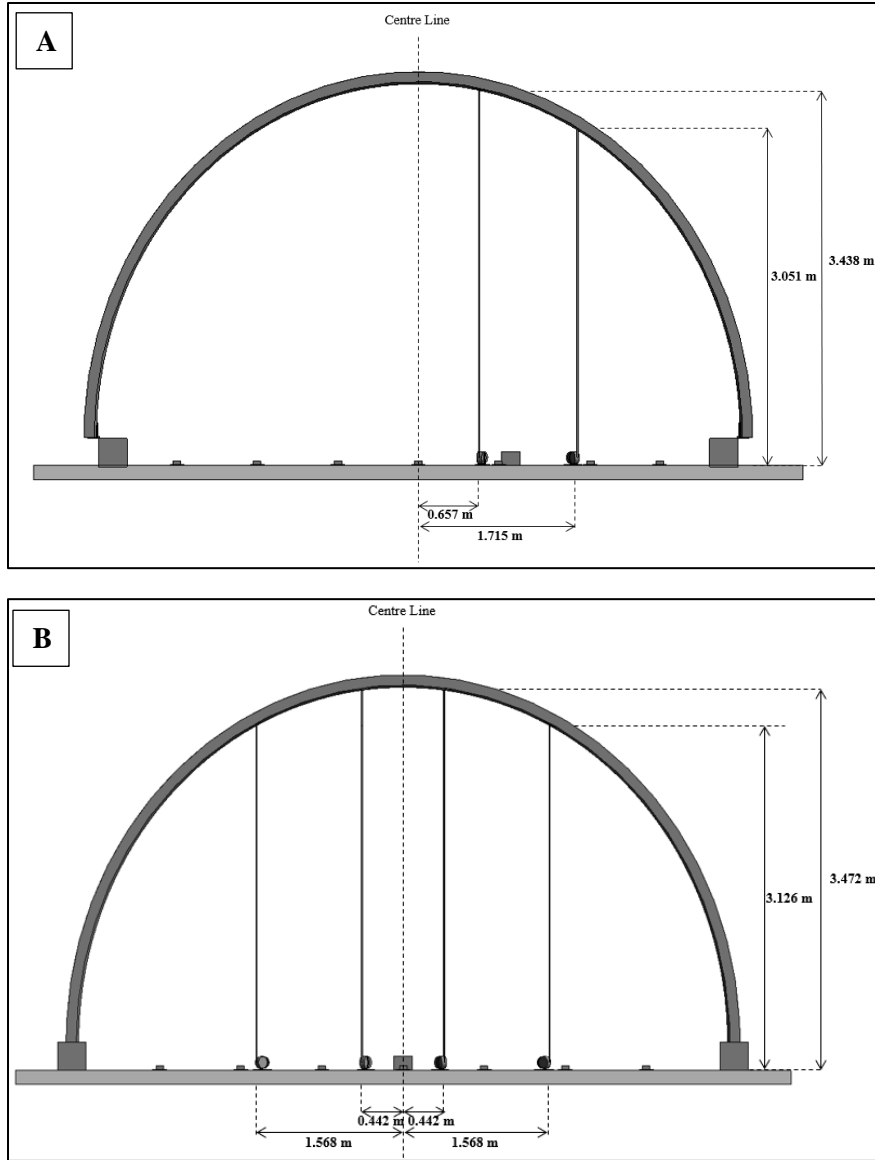


Figure 4-5: Pinned Support Condition Specimen with Unbalanced Loading Pattern (A) and Fixed Support Condition Specimen with Balanced Loading Pattern Schematic (B)

4.3.3 Instrumentation

In order to compare the behaviours between all test specimens, various types of instrumentation were used. A naming convention, found in Table 4-2, was assigned to all the different types of instrumentation, based on their location along the span and width of the structure. The letter identifier was used for the type of instrumentation and the direction of the measurement, and a number identifier was used for its location.

Table 4-2: Instrumentation Identifiers

Instrument Name	Code
Vertical Linear String Potentiometer	S

Horizontal Linear String Potentiometer	SH
Longitudinal Linear String Potentiometer	SL
Load Cell	LC
Linear Variable Differential Transformer	LVDT

A total of 17 load cells were part of the loading assembly to measure the load experienced on each loading point. All loads were applied by the actuator operating under displacement control. Linear string potentiometers were used to measure vertical, horizontal, and longitudinal displacements along the structure. A total of 14 potentiometers measured the middle two panels at every 0.875 m or 1/8th diameter spacing at the base of the structure, 4 other potentiometers measured the horizontal displacement, and finally, the last potentiometer measured the lateral displacements. Linear variable differential transformers (LVDT) were used on the hinges and concrete slab to monitor rotational deformations. Horizontal displacements were measured at the following four locations: at the 1/8th-diameter distance from each end-support for SB1H and SB7H, and at the 1/4th-diameter distance from the end-supports for SB2H and SB6H, aligning with the vertical string potentiometers of S1, S2, S6 and S7. The positions of the vertical and horizontal potentiometers are presented in Figure 4-6.

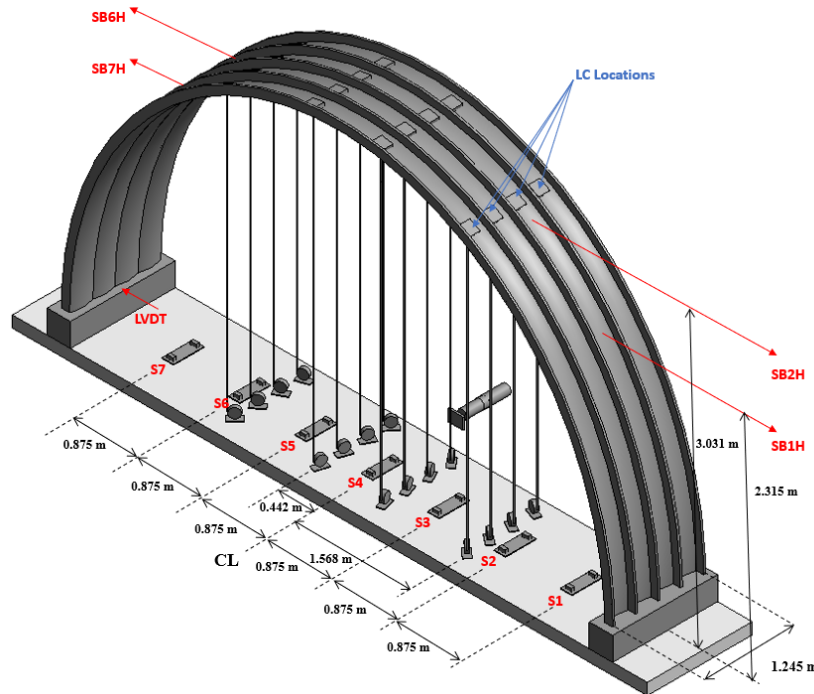


Figure 4-6: Linear String Potentiometer Instrumentation Positioning

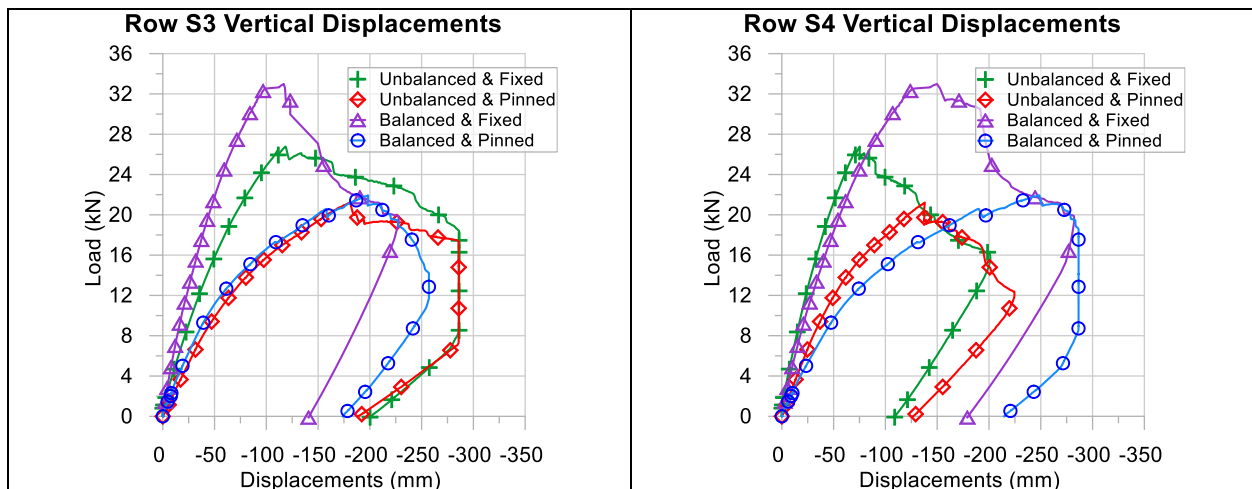
4.4 Experimental Results and Discussion

The experimental results were obtained for all four specimens by loading the structures beyond their maximum capacity. The vertical and horizontal displacements, as well as the buckling and deformation observations were recorded and the results for all test specimens were compared. The permanent and post-buckling deformations demonstrated a structure capable of resisting high loads but flexible throughout the

loading process. Results for vertical and horizontal displacements as well as displacement profiles are graphically presented in Figures 4-7, 4-8 and 4-9. The load-deflection graphs for each specimen demonstrate different behaviour patterns and resistance capacity throughout the full range of loading. Although each specimen did experience large deflections before any buckling behaviour was observed or failure occurred, each specimen demonstrated a clear difference in their maximum loading capacity, their panels' stiffness and the structure's residual strength after failure. Specifically for the balanced loading pattern and fixed support condition, the specimen was loaded and unloaded in three stages still within its elastic region, resulting in a single displacement curve of accumulated displacement results, excluding the unloading results in each stage.

Figure 4-7 presents the vertical displacements for rows S3, S4, S5, and S6 of each specimen where the largest displacements were observed. On the X-axis, negative displacements represent downward deflections, and positive displacements, upwards deflections. On the Y-axis, the load represents the cumulative load of all loading points on the specimen as measured by the load cell on the hydraulic actuator. The markers on the graph are used to differentiate each test specimen and are not related to the rate of data acquisition. During the loading of the specimens, the observed displacements were generally larger in the vertical direction than the horizontal displacements. The fixed base support specimens, in balanced and unbalanced loading patterns respectively, showed a 40% and 24% larger load capacity compared to their equivalent pinned base support loading pattern specimens. The specimen which had the largest load capacity was the fixed support - balanced loading pattern, with a total ultimate load of 33.0 kN distributed over the whole surface. This specimen demonstrated a uniform downward deflection across all loading rows.

Both fixed support specimens exhibited significantly higher stiffness than the pinned base support specimens. Although the fixed base support specimens for each loading pattern recorded maximum vertical displacements at the centre of the structure of 150 mm and 119 mm at the ultimate load for the balanced and unbalanced loading patterns respectively, the deflections were 49% and 41% lower when compared to the pinned base support specimens equivalent loading patterns. As the load increased, larger stiffness of the panels was observed for both fixed support loading patterns on the load-displacement graphs, as displacements increased steadily for all instrumented rows. Once ultimate load was reached, the fixed base support balanced loading pattern specimen's material demonstrated little resistance before losing the majority of its strength.



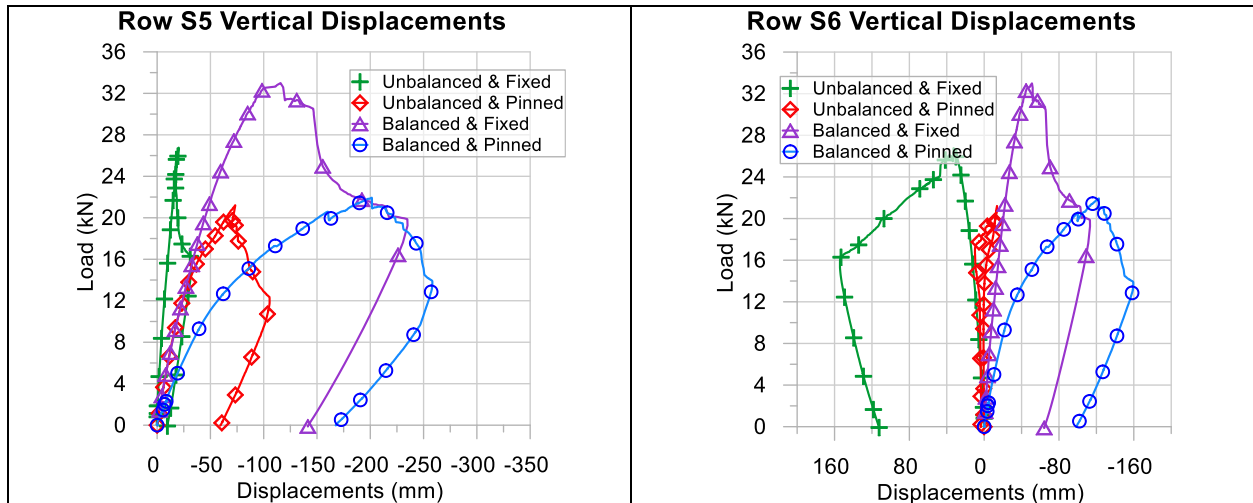


Figure 4-7: Vertical Displacements at SP locations S3, S4, S5, and S6

The fixed base support unbalanced loading pattern specimen demonstrated a higher residual strength after ultimate load where large deformations were generally observed with less significant drop in capacity. Since the loading pattern was unbalanced, the largest displacements occurred near the applied loading, at row S3. As presented in Figure 4-8 for a loading of 21 kN, for the unbalanced pattern specimen, as the loading side experienced large downward vertical displacements, the other half of the specimen underwent upwards movement as the panels “bulged” outwards. As a result, row S6 in Figure 4-7 had positive displacements, and row S5 experienced minimal displacements. As the specimen was only loaded on one side, the specimen experienced greater vertical displacements compared to the fixed base support balanced loading pattern specimen.

Figure 4-8 demonstrates an exaggerated 2D comparison of all 4 tests. Each circle in this graph represents a point in which displacement measurements were taken and includes the combination of all seven vertical measuring points as well as the four horizontal measuring points. The trendlines between the measured points approximate the deformation, based on the measured values. The deformation in the figure has been magnified three times to demonstrate the difference more clearly between each test.

Both pinned base support specimens underwent much larger vertical deformations at their ultimate loads than the fixed base support cases, reaching displacements of 249 mm and 181 mm for the balanced and unbalanced loading pattern specimens respectively. The pinned base support specimens demonstrated much less stiffness during the loading process than the fixed base support specimens. The use of pinned supports also greatly reduced the maximum load capacity of the K-Span panels, reaching only 21.9 kN for the balanced loading pattern specimen and 21.0 kN for the unbalanced loading pattern specimen.

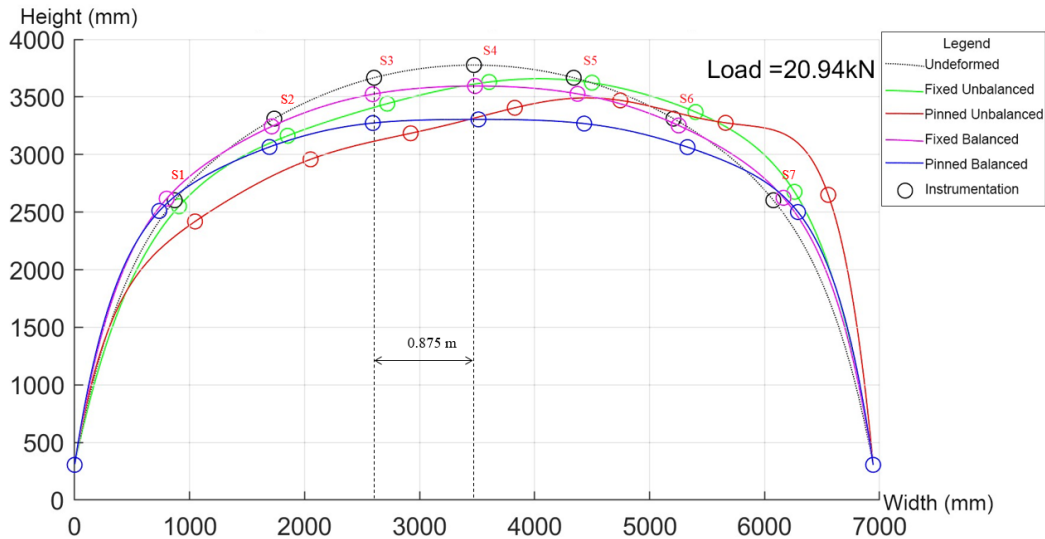


Figure 4-8: K-Span 3 Times Magnified Shape After Loading for Each Loading Pattern Specimen

The pinned base support balanced loading pattern specimen experienced constant and symmetrical downwards deflections across all rows. Once the ultimate load was reached, this specimen demonstrated very little residual strength, and quickly lost load capacity. This specimen also experienced the largest vertical displacement across all specimens. During the loading process, there were instances where the load suddenly reduced before increasing again, caused by localized buckling at the lips and along the seamed connection of the panels near the top centre of the specimen. As presented in Figure 4-7 for the pinned base support balanced loading pattern specimen, each drop in load, specifically at 17.3 kN, 20.6 kN and 21.9 kN, prior to reaching the ultimate load, can be associated with localized buckling of the lips. Although the specimen had not reached its maximum capacity, the localized buckling of the lips created instabilities in the loading pattern, which likely precipitated redistribution of the load between the panels and notable differences in load levels (of up to 90%) between rows.

The pinned base support unbalanced loading pattern specimen also demonstrated large vertical displacements. Similar to its equivalent fixed support specimen, this specimen also recorded its largest displacements in row S3, in which the linear string potentiometer reached its stroke limits. Since this specimen had such large vertical displacements on half of its surface, row S6 recorded minor vertical displacements, being on the opposite side of row S3. The pinned base support unbalanced loading pattern specimen that represented severe snow-loading conditions proved to be the worst-case scenario under loading with regards to vertical displacements and ultimate capacity. The unbalanced loading pattern specimens, whether their base supports are pinned or fixed, had lower overall capacities compared to the balanced loading pattern specimens, however the post-ultimate structural performance was notably different in that large displacements were observed at the heaviest load location with more gradual capacity loss than fixed specimens. After ultimate load, the softening slope of the unbalanced specimen was less steep than the balanced conditions which may allow for better load sharing and redistribution along a K-Span length if there are inconsistencies in snow loading along the length of a structure.

Each specimen also experienced horizontal displacements, as presented in the load-displacement graphs in Figure 4-9. Positive displacements represent outward deformations, whereas negative displacements represent inwards deformations. The differences in the specimens' structural displacements are more pronounced for horizontal displacements compared to vertical displacements. Likely due to uneven loading present within the specimens, the horizontal displacements are not as symmetric as the

vertical displacements for the balanced loading pattern specimens. The presence of small imperfections likely led to premature instabilities causing the specimen to lean in one direction.

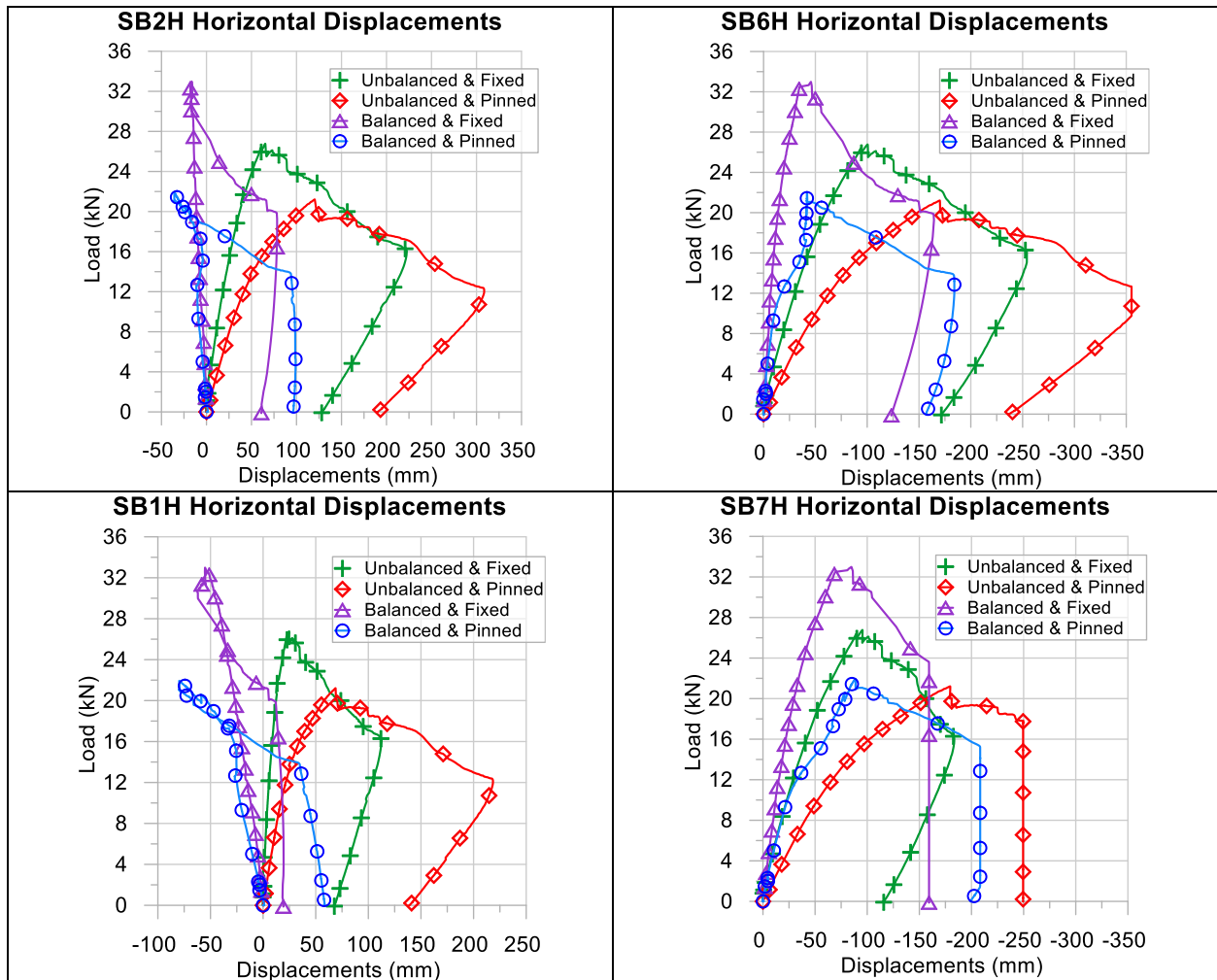


Figure 4-9: Horizontal Displacements

Both fixed support specimens demonstrated significantly lower displacements compared to the vertical displacements before ultimate capacity was reached. Both balanced and unbalanced loading pattern fixed support specimens displaced horizontally by 85 mm and 100 mm at the ultimate load capacity. The difference in horizontal displacements was much greater for the unbalanced loading pattern where the equivalent pinned support specimens had 43% higher displacements compared to the fixed support specimen, whereas the difference between the balanced loading patterns was only 8%. For the fixed support specimens, the load-displacement curves had linear displacements and constant loading for each row prior to reaching their maximum capacity.

Once ultimate load was reached, the fixed base support balanced loading pattern specimen demonstrated very little residual strength and started to deform in one direction, as noted in the graphs for SB1H and SB2H, where a sudden change of direction in displacement occurred after the specimen started to lose load capacity. The fixed base support balanced loading pattern specimen deformed more vertically than horizontally, and is the test specimen that experienced the least horizontal displacements.

Figure 4-9 demonstrates that the fixed base support unbalanced loading pattern specimen experienced significant deformations after ultimate load was reached. The majority of the deformations occurred near the 1/8th to 1/4th diameter distance from the base supports. The horizontal displacements on each side of the specimen remained constant and displaced in a similar pattern. The SB1H and SB2H only had 117% and 42% difference between their opposite side SB7H and SB6H linear string potentiometer measurements.

The pinned base support balanced loading pattern specimen experienced the most unstable horizontal displacements. On one side of the specimen, SB6H and SB7H, the panels were very stiff experienced little horizontal displacement until the total loading reached 12.0 kN, where a sudden change of rate for horizontal displacement increase occurred. The specimen started to displace more until it reached a total loading of 16.0 kN where the specimen became stiff again, until reaching the ultimate load of the specimen. The opposite effect occurred on the other side of the specimen, at SB1H and SB2H, where at the same 12.0 kN range of loading, the specimen became suddenly very stiff, then at 16.0 kN, started to displace again. Prior to reaching ultimate load, each side of the specimen displaced in opposite directions, and panels bulged outwards as presented in Figure 4-8, following the same trend as the fixed base support balanced loading pattern specimen.

The fixed base support balanced loading pattern specimen showed a more balanced and similar load-displacement curve when comparing each side of the specimens than its equivalent pinned support. The difference in horizontal displacements prior to reaching ultimate load is not as severe when compared to the vertical displacements. The highest horizontal displacement experienced by the fixed base support balanced loading pattern specimen was only 85 mm at ultimate load, which happened at SB7H. Contrary to the vertical displacements after reaching ultimate load, the pinned base support balanced loading pattern specimen demonstrated very different behaviour in terms of horizontal deflections. As soon as localized buckling occurred in the specimen, the panel displacements on the SB1H and SB2H side suddenly changed direction, where the whole specimen moved horizontally towards the opposite side. The majority of displacements occurred once the specimen lost capacity, where displacements over 210 mm were recorded at the SB7H location before the linear string potentiometer could no longer measure stroke.

The pinned base support unbalanced loading pattern specimen had the greatest horizontal deflections. This specimen moved in one direction due to its unbalanced loading pattern and demonstrated larger horizontal displacements on the side on which the loading was not present. The opposite effect was observed in Figure 4-7, where the majority of the vertical displacements occurred near the loading points. As the specimen moved sideways, the structure experienced the largest displacements before reaching ultimate load. The pinned base support unbalanced loading pattern specimen reached displacements of 120 mm on the loading side (SB2H) and 170 mm for the unloaded side (SB6H), for a difference of 34%. The load-displacement curves for each side show a similar displacement pattern between SB1H and SB2H, as well as between SB6H and SB7H.

After reaching ultimate load, the pinned base support unbalanced loading pattern specimen retained substantial residual capacity, retaining the majority of its load-bearing capacity while deforming horizontally after ultimate load. Although, a significant reduction in capacity happened once ultimate load was reached, the specimen continued to carry load while large displacements were observed, reaching displacements up to 350 mm for the SB6H horizontal linear string potentiometer measurement.

Throughout testing, the loading points were positioned to simulate the NBCC's specified snow load on roof. The intent was to induce constant and equilibrated values for each loading row and point going across the specimen. Some variation in load was noted in the loading cells along both the width and the

length of specimens. For three of the specimens, this variation between the averages of load across the widths of the specimens had a maximum percentage difference of 20%. For the pinned balanced loading condition, the largest difference was noted near the ultimate load of the specimen between the heaviest loading in the centre of the structure and the outside loading with an average percentage difference of 82%, reaching a maximum of 90% difference at load levels approaching ultimate load. Although this may have resulted in a low-capacity estimate of this particular specimen, it is reflective of the high central loading and lower outer sloped surface loadings that are likely to occur in the balanced snow conditions that may exist in field conditions. As some of the panels started to experience localized buckling and large deformations, re-distribution of load would occur wherein some panels within the specimen would take on load, and others would lose strength, leading to sideways movement in the specimen, as presented in Figure 4-8. The ductility of the material and deformability of the panels contributed to the specimens experiencing not only larger vertical and horizontal displacements in certain areas, but also load re-distribution and lateral movement during the loading process of the experimental program.

Four different common plastic deformations and localized buckling patterns were noted throughout the experimental program. Figure 4-10 presents the deformations around the base supports for both the fixed (A) and pinned (D) support conditions, the localized buckling of the lips (C) and the crimping of the bottom webs (B) of the panels. The first deformations noted for each specimen occurred near the base supports. For the pinned support specimens, the deformations were caused by the rotation of the steel hinges. As the L-shaped steel member rotated outward, the panels that were bolted to the steel hinge folded above the steel member. This plastic deformation increased the magnitudes of the vertical displacements for both pinned support specimens. No slipping effect from the seam connections between panels were observed. The crimping of the seam connections proved to be an effective joining method and appeared to be an issue of no concern for these specimens.

The fixed support specimens experienced a different type of localized buckling near the base supports, or Zone 1 seen in Figure 4-11. For semi-circular structures such as K-Spans, in which the arch is fixed in concrete, large positive bending moments are likely to occur near the base supports, which causes higher stresses and localized buckling at the lips on the outside of the specimens, where the panels are crimped together. The lips continued to deform throughout the loading process likely maintaining moment resistance of the section contributing to both the stiffness and ultimate strength of the structure.

One common permanent deformation noted in all the specimens occurred on the bottom web portion of the panels, at 1/8 to 1/4 length of the diameter distance from the base supports, in Zone 2 seen in Figure 4-11. This “accordion crimping effect”, as described by Walentynski et al. [11], started to form as the load approached the ultimate capacity of the specimens. The deformations occurred where the transverse corrugation meets the corners of the webs of the panels, as the corrugation undergoes a squeezing effect, presented in Figure 4-10 (B). The negative bending moments caused by the loading of the specimens generated the accordion crimping deformation. As the load increased, the crimping deformations worsened. The presence of these deformations should be used as a warning sign that the ultimate load is approaching. Upon reaching the ultimate load, this accordion behaviour worsened and created a hinge in the panels, precipitating more pronounced horizontal displacements. The location of the hinge in the panel would then dictate the direction in which the specimens would move horizontally.

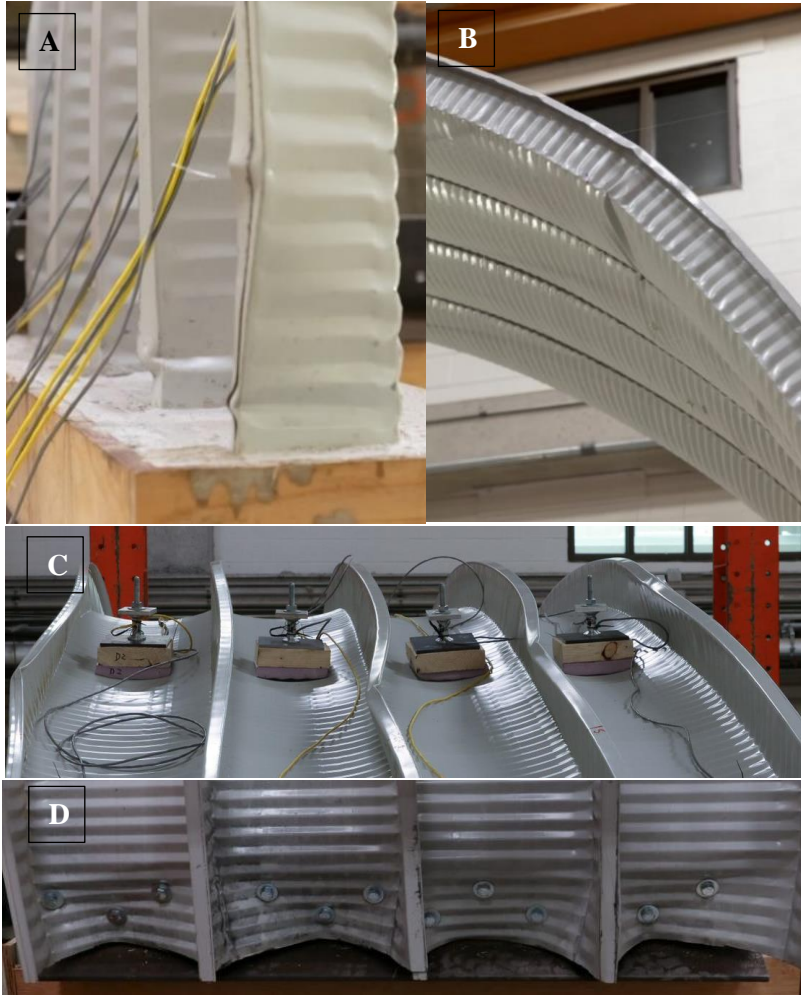


Figure 4-10: Localized Buckling and Plastic Deformations of Specimens (Photographs taken by Louis Saulnier)

The final-forming local deformation observed, common to all specimens, was the buckling of the crimped lips and occurred on the top portion of the panels, between the $1/2$ to $1/3$ diameter distance from the base supports, as presented by Zone 3 in Figure 4-10. This localized buckling pattern, caused by positive bending moments, presented in Figure 4-10 (C), led to the overall loss of capacity in all specimens. As soon as a seam connection buckled, loss of capacity would ensue. The loss of capacity due to localized buckling was prevalent in the pinned base support balanced loading pattern specimen. As the loading and the positive bending moments increased, the lips and flanges of the panels would deform and separate. As the separation between flanges increased, localized buckling would then occur. Imminent structural failure should be a concern as soon as these buckling patterns are noticed on K-Spans, as the combination of the lips buckling and the crimping of the webs leads to sudden loss of capacity and more pronounced displacements.

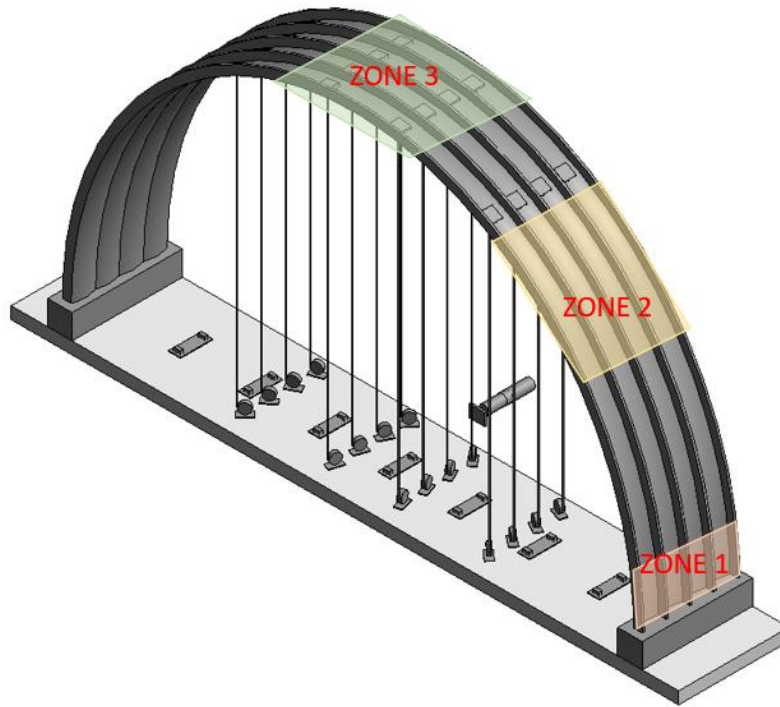


Figure 4-11: Localized buckling Zones Along Specimens

Overall, the fixed support specimens demonstrated higher capacities of 24% for the unbalanced and 40% for the balanced loading patterns and lower deformations at ultimate of 41% for the unbalanced to 49% for the balanced loading patterns when compared to the pinned support specimens. Encasing the base of the K-Span panels in concrete increases the structure’s stiffness. The balanced loading pattern specimen quickly lost load bearing capacity and did not demonstrate similar post-ultimate capacity when compared to its unbalanced loading pattern specimen, where loading was less severe. The post-ultimate capacity may be significant, on occasion, because it may facilitate load redistribution in multi-panel structures subjected to “real” snow events. However, the unbalanced loading pattern created instabilities in the specimen and led to large horizontal displacements and lower ultimate capacities, generally making it the worst-case snow fall scenario for K-Span structures, that may be subject to drifting effects.

The pinned support specimens led to larger displacements and less load capacity. Both pinned support specimens followed a similar behaviour to their equivalent fixed support specimens. The large displacement that occurred in the pinned specimens worsened the localized buckling present in the panels, which led to failure.

4.5 Numerical Modelling Program

4.5.1 Model Description

The numerical model was constructed using the finite element software ANSYS to analyze and replicate the full-scale testing of the K-Span model of a representative seamed assembly of 4 panels, without end-walls. The modelled arch structure had a diameter of 7 m, as did the experimental specimens. Similar to the experimental work, the numerical model was analyzed using the same balanced and unbalanced loading patterns to determine and compare the overall deflections in the vertical and horizontal directions (X and Y axes). The value of loads recorded during the experimental program for each loading point were

used for the loading of the numerical models. The numerical models were evaluated using large deflections and used shell elements for the panels. The top of the lip of one panel and the bottom of the lip of the next panel were bonded together to simulate the seamed connection in the experimental specimens.

Linear properties were used, as plasticity was not necessary to achieve the comparison in displacements between two different support conditions at levels below the ultimate capacity. The difference in stiffness and overall behaviour could be observed and compared at lower load levels avoiding the inclusion of plasticity. The prediction of ultimate loads of the numerical models and buckling patterns would require a more detailed modelling to include plasticity and corrugation of the panels.

4.5.2 Material Properties

Galvanized steel was the material used for the construction of the K-Span numerical models and was assigned linear-elastic material properties as shown in Table 4-3.

Table 4-3: Material Properties

K-Span Steel Panels	
Elasticity Modulus	200 000 MPa
Poisson Ratio	0.3

4.5.3 Model Geometry

The geometry of the numerical model was based off the dimensions of the experimental specimens as well as the dimensions found in research papers by A. MacDonald [4], Cybulski et al. [6] and G. Lépine [16]. Dimensions were also confirmed through laboratory measurements. For the purpose of this research, the geometry of the numerical model was simplified to exclude the double corrugation created by the forming process. The simplification of the geometry facilitated a focus on the overall behaviour of the structure and circumvented the preparation of models that were excessively large or with unnecessarily complex geometries. This reduced the number of nodes and elements required to analyse the numerical model. Because the numerical model is simplified, the impact and effects from the double corrugation are not fully represented throughout the numerical solution. Unless accounted for, as described by the thickness modification below, this simplification is likely to result in a model with significantly higher stiffness than the actual K-Span panels. Furthermore, the simplified model will exhibit stronger capacity than the actual specimens.

The numerical model had a diameter of 7 m, and the set of 4 panels were 1.245 m wide. The structure formed a perfect semicircle, and the shell elements were assigned a thickness of 0.7 mm versus the 1.016 mm of the experimental program. This difference in thickness accounted for the reduction in the effective area and purposely increased the flexibility of the panels to compensate for the exclusion of the double corrugation in the numerical model. This approach was adopted from recommendations for the reduction in effective area used in the Technical Specification for Arched Corrugated Steel Roof Standard Trial (CECS 167: 2004) [15]. Since the seamed connection is only represented in the numerical model by two shell layers and did not include the four layers of folded steel material found in the experimental program as presented in Figure 4-12, a thickness of 1.4 mm was assigned for the thickness of each flat lip.

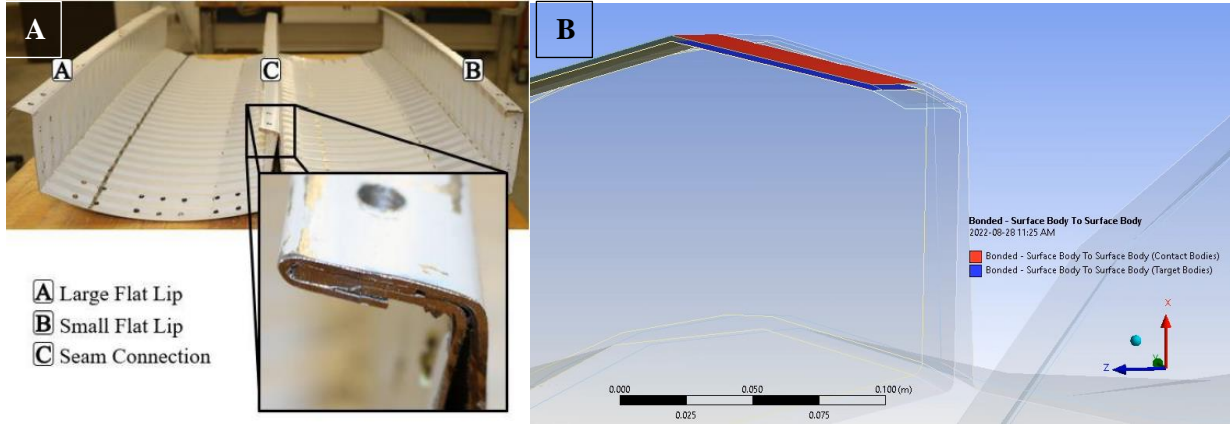


Figure 4-12: Crimping of Lips [16] (A) (Photographed by G. Lépine) and Numerical Representation (B)

The pinned base support numerical models included the addition of a steel rod to simulate the experimental hinge assembly. The numerical circular rod was defined to be the same size as the bar that connected both steel angles to the concrete supports and K-Span specimens. The steel angles of the hinge assembly were excluded from the numerical model for simplification, as was accounted for by the boundary and contact conditions.

The full arch geometry of the numerical model was split into 11 sections for the balanced loading pattern specimens, and 7 sections for the unbalanced loading pattern specimens, as represented in Figure 4-13 and Figure 4-14. The geometry was split across all panels in order to assign boundary conditions for the base supports and to assign loading conditions along the length of the model, replicating the loading of the experimental specimens.

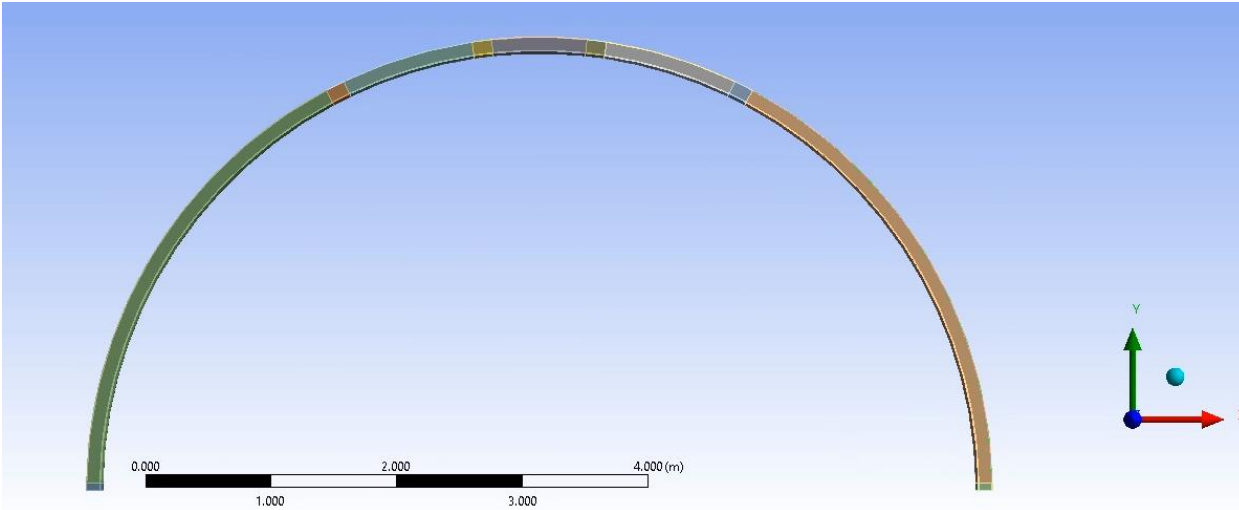


Figure 4-13: Numerical Model Geometry Split Diagram for Balanced Loading Pattern

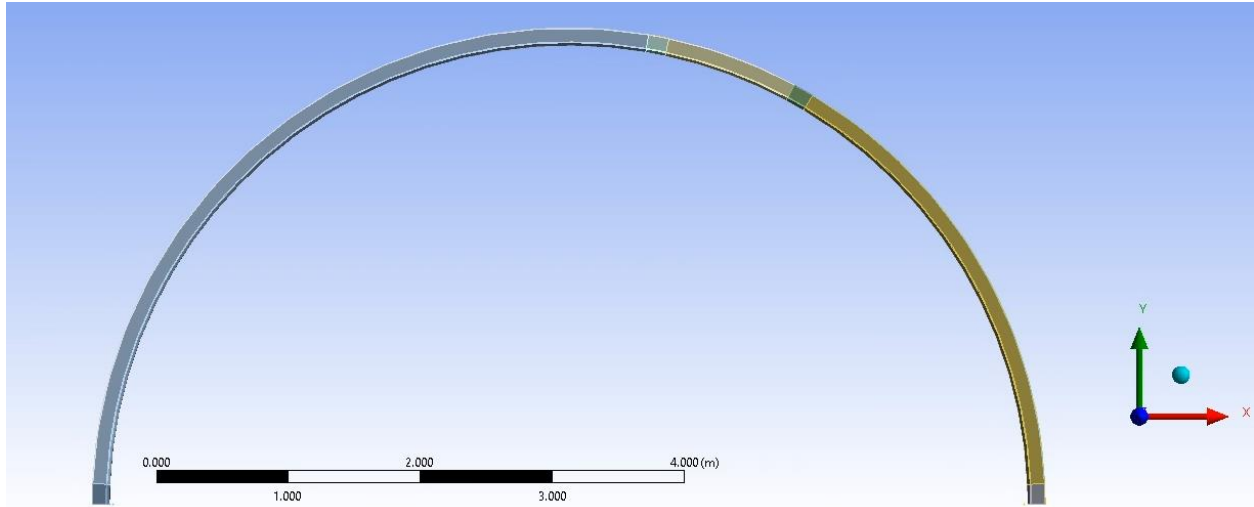


Figure 4-14: Numerical Model Geometry Split Diagram for Unbalanced Loading Pattern

4.5.4 Boundary and Loading Conditions

Boundary conditions were included in the numerical model to simulate both types of base supports studied in the experimental program. No end-walls or lateral supports were included in the numerical models. The first boundary condition assigned to the model was the fixed base support, where the ends of the specimens were encased in concrete in the experimental program. Since the geometry was split into multiple sections, the ends of the K-Span were assigned a fixed boundary condition where the end of the panels were prevented from rotating, and given a zero displacement in the X, Y, and Z directions. The second boundary condition assigned to the model was the pinned base support, where the bottom surface of the panels was bolted onto steel hinges in the experiment. In order to simulate the rotational effects of hinges in the numerical model, the steel bar was assigned a fixed boundary condition and the bottom surface of the panels, which needed to rotate, were assigned a revolute joint, to be able to rotate around the surface of the steel bar. This allowed the panels to move in the same direction as the experimental specimens, rotating around the Z axis as presented in Figure 4-15.

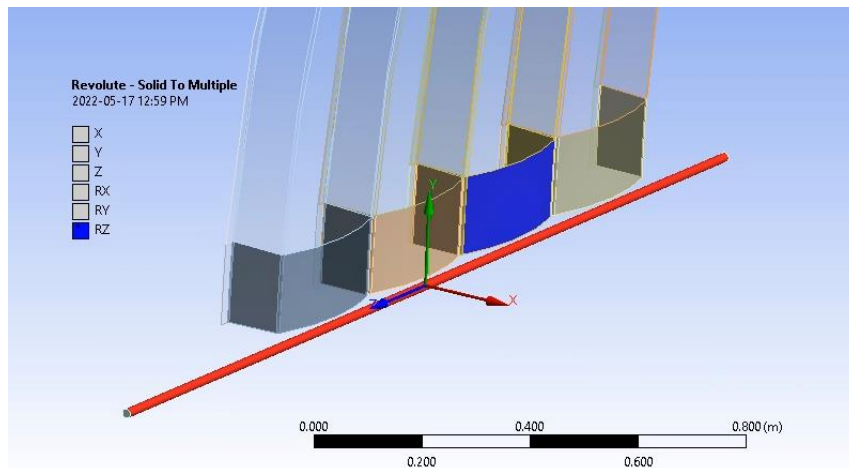


Figure 4-15: Hinge Numerical Representation

To simulate the experimental seamed connection between panels, a small gap between the flat lips was designed during the creation of the geometry, and a bonded contact between the bottom and top surface of the flat lips were assigned, as presented in Figure 4-12 (B). The simplification of the bonded contact and different thickness assignment of the material along the circumference of the lips accurately replicated the seamed connection, as there was no slipping between the panels observed during the experimental program, making the bonded contact an acceptable representation. If further analysis of the seamed connection was required, a complete modelling of the folded steel material with further definitions and more refined meshing techniques to perfectly represent the seamed connection would be necessary.

The numerical panels were also loaded vertically like the experimental specimens, both in a balanced and unbalanced loading pattern. Since the experimental load measured for each row was unequal during the loading process of the experimental work, as shown in Appendix A, Figure A-17, A-18, A-19, and A-20, the numerical model loading rows were progressively assigned load steps consistent with the recorded loads from the experimental results, until the yielding of the material was reached (stresses above 360 MPa were observed). Load increments applied to the models were 4 kN for the fixed support models and 2 to 3 kN for the pinned support models.

4.5.5 Analysis Solution Method

The application of the numerical model consisted of a static structural analysis of shell elements utilizing the full Newton-Raphson non-linear solution procedure. The model was composed of 2D-higher-order quadratic shell elements of 8 nodes, for a total element count of 24120 and total nodal count of 70624. The same mesh and element sizing was used throughout the shell bodies of the numerical model. As the model was used to analyse the global deformations and observe the reactions of the panels overall, no mesh refinement was given in the fillet areas or corners of the panels because of the large scale of the model. A convergence study on mesh and element sizing refinement was conducted to ensure accuracy of the displacement values for areas of interest. Convergence of displacement results was achieved, with negligible variations between iterations ($\approx 1\%$), and as such, a surface meshing size of 40 mm was assigned to the shell elements of the numerical model, as shown in Figure 4-16.

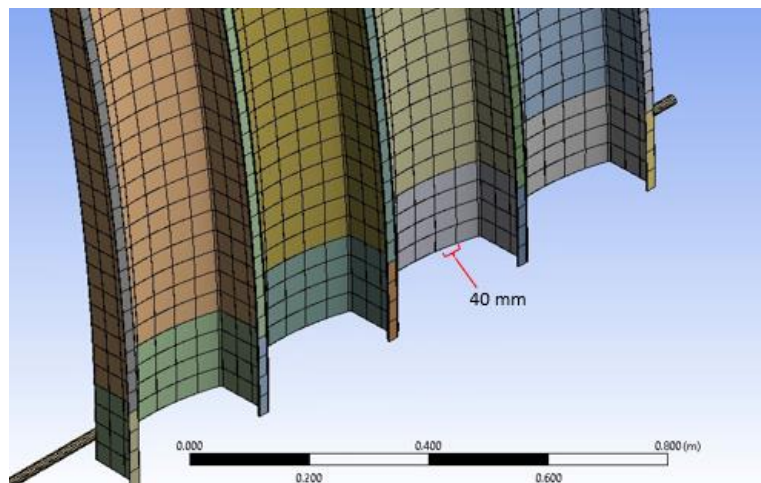
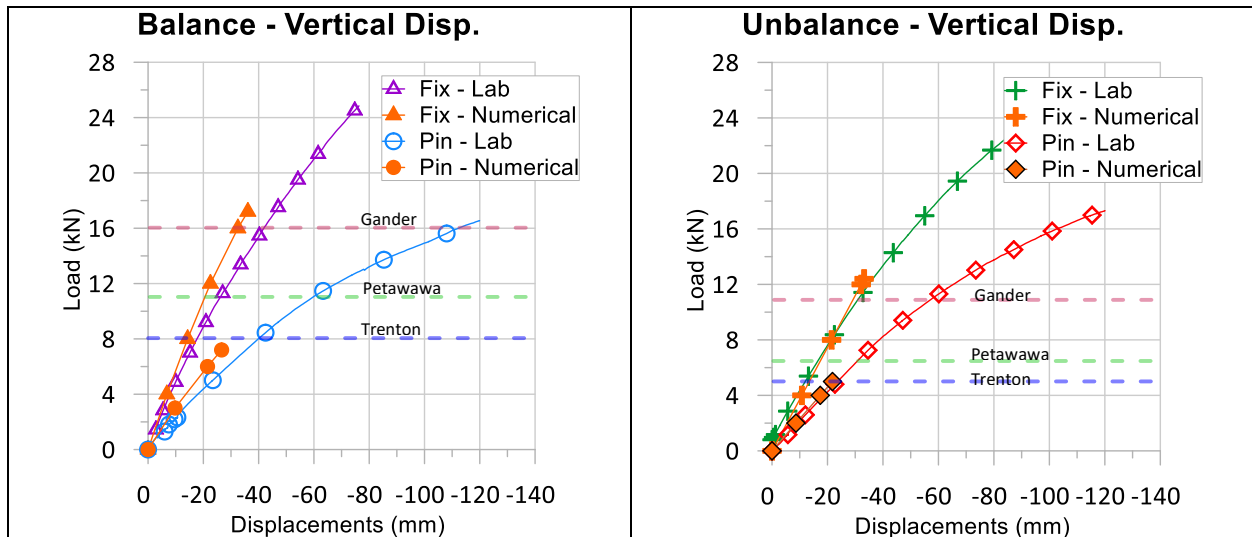


Figure 4-16: Meshing Sizing for K-Span Panels

4.6 Numerical Model Results and Discussion

The numerical results obtained for each test specimen demonstrated the success of the numerical model in analysing the structure's initial overall displacement behaviour. Vertical and horizontal displacements, as well as overall structural behaviour, were compared to experimental results. Although the numerical model was not able to reach the same ultimate loads as the experimental specimens, the displacements recorded, and areas of localized deformations were comparable to the experimental findings. Figure 4-17 provides a comparison of both the vertical and horizontal displacements for all numerical and experimental specimens. Vertical displacement results for the experimental and numerical balanced pattern are taken from Zone A, represented in Figure 4-11, and the vertical displacements for the unbalanced patterns and all horizontal displacements are taken from Zone B.

Three lines were added to the graphs in Figure 4-17 to represent, in kN, the NBCC's calculated 1-in-50 year ground snowfall design loads for a 7 m-diameter K-Span. The unfactored design loads from the NBCC were converted from a surface load of kPa units to a cumulative load of the whole specimen surface in kN to match experimental testing results. The red, green and blue lines were added to represent, respectively, the worst-case snow accumulation for Gander (NL), Petawawa (ON) and Trenton (ON). These three cities expect different amounts of ground snow loads per year, as the NBCC values for 1-in-50-year ground snow load are 1.6 kPa for Trenton, 2.6 kPa for Petawawa, and 3.7 kPa for Gander. These three cities host a CAF base, one of which, Petawawa, had a K-Span failure occur in 2019. The load-displacement curve only represents the initial portion of the experimental displacements recorded until yielding of the material is achieved.



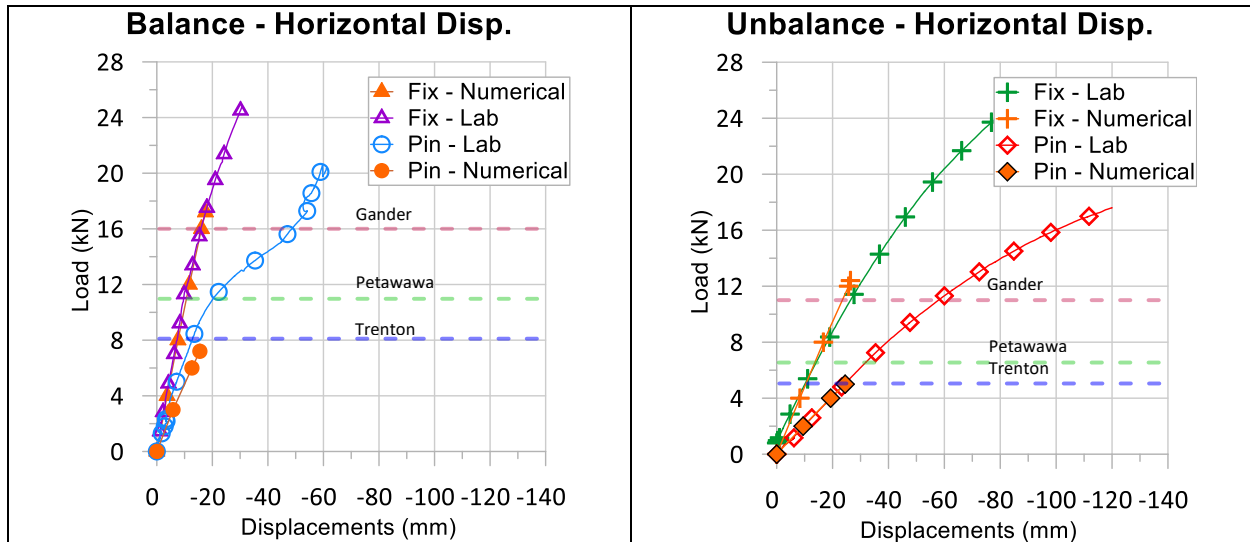


Figure 4-17: Numerical and Experimental Displacement Results Comparison

As shown in Figure 4-17, all experimental results for the fixed support specimen surpassed the NBCC’s ultimate load limits for both balanced and unbalanced loading pattern specimens. Balanced and unbalanced service loading pattern limits for the 7 m diameter arched specimens are respectively 8.0 kN and 5.3 kN for Trenton, 11.3 kN and 7.6 kN for Petawawa and 16.3 kN and 11.0 kN for Gander. The experimental specimens were all capable of resisting larger loads than could be predicted by analysis, but they all deformed significantly under the simulated loading patterns representing Canadian snow loads. As for the numerical model, the replicated fixed support specimens were also able to surpass the Code service limits for each city listed, but the pinned support specimens were unable to get past the lowest city limits. Further analysis with larger diameter models would be required to determine if the load limits for each city still meet the NBCC ultimate load limits. These numerical models were analyzed using the experimental loading, which demonstrated larger deflections in both the vertical and horizontal directions. When loaded using NBCC balanced and unbalanced loading patterns, the numerical models demonstrated lower displacements and larger capacity, as the loading scenarios were better distributed and consistent, but not realistic compared to a real snow accumulation scenario.

The comparison between numerical and experimental results presented in Figure 4-17 showed similarities in the vertical and horizontal displacement results. The fixed base support balanced loading pattern numerical model reached stress levels consistent with yielding of the material at a load of 17.2 kN. At the numerical ultimate converged load, the difference between numerical and experimental displacements, both vertically and horizontally, were 24% and 31% respectively. The numerical horizontal displacement curve followed the same trend as the experimental specimens. However, the numerical vertical displacement curve demonstrated a small difference from the experimental specimen. The numerical model captured the stiffness of the fixed base support balanced loading pattern specimen, as well as the difference in capacity between all specimens.

The fixed base support unbalanced loading pattern numerical model had a load at the yielding of the material of 12.4 kN. The fixed base support unbalanced loading pattern numerical model best represented the experimental results, with a 9% difference for vertical displacements and 16% difference for the horizontal displacements at the load consistent with stresses where yielding of the steel was anticipated.

The pinned base support balanced loading pattern numerical model had much more difficulty in reaching force convergence, caused by the flexibility and rotational joints assigned to the numerical models. The numerical model converged at 7.2 kN, with vertical displacements of 27 mm and horizontal displacements of 16 mm. The percentage difference for vertical and horizontal displacements between the numerical model and experimental specimens was 27% and 3%, respectively. The numerical model achieved acceptable results replicating the beginning of the experimental program.

The pinned base support unbalanced loading pattern numerical model also had difficulty in reaching the same maximum load as the experimental specimen. The large displacements caused the material to reach yield stress values at very low loads, reaching a load of 5 kN. Vertical and horizontal displacements were respectively 22 mm and 25 mm. The difference in vertical and horizontal displacements between the numerical model and experimental specimen is respectively 9% and 1%.

Although both pinned support numerical models were unable to reach the maximum load of Trenton's and Petawawa's snowfall loads, further modelling to include non-linear properties may prove that the models are capable to reach even the NBCC's snow load limits for Gander.

The overall deformations are well represented within the numerical models as seen in Figure 4-18. Although Figure 4-18 shows the displacements recorded at the numerical yielding limits, the overall deformations in the X, Y and Z axes accurately portray the behaviours of the experimental program. A common effect experienced by all the numerical models was the movement of the lips and seamed connections at the top of the K-Span models. This behaviour was also noted during the experimental program, where the lips and seamed connections would separate from each other near the top portion of the structure. These large displacements were more severe near the exterior panels where the lips were not seamed to other panels or end walls.

As seen in the load-displacement diagrams of Figure 4-17, the fixed base support balanced loading pattern model demonstrated a stiffer structure with lower deflections compared to the remainder of the models. As can be seen in by the red and yellow contours on Figure 4-18 (A), the majority of the deflections experienced by the model occurred vertically, near the centre of the arch. The fixed base support unbalanced loading pattern model (B) also behaved like the experimental specimen, where the majority of the displacements occurred near the loading points, creating an outward movement of the panels situated on the unloaded side. The fixed base support unbalanced loading pattern model demonstrated more sideways movement than its balanced counterpart but remained stable and its deformations were still localized.

As for the pinned base support models (C and D), the global deformations reached similar values while reaching stress level in the model, consistent with yielding, at lower applied load levels. The pinned support model clearly demonstrated that K-Spans built using hinges are less stiff with larger deformations at lower levels.

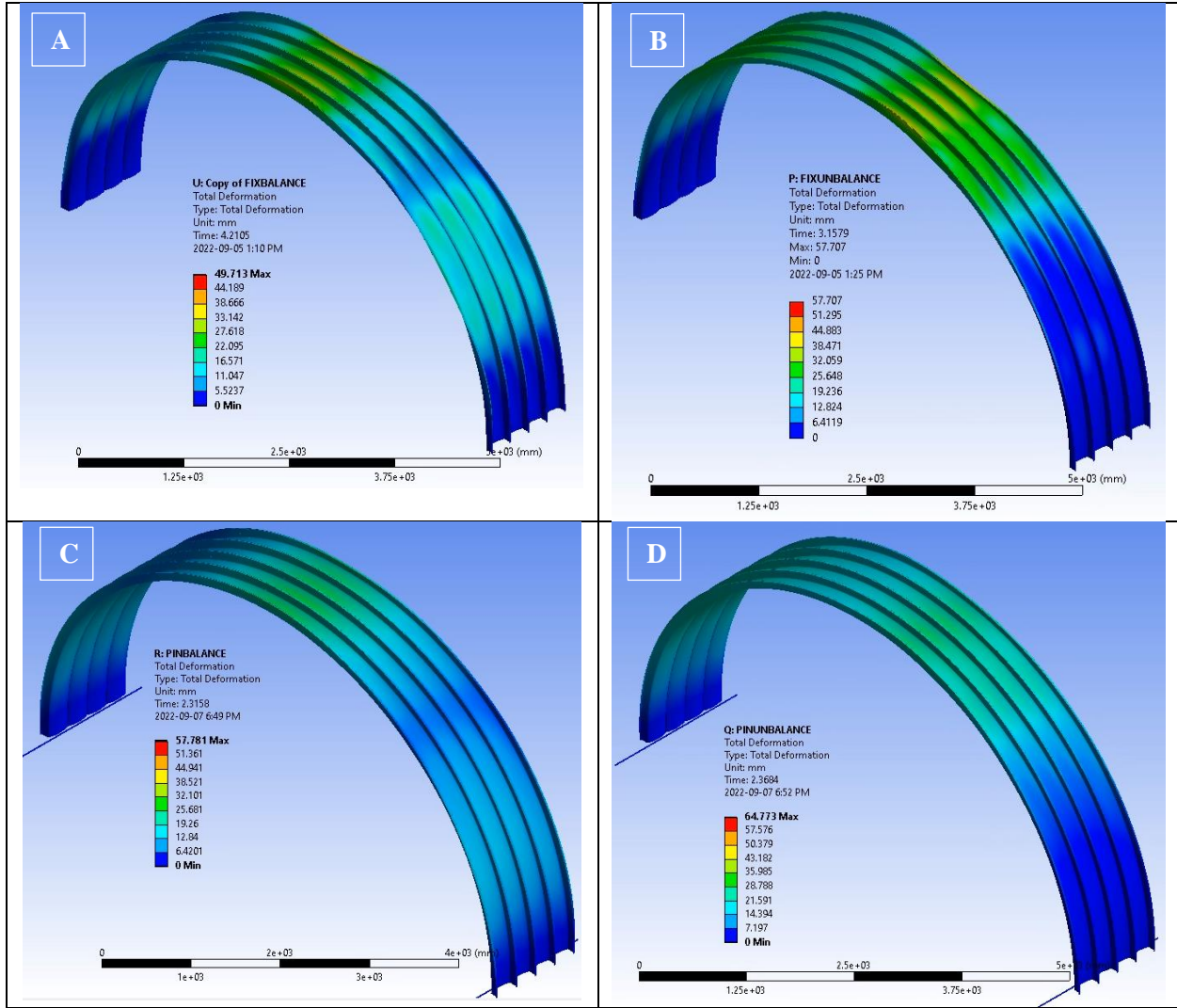


Figure 4-18: Total Deformation Comparison for Fixed and Balanced Model (A), Fixed and Unbalanced Model (B), Pinned and Balanced Model (C) and Pinned and Unbalanced Model (D) once Yielding Limit is Reached

Overall, the numerical models were unable to converge at the ultimate loads of the experimental specimens. The numerical models were also unable to record deformations past the ultimate load and localized buckling, but the initial deformation behaviours of the specimens were accurately represented up to the level where the stresses were consistent with the yield limits of the material properties. All numerical models demonstrated similar vertical and horizontal displacement patterns and recorded the initial plastic deformations and localized buckling near the base supports and crimping of the webs. Further advanced modelling and inclusion of post-buckling analysis would be required to capture the behaviour of the experimental specimens nearer loads related to their ultimate capacity. It may be possible to scale these models to study the serviceability load-deflection behaviour of larger-span specimens.

4.7 Summary and Conclusions

The experimental work for this research evaluated the strength capacity and deformations experienced by loading a set of four panels of ABM-120 K-Spans. These results were compared to numerical models which attempted to replicate the same results as the experimental program. Results for vertical and horizontal displacements were obtained and investigated in order to draw conclusions and have a better understanding regarding the behaviours of K-Spans.

The observed behaviours confirmed the flexibility and potential instabilities that arise from these types of structures. The unique design of doubly corrugated steel for K-Span panels, with local deformations generated during the forming process, although necessary to properly have a continuous curved panel, precipitates distinctive localized buckling patterns at high levels of loading. The flexibility of the panels made the structure exhibit large displacements under loading conditions. Although all the experimental tests for a 7m-diameter K-Span structure were capable of reaching loads up to the ultimate snow load factors for many cities in Canada, the serviceability of the pinned structures could be at risk under large snow loads, especially for larger span structures. Maintenance systems, such as sprinklers or indoor lighting, must be considered as an added load on the structure, and should be flexible to accommodate any potential deformations.

Another important observation is that the use of hinges to connect the panels to the base supports is a much less effective way to assemble a K-Span if structure must resist significant snow loading. This method of construction may be faster and less costly by only bolting the panels to a steel angle but deviating from the manufacturer's specifications have caused the structures to not only have lower ultimate capacity resistance, but also causes the structure to have larger displacements.

The finite element numerical models were able to accurately determine the vertical and horizontal displacements under the same loading conditions as the experimental specimens. Further refinement of elements in areas of high stresses would be needed to accurately capture the local buckling behaviour experienced by the experimental specimens that could indicate imminent failure of the structure.

K-Spans are versatile cost-effective structures that can be built in both industrial and military settings. However, K-Spans that were built by connecting the panels to steel angles and hinges may have insufficient capacity to support the ultimate snow loads for certain regions in Canada. Further monitoring and analysis of larger sized K-Spans of over 15 to 18 meters diameter (50 to 60 ft diameter) is required to better understand the effect of base support conditions of K-Span structures subjected to heavy snow loads.

A summary of all key results, findings and observations for the large-scale experimental testing of K-Spans are listed below:

1. 7 m diameter K-Span specimens demonstrated that they could resist 24% to 40% higher loads when built using fixed base supports vice pinned supports for both unbalanced and balanced loading patterns respectively.
2. 7 m diameter K-Spans built using hinges appear to displace more than structures built using fixed supports, and displacements were observed to be up to 49% greater.
3. Localized permanent deformations occur near the base supports for both pinned and fixed supports when loaded. For fixed base supports, the deformations are caused by the large bending moments, whereas for pinned base supports, it is the rotation of the hinges that bend the end of the panels that cause the deformations.

4. The ultimate capacity of a K-Span structure is immediately precipitated by localized buckling near the top lips of the structure and crimping of the webs at the 1/8 to 1/4 length distance from supports.
5. Reducing the effective thickness of elements in numerical models appeared to be a suitable simplified method to represent the double corrugation that reduces the stiffness and strength of the flat panels. It may not fully capture the behaviour of the specimens but appeared to capture accurate displacements ranging from a 1% to 31% difference between experimental and numerical displacement results. Further analysis using larger diameter K-Spans should be studied to correlate appropriate effective thicknesses for these larger diameter structures.

4.8 References

- [1] Sweeney, S., Briassoulis, D., & Kao, A. (1991, January). *Evaluation of K-Span as a Rapidly Erectable Lightweight Mobilization Structure (RELMS)* (TR M-91/06). US Army Construction Engineering Research Laboratory.
- [2] M.I.C. Industries. (1993, March). *MIC-120 ABM (K-Span) Automated Building Machine Training Manual*.
- [3] Biegus, A., & Kowal, A. (2013). Collapse of halls made from cold-formed steel sheets. *Engineering Failure Analysis*, 31, 189–194. <https://doi.org/10.1016/j.engfailanal.2012.12.009>
- [4] MacDonald, A. (2021). Two-dimensional finite element analysis of the automatic bending machine (ABM)-120 K-Span structure subjected to asymmetric snow loads. *Defence Research and Development Canada (DRDC), DRDC-RDDC-2021-D038*.
- [5] Piekarczyk, A., Więch, P., Kuczyński, K., & Walentyński, R. (2021). Experimental and computational approaches to the evaluation of double corrugated arch structures. A review of the latest advancements. *Archives of Civil Engineering*, LXVII(2). <https://doi.org/10.24425/ace.2021.137152>
- [6] Cybulski, R., Walentyński, R., & Cybulska, M. (2014). Local buckling of cold-formed elements used in arched building with geometrical imperfections. *Journal of Constructional Steel Research*, 96, 1–13. <https://doi.org/10.1016/j.jcsr.2014.01.004>
- [7] American Iron and Steel Institute & Canadian Standards Association. (2016). *North American Specification for the Design of Cold-formed Steel Structural Members 9th Ed* (9th ed.). Canadian Standards Association.
- [8] National Research Council of Canada & Canadian Commission on Building and Fire Codes. (2015). *National Building Code of Canada, 2015* (14th ed.). National Research Council Canada.
- [9] Cybulski, R., & Koziel, K. (2011). *Introduction of stiffness investigation of ABM K-span arch structures*. IV International Interdisciplinary Technical Conference of Young Scientists, Poznań, Poland.

- [10] Piekarczyk, A., Więch, P., & Cybulski, R. (2019). Experimental method to evaluate the load-carrying capacity of double corrugated sheet profiles. *Thin-Walled Structures*, 144, 106283. <https://doi.org/10.1016/j.tws.2019.106283>
- [11] Walentynski, R., Cybulski, R., & Koziel, K. (2013). Local buckling and post-buckling investigation of cold-formed self-supported elements. *Computer Methods in Mechanics*.
- [12] Xu, L., Gong, Y., & Guo, P. (2001). Compressive tests of cold-formed steel curved panels. *Journal of Constructional Steel Research*, 57(12), 1249–1265. [https://doi.org/10.1016/s0143-974x\(01\)00048-7](https://doi.org/10.1016/s0143-974x(01)00048-7)
- [13] Airumyan, E., & Boyko, O. (1997). Full-scale testing and design of frameless arch steel roof. *Structural Assessment*.
- [14] Piekarczyk, A. (2019). Experimental and numerical studies of double corrugated steel arch panels. *Thin-Walled Structures*, 140, 60–73. <https://doi.org/10.1016/j.tws.2019.03.032>
- [15] Association Standard of the People’s Republic of China. (2005). *Technical specification for arched corrugated steel roof trial* (CECS 167: 2004).
- [16] Lépine, G. (2021). *Structural Capacity of Thin-Walled Cold-Formed Steel Doubly-Corrugated Arch Panels*. Royal Military College of Canada.
- [17] Leontovich, V. (1959). *Frames and Arches; Condensed Solutions for Structural Analysis*. McGraw-Hill Book Company.

CHAPTER 5: CONCLUSIONS AND RECOMMENDATIONS

5.1 General

This research was focused on evaluating the structural behaviours and deformations experienced by 7-meter full-scale K-Span specimens under severe snow loading patterns. Two types of base support connections were used, with either the K-Span panels embedded in concrete, making it a fixed support, or the panels were bolted to steel hinges, making it a pinned support. Results were used to observe the deformation behaviour and replicate this behaviour using finite element analysis.

The project consisted of 4 seamed ABM-120 panels, tested in 4 different scenarios: fixed-balanced, pinned-balanced, fixed-unbalanced and pinned-unbalanced. With the combination of aircraft steel cables, pulleys and a loading assembly, which consisted of instrumentation, and steel and aluminum loading plates, the snow loading patterns were simulated by pulling the structure downwards with a 100kN actuator, creating large deformations and loading the K-Span specimens to their ultimate capacity limits. The 1.016 mm-thick doubly-corrugated cold-formed steel members, shaped as a semicircle, were also represented through finite element analysis. All experimental tests and numerical simulations were compared and loaded following the same boundary conditions and loading patterns.

The project successfully replicated real-life construction K-Spans to better understand the risk, capacity and behaviour of the current infrastructure found within DND's portfolio. Some of the existing K-Spans owned by DND were built using steel hinges connected to the supports, which may result in significant instabilities at lower loads than anticipated and lower structural capacity than expected. Overall summary conclusions from this research are provided in Section 5.2 and recommendations for future work are given in Section 5.3.

5.2 Summary and Conclusion

The displacement results of both the numerical models and experimental specimens demonstrated that K-Span structures are capable of supporting large loads. However, the inclusion of the double corrugation and the presence of imperfections in the forming process of the panels create potential instabilities and distinctive localized buckling patterns. The flexibility of the members causes the structure to largely displace under loading. Although all specimens were capable of meeting the ultimate limit states for geographical areas such as Gander (NL), the serviceability limit states of the structure are of great concern due to the deflections experienced under loading.

K-Span structures can be constructed with very small labour crews, at minimal cost and on-site, within very fast timelines. The inclusion of different base supports connections such as steel hinges, to minimize the construction timelines and facilitate the construction process, creates a risk to the structure in certain areas of Canada, especially those that are known to have large snowfalls. The steel hinges, found in many of DND's current infrastructure inventory, behave as pins and allow the structure to displace significantly more in the lateral and vertical directions than if the structure was embedded in concrete with a fixed base support condition. Localized buckling occurs much sooner, and the structure starts to sway in one direction as soon as there is presence of uneven loading.

Through finite element analysis, numerical models were used to replicate deflections and loads for large scale K-Span models. Although the inclusion of the double-corrugation would provide more accurate results, reducing the effective area [2] [23] has proven to be an effective method to estimate the initial

locations of localized buckling and the overall displacements of the structures. This method lessens the number of nodes and elements required, which in turn reduces the computation time, while providing good displacement results and confirmed areas of interest for localized buckling.

A summary of all key results, findings and observations for the large-scale experimental testing program of K-Spans are listed below:

1. 7 m diameter K-Span specimens demonstrated that they could resist 24% to 40% higher loads when built using fixed base supports vice pinned supports for both unbalanced and balanced loading patterns respectively.
2. K-Spans built using steel hinges appear to displace more than structures built using fixed base supports and exhibited displacements up to 49% greater.
3. Localized permanent deformations occur near the base supports for both pinned and fixed supports. For fixed base supports, the deformations are caused by the large bending moments, whereas for pinned base supports, it is the rotation of the hinges at the end of the panels that cause the deformations.
4. Once localized buckling occurs at the lips near the top of the structure and crimping of the webs occurs at the 1/8 to 1/4 length distance from supports, the K-Span structure approached its capacity limits.
5. Reducing the effective area for numerical models has proven to be a possible method to represent the double corrugation that reduces the strength and stiffness of the K-Span panels but it does not capture the full behaviour of the specimens once yielding of the material is present.
6. No slipping effect at the seams between panels was noticed during the experimental program.
7. Serviceability limit states are of concern for large diameter K-Span structures which are connected to hinges rather than embedded in concrete.

5.3 Recommendations

Based on the experimental program conducted and scope of this research, the following recommendations should be considered for future K-Span constructions within Canada and future research related to ABM-120 K-Span structures.

1. Future K-Span structures should be built using fixed base supports, by having panels set inside concrete. Any design that deviates from these support conditions, should only be conducted after extensive and thorough analysis by qualified engineering personnel.
2. Future studies are recommended to provide data for fixed and pinned K-Span structures having spans of 15- to 20-meter diameters, greater than the 7 m span monitored in this study. This may be done by monitoring existing structures under deliberate loading or actual large snow events. This work should be supplemented with parametric studies using similar finite element models to the one used in this research.

3. Due to the flexibility of the panels, maintenance systems and utilities, such as sprinklers and indoor lighting, should be as flexible as possible to accommodate the large displacements experienced by the structure.
4. When considering building K-Span structures, utilizing the maximum allowable steel thickness will help increase the stiffness of the panels, which in turn will have more strength capacity. Changes to the design tables may be required to ensure adequate stiffness in these structures.
5. Further research should be conducted on the stress experienced in areas near the base supports, in the quarter length web portion of the span, and the seamed lips near the top of the arch, to capture localized buckling. This should be conducted with the use of digital correlation cameras (DIC) or Fibre Optic Sensors (FOS).
6. Further modelling in finite analysis software should be done to represent the behaviour of K-Spans at ultimate load.
7. A strengthening method should be developed to reduce the displacements and movements of K-Span structures that were built using steel hinges as pinned base support conditions.
8. Further studies should be conducted on the effects of the end walls of the structure and its influence on the overall behaviour of the panels.

REFERENCES

- [1] K Span General Construction Contractor UAE. (n.d.). *K Span Roofing System*. K-Span Roofing System WordPress. Retrieved July 22, 2022, from <https://kspanroofingsystem.wordpress.com/>
- [2] Cybulski, R., Walentyński, R., & Cybulska, M. (2014). Local buckling of cold-formed elements used in arched building with geometrical imperfections. *Journal of Constructional Steel Research*, 96, 1–13. <https://doi.org/10.1016/j.jcsr.2014.01.004>
- [3] Canadian Commission on Building and Fire Codes & National Research Council of Canada. (2015). *National Building Code of Canada, 2015* (14th ed.). National Research Council Canada.
- [4] Division of Graduate Studies. (2015, May). *Thesis Preparation Guidelines*. Royal Military College of Canada.
- [5] Piekarczyk, A., Malowany, K., Więch, P., Kujawińska, M., & Sulik, P. (2015). Stability and bearing capacity of arch-shaped corrugated shell elements: experimental and numerical study. *Bulletin of the Polish Academy of Sciences Technical Sciences*, 63(1), 113–123. <https://doi.org/10.1515/bpasts-2015-0013>
- [6] Sweeney, S., Briassoulis, D., & Kao, A. (1991, January). *Evaluation of K-Span as a Rapidly Erectable Lightweight Mobilization Structure (RELMS)* (TR M-91/06). U.S. Army Construction Engineering Research Laboratory (USACERL).
- [7] Walentyński, R., & Cybulski, R. (2012, October). Modern investigation techniques for doubly corrugated cold formed structural elements. *10th International Conference on New Trends in Statics and Dynamics of Buildings*, Bratislava, Slovakia.
- [8] *K-Span Buildings*. (n.d.). EMROOZ Engineering & Construction. Retrieved June 10, 2022, from https://www.emrooz-ec.org/?page_id=105&hcb=1
- [9] MacDonald, A. (2021, February). *Two-Dimensional finite element analysis of the automatic bending machine (ABM)-120 K-Span structure subjected to asymmetric snow loads* (DRDC-RDDC-2021-D038). Defence Research and Development Canada (DRDC).
- [10] *MIC-120 ABM (K-Span) Automated Building Machine Training Manual* (Vol. 2). (1993). M.I.C. Industries.
- [11] Dubina, D. (2014, October 16–17). *Cold-formed Steel Design* [Joint Research Center]. European Convention for Constructional Steelwork, Brussels, Belgium.
- [12] Lépine, G. (2021). *Structural Capacity of Thin-Walled Cold-Formed Steel Doubly-Corrugated Arch Panels*. Royal Military College of Canada.
- [13] S136-16. (2016). *North American Specification for the Design of Cold Formed Steel Structural Members (AISI Standard)*. CSA Group.

- [14] Biegus, A., & Kowal, A. (2013). Collapse of halls made from cold-formed steel sheets. *Engineering Failure Analysis*, 31, 189–194. <https://doi.org/10.1016/j.engfailanal.2012.12.009>
- [15] Piekarczyk, A., Więch, P., Kuczyński, K., & Walentyński, R. (2021). Experimental and computational approaches to the evaluation of double corrugated arch structures. A review of the latest advancements. *Archives of Civil Engineering*, 67(2), 7–35. <https://doi.org/10.24425/ace.2021.137152>
- [16] Walentyński, R., Cybulski, R., & Mazurkiewicz, J. (2013). Doubly corrugated cold-formed arch roof panels. Advanced identification of geometrical and material properties. *Architecture Civil Engineering Environment (ACEE)*, 1.
- [17] Airumyan, E., & Boyko, O. (1997). Full-Scale Testing and Design of Frameless Arch Steel Roof. In *Structural Assessment: The Role of Large & Full- Scale Testing* (pp. 211–217). E & FN Spon.
- [18] Leontovich, V. (1959). *Frames and Arches; Condensed Solutions for Structural Analysis*. McGraw-Hill Book Company.
- [19] Marzouk, O. A., & Abdel-Sayed, G. (1975). Stability of Half-Barrel Orthotropic Shells. *Journal of the Structural Division*, 101(7), 1517–1530. <https://doi.org/10.1061/jsdeag.0004103>
- [20] Xiliang, L., Yong, Z., & Fuhai, Z. (1999). *Experimental Study on Full-sized Models of Arched Corrugated Metal Roof*.
- [21] Piekarczyk, A. (2019). Experimental and numerical studies of double corrugated steel arch panels. *Thin-Walled Structures*, 140, 60–73. <https://doi.org/10.1016/j.tws.2019.03.032>
- [22] Piekarczyk, A., Więch, P., & Cybulski, R. (2019). Experimental method to evaluate the load-carrying capacity of double corrugated sheet profiles. *Thin-Walled Structures*, 144, 106283. <https://doi.org/10.1016/j.tws.2019.106283>
- [23] Tianjin University. (2005). *Technical specification for arched corrugated steel roof* (CECS 167:2004 ed.). China Association for Engineering Construction Standardization.
- [24] Litong, S., & Chen, L. (2010). Computer Nonlinear Analysis of Ultimate Bearing Capacity of Corrugated-arch Metal Roof. *2010 International Conference on Intelligent Computation Technology and Automation*. <https://doi.org/10.1109/icicta.2010.474>
- [25] Piekarczyk, A., Malesa, M., Kujawinska, M., & Malowany, K. (2012). Application of Hybrid FEM-DIC Method for Assessment of Low Cost Building Structures. *Experimental Mechanics*, 52(9), 1297–1311. <https://doi.org/10.1007/s11340-012-9616-2>
- [26] Walentynski, R., Cybulski, R., & Koziel, K. (2013). Local buckling and post-buckling investigation of cold-formed self-supported elements. *Computer Methods in Mechanics*.

- [27] Cybulski, R., & Koziel, K. (2011). *Introduction of stiffness investigation of ABM K-span arch structures*. IV International Interdisciplinary Technical Conference of Young Scientists, Poznań, Poland.
- [28] Xu, L., Gong, Y., & Guo, P. (2001). Compressive tests of cold-formed steel curved panels. *Journal of Constructional Steel Research*, 57(12), 1249–1265. [https://doi.org/10.1016/s0143-974x\(01\)00048-7](https://doi.org/10.1016/s0143-974x(01)00048-7)

APPENDIX A - GRAPHICAL LOAD AND DISPLACEMENTS RESULTS

The following figures presented in Appendix A consist of all the experimental and numerical results displacement curves described in Chapter 3, as well as other experimental and numerical load and displacement results which have not been discussed in this research paper, but may be pertinent for future studies.

Row 1 Vertical Displacements

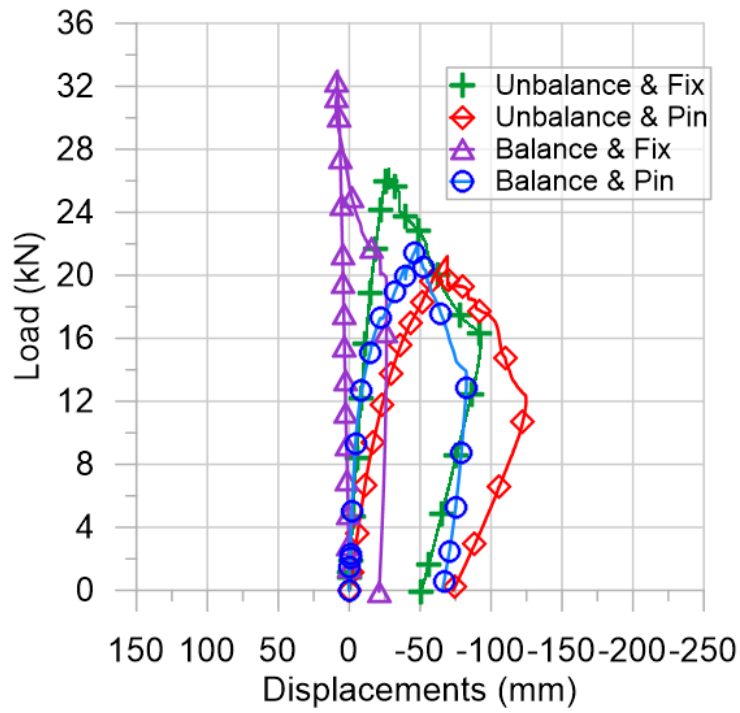


Figure A-1: Vertical Displacements for Row S1

Row 2 Vertical Displacements

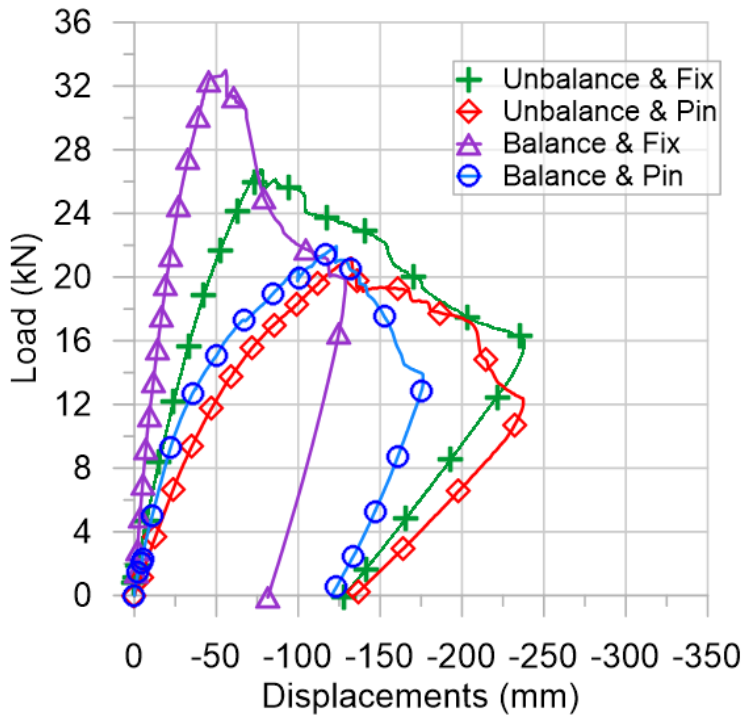


Figure A-2: Vertical Displacements for Row S2

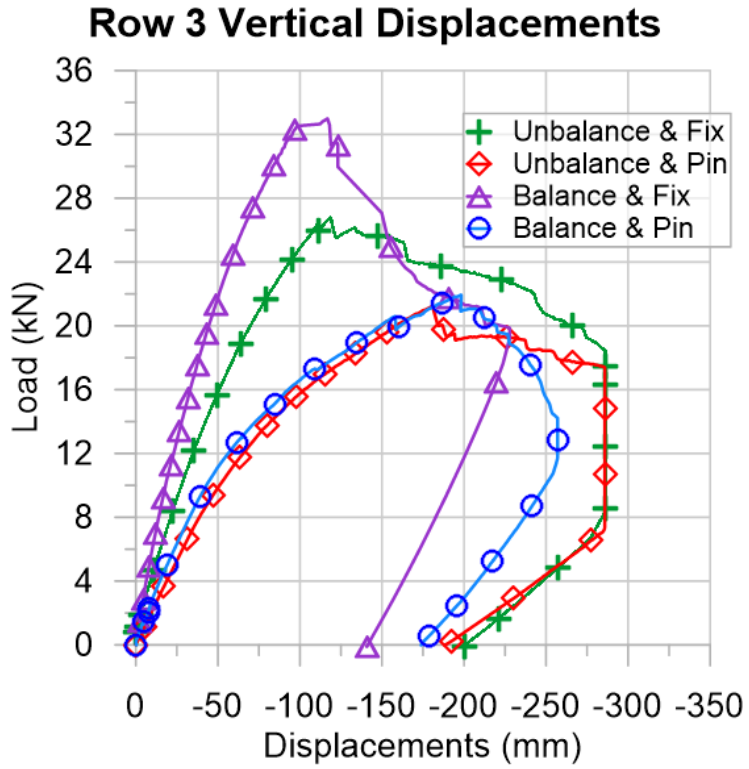


Figure A-3: Vertical Displacements for Row S3

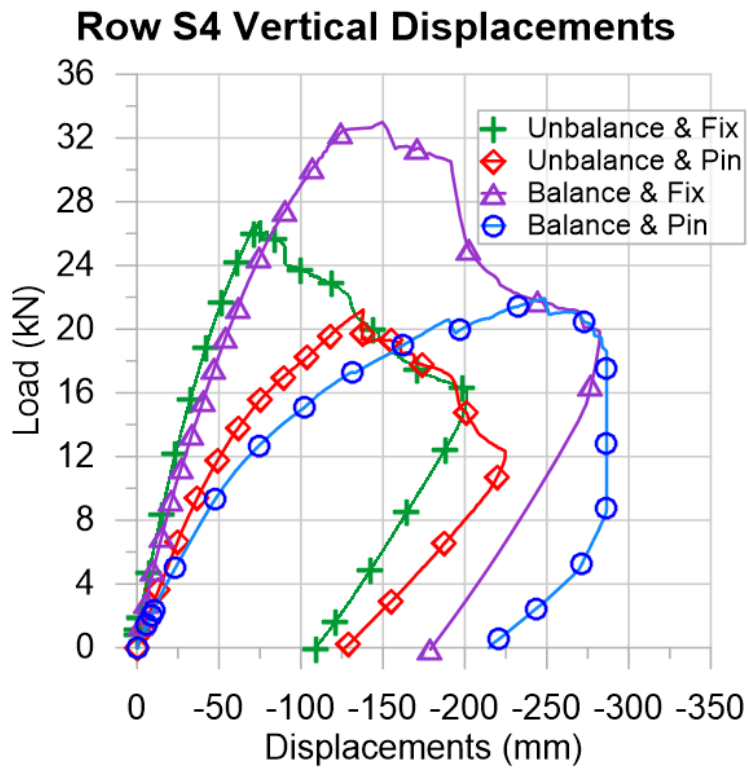


Figure A-4: Vertical Displacements for Row S4

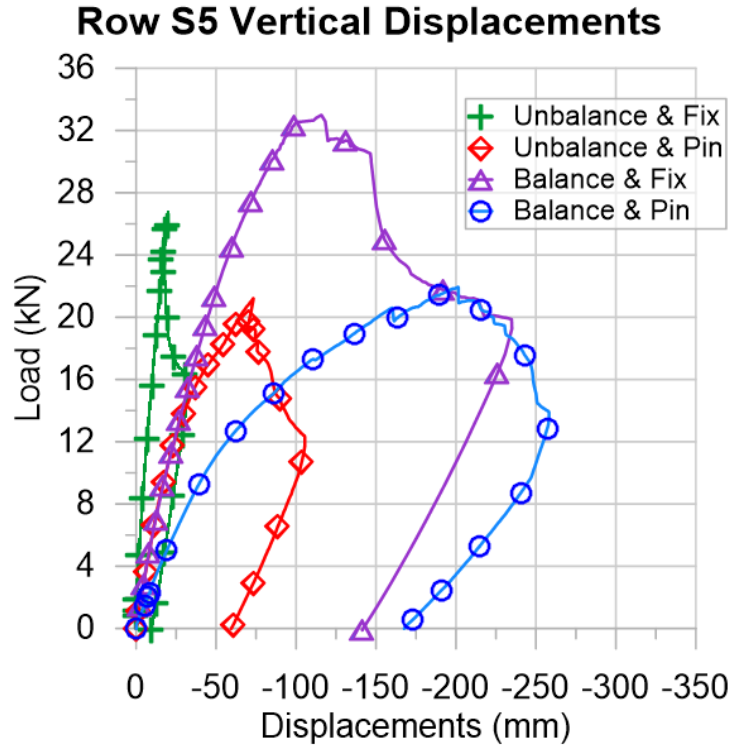


Figure A-5: Vertical Displacements for Row S5

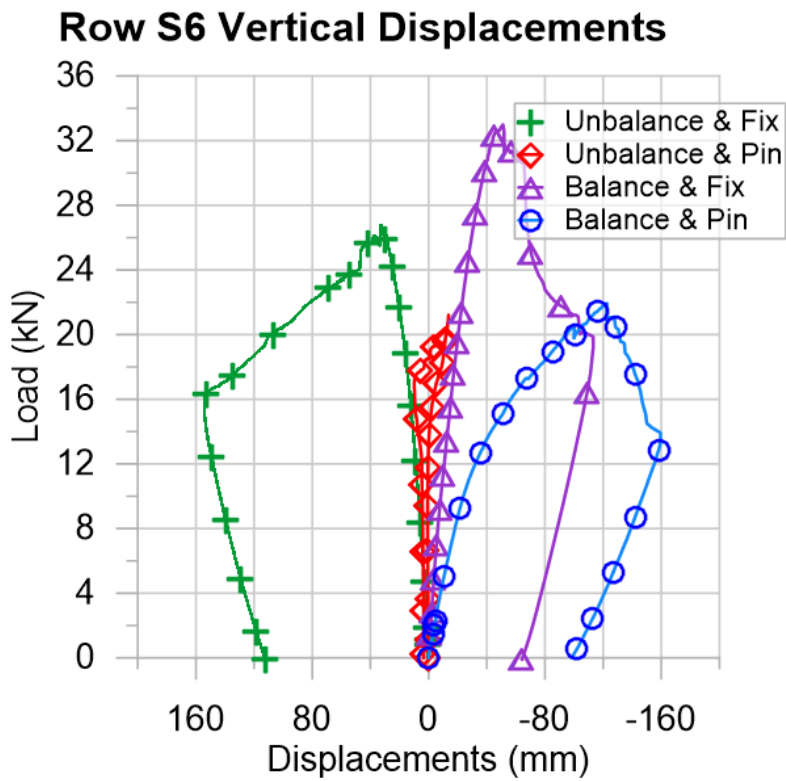


Figure A-6: Vertical Displacements for Row S6

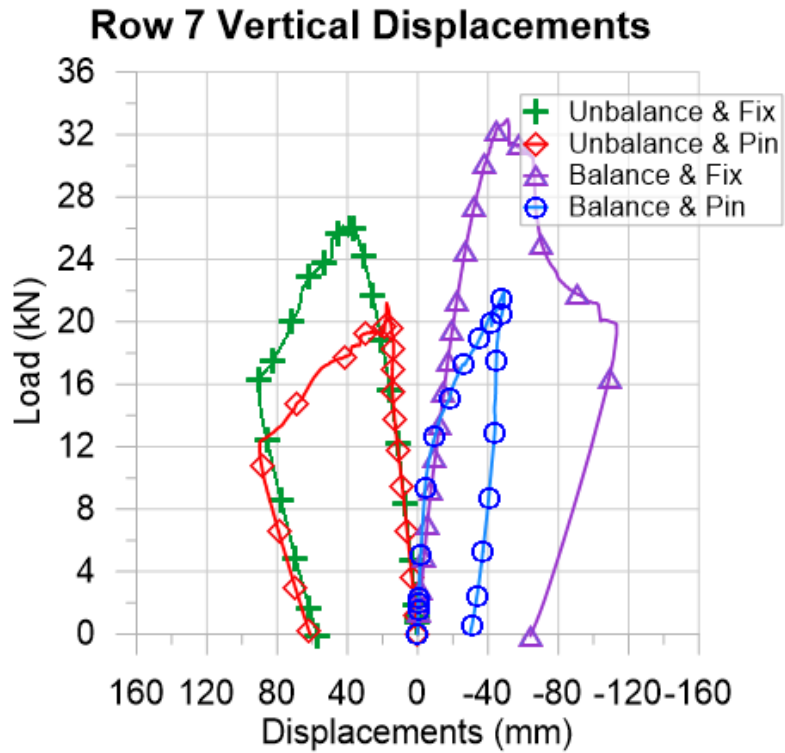


Figure A-7: Vertical Displacements for Row S7

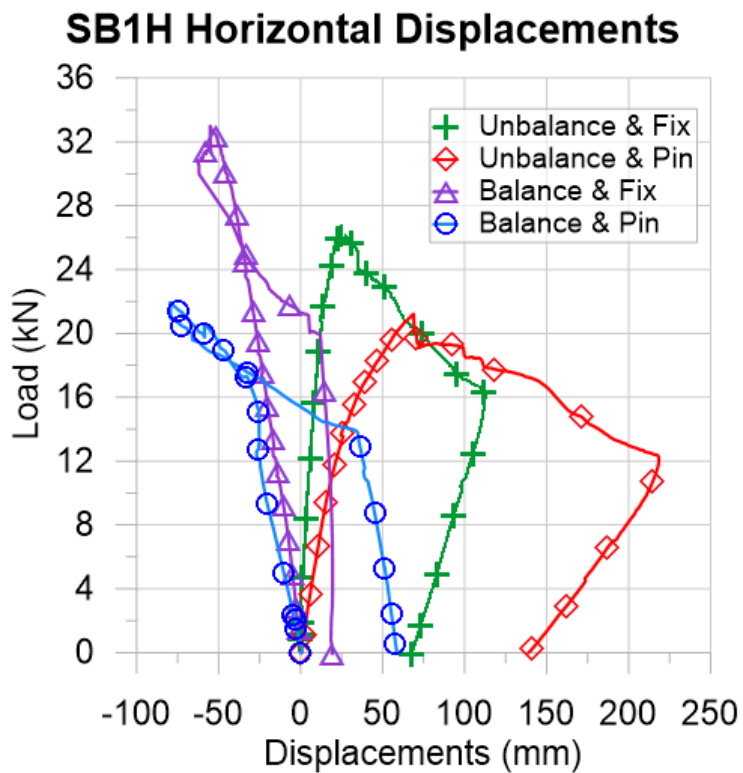


Figure A-8: Horizontal Displacements for SB1H

SB2H Horizontal Displacements

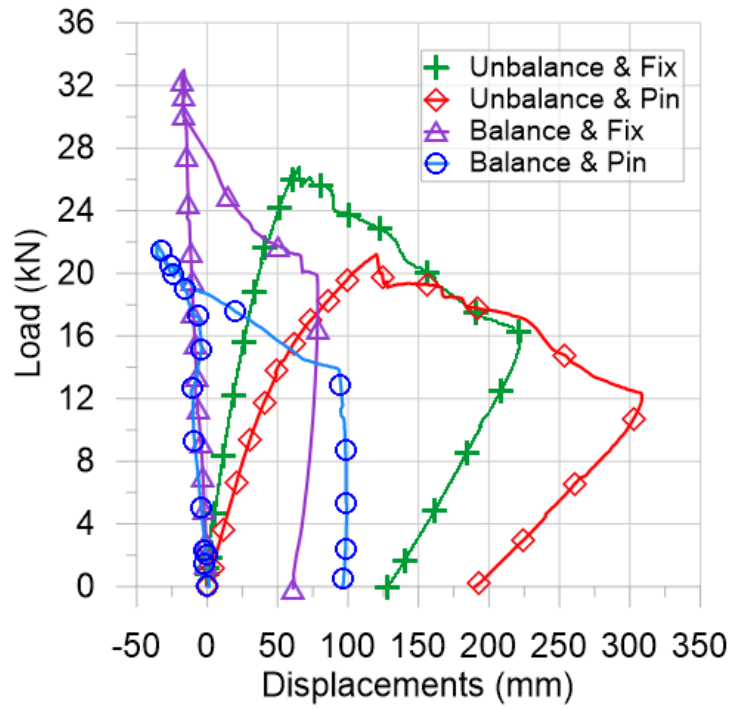


Figure A-9: Horizontal Displacements for SB2H

SB6H Horizontal Displacements

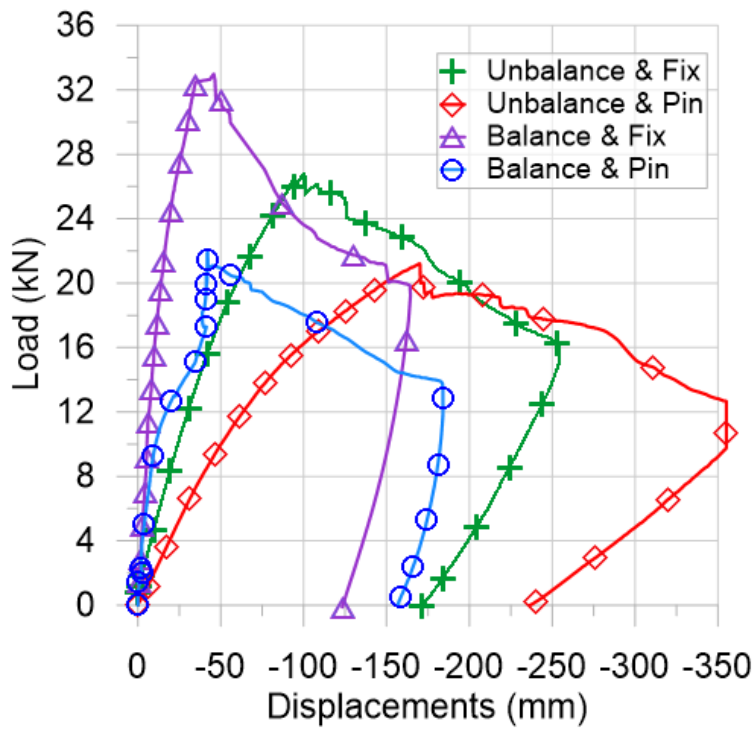


Figure A-10: Horizontal Displacements for SB6H

SB7H Horizontal Displacements

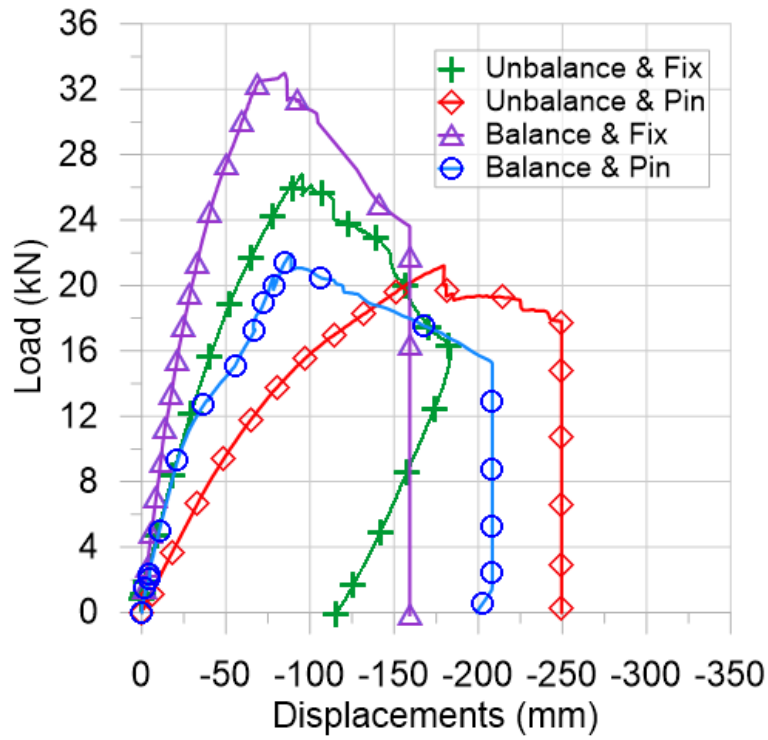


Figure A-11: Horizontal Displacements for SB7H

SL4 Longitudinal Displacements

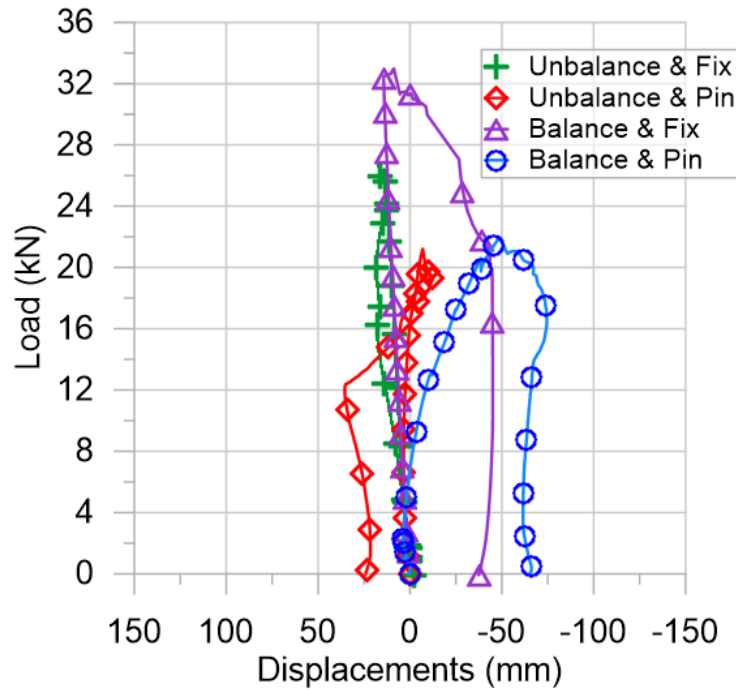


Figure A-12: Longitudinal Displacements for SL4

Balance - Vertical Disp.

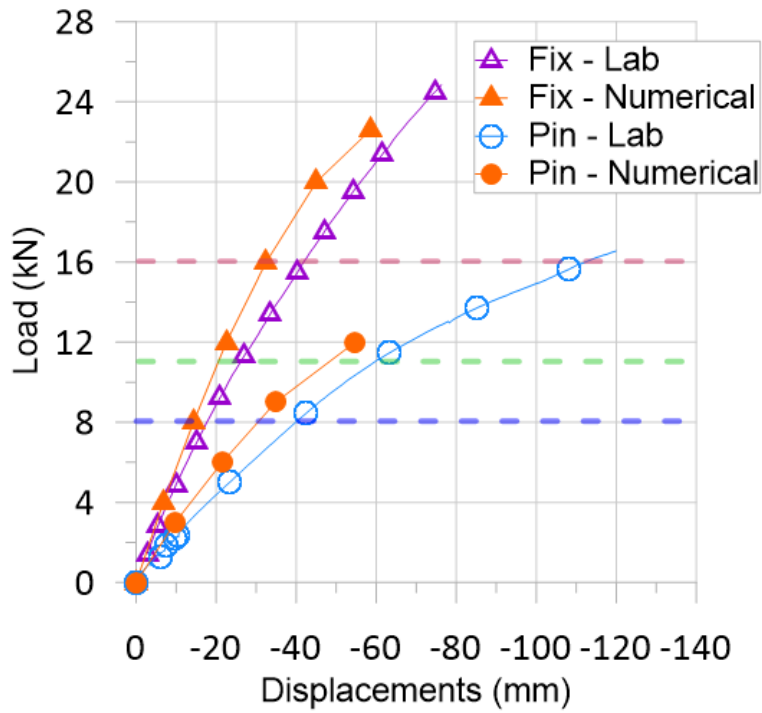


Figure A-13: Vertical Displacement Comparison for Balanced Loading Pattern Specimens

Unbalance - Vertical Disp.

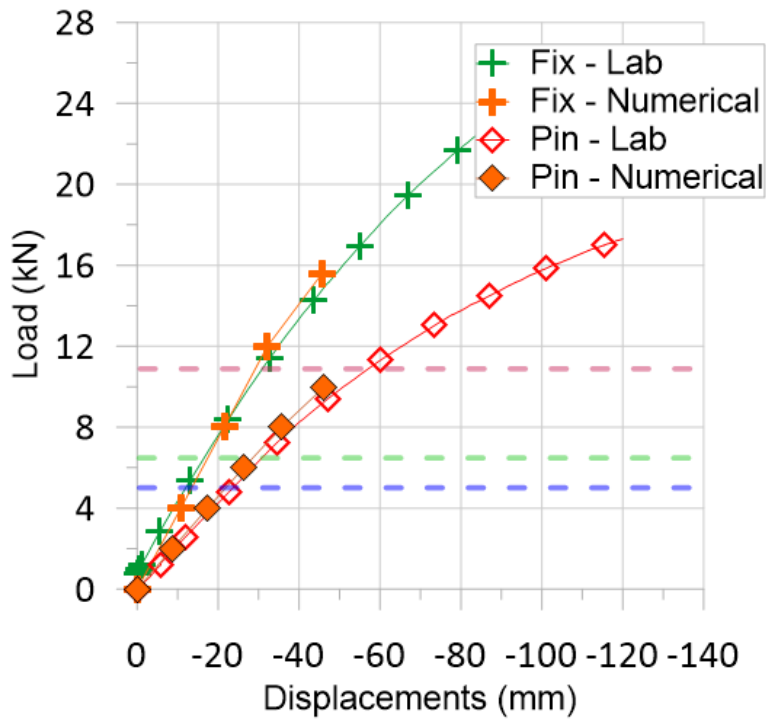


Figure A-14: Vertical Displacement Comparison for Unbalanced Loading Pattern Specimens

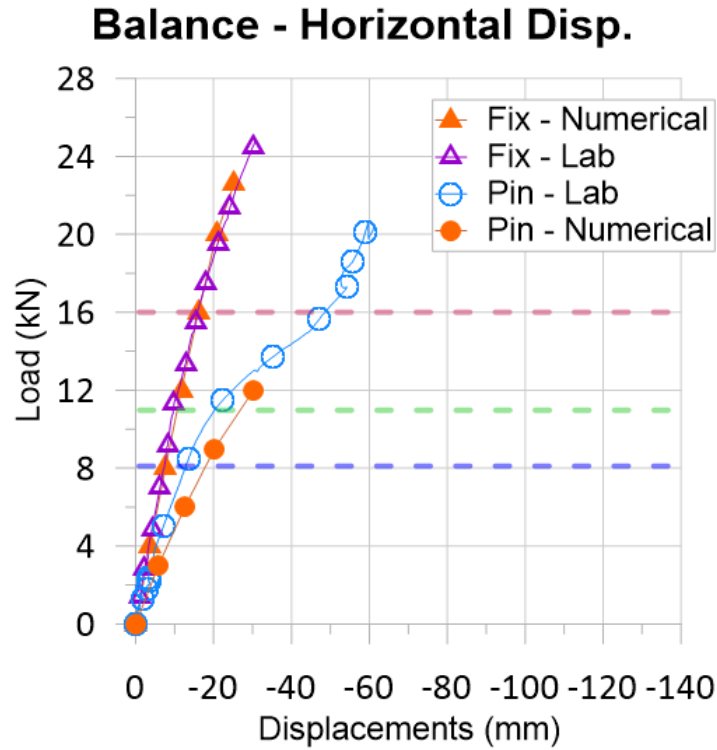


Figure A-15: Horizontal Displacement Comparison for Balanced Loading Pattern Specimens

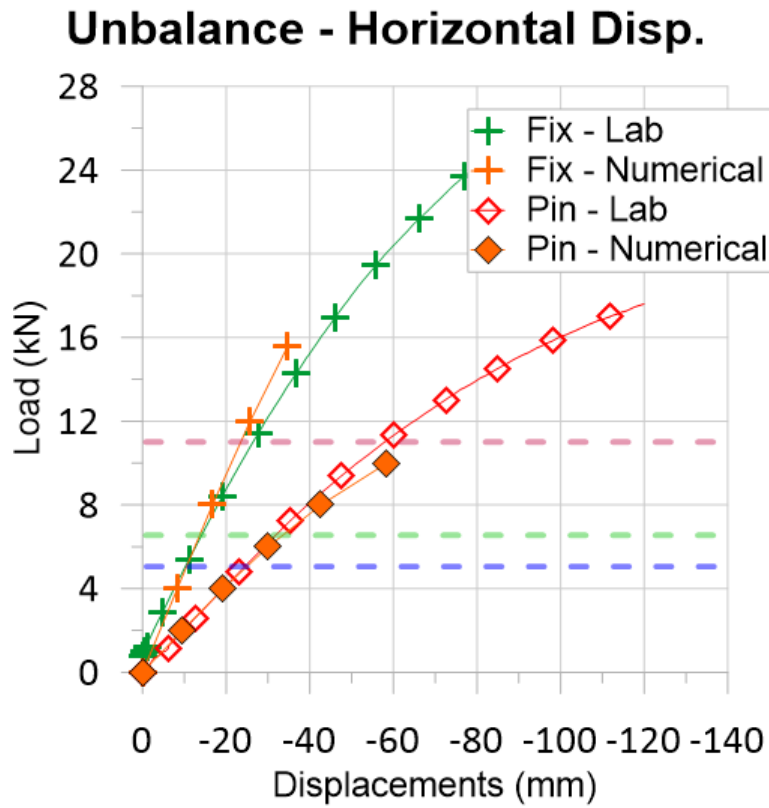


Figure A-16: Horizontal Displacements Comparison for Unbalanced Loading Pattern Specimens

Balance & Fix - Row Load Distribution

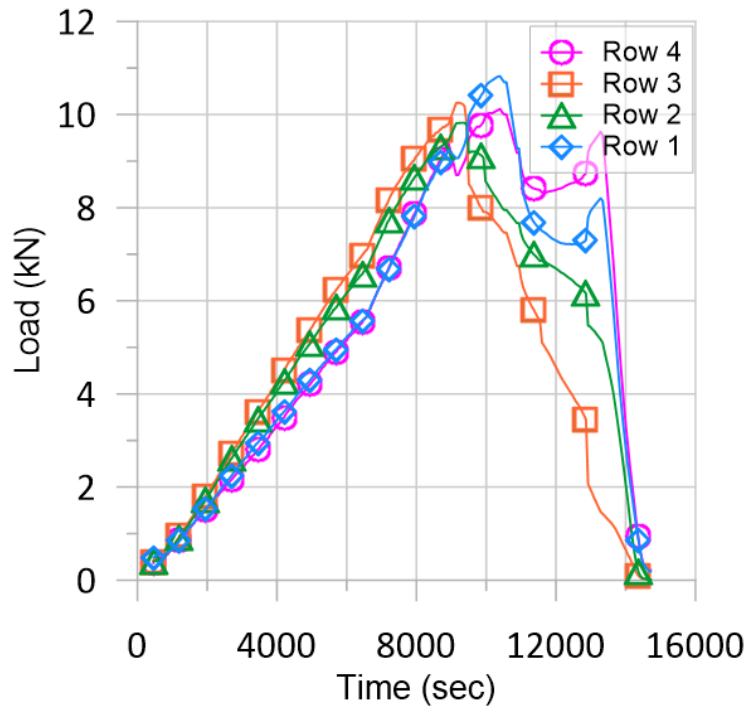


Figure A-17: Loading Distribution per Row for Balanced Loading Pattern & Fixed Support Specimen

Balance & Pin - Row Load Distribution

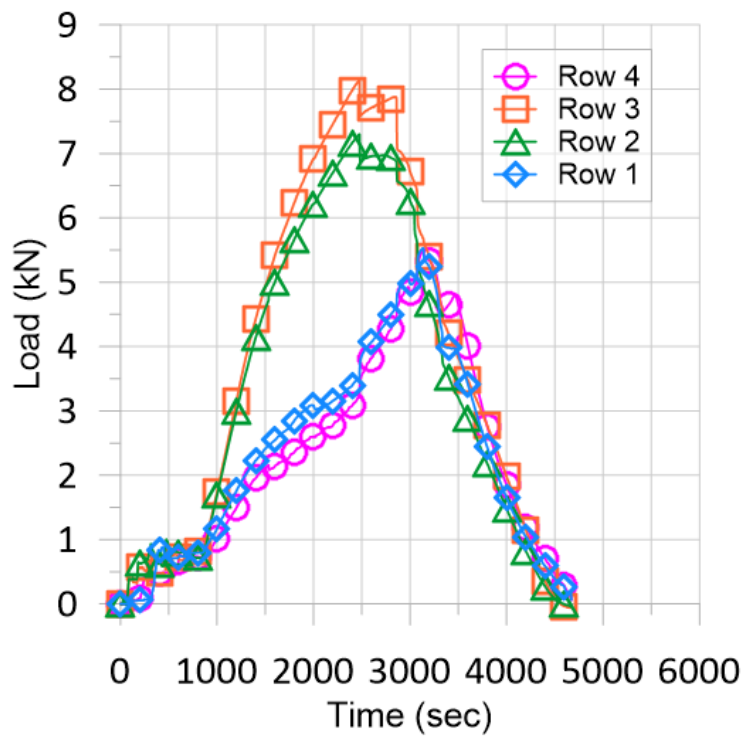


Figure A-18: Loading Distribution per Row for Balanced Loading Pattern & Pinned Support Specimen

Unbalance & Fix - Row Load Distribution

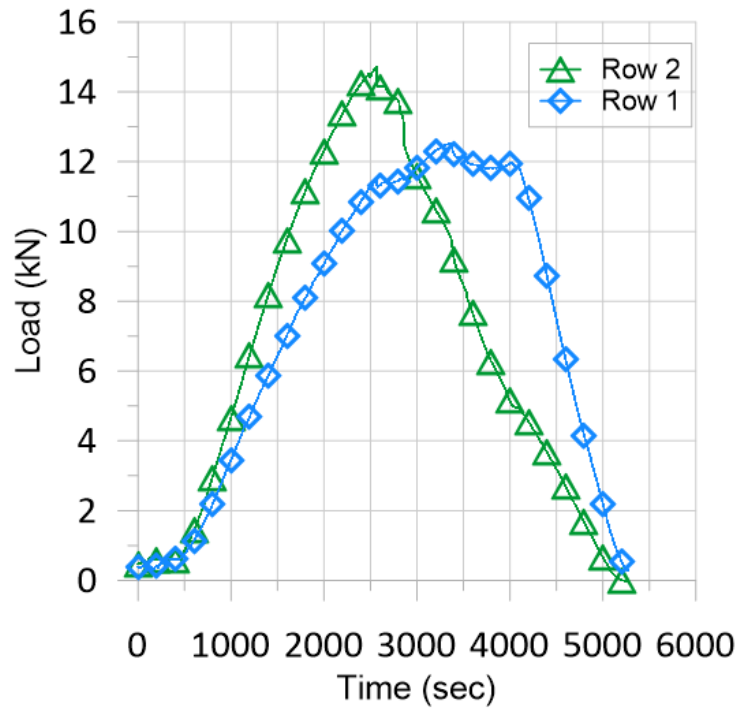


Figure A-19: Loading Distribution per Row for Unbalanced Loading Pattern & Fixed Support Specimen

Unbalance & Pin - Row Load Distribution

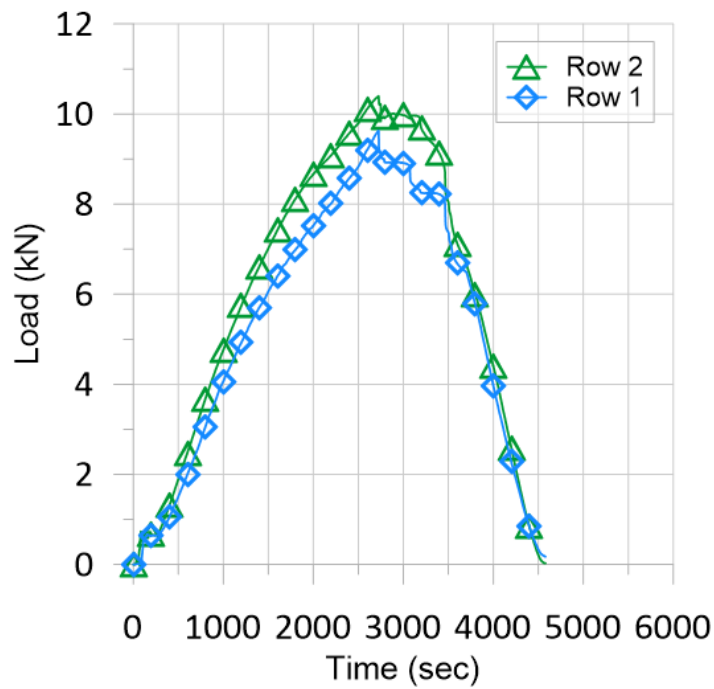


Figure A-20: Loading Distribution per Row for Unbalanced Loading Pattern & Pinned Support Specimen

APPENDIX B - LARGE SCALE K-SPAN SPECIMEN SCHEMATICS AND DIMENSIONS

The following figures presented in Appendix B are all the experimental plans and schematics used to build the full-scale experimental set-up, loading of the specimens and instrumentation positioning. This Appendix is meant to supplement the research paper to provide a better understanding and overview of the scale of the experimental results.

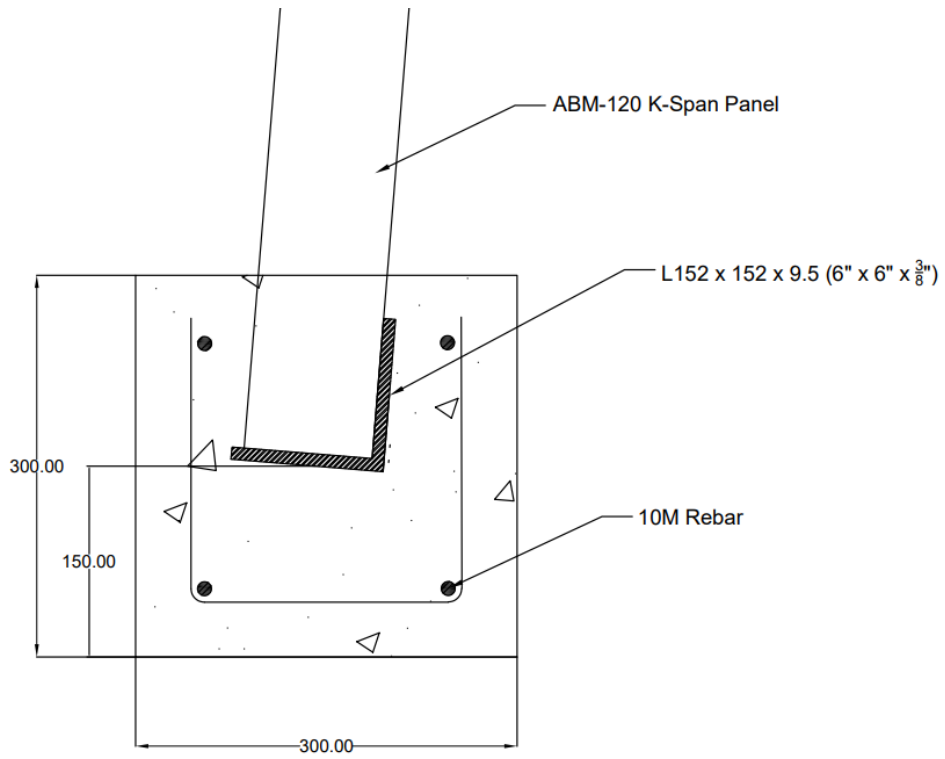


Figure B-1: Fixed Concrete Support Side View

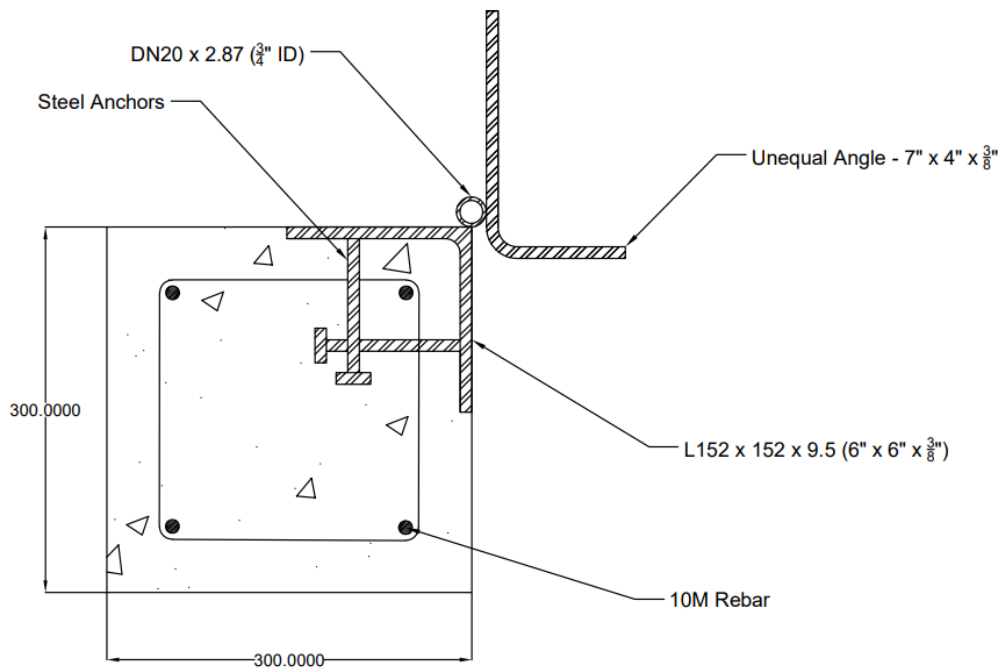


Figure B-2: Pinned Concrete Support Side View

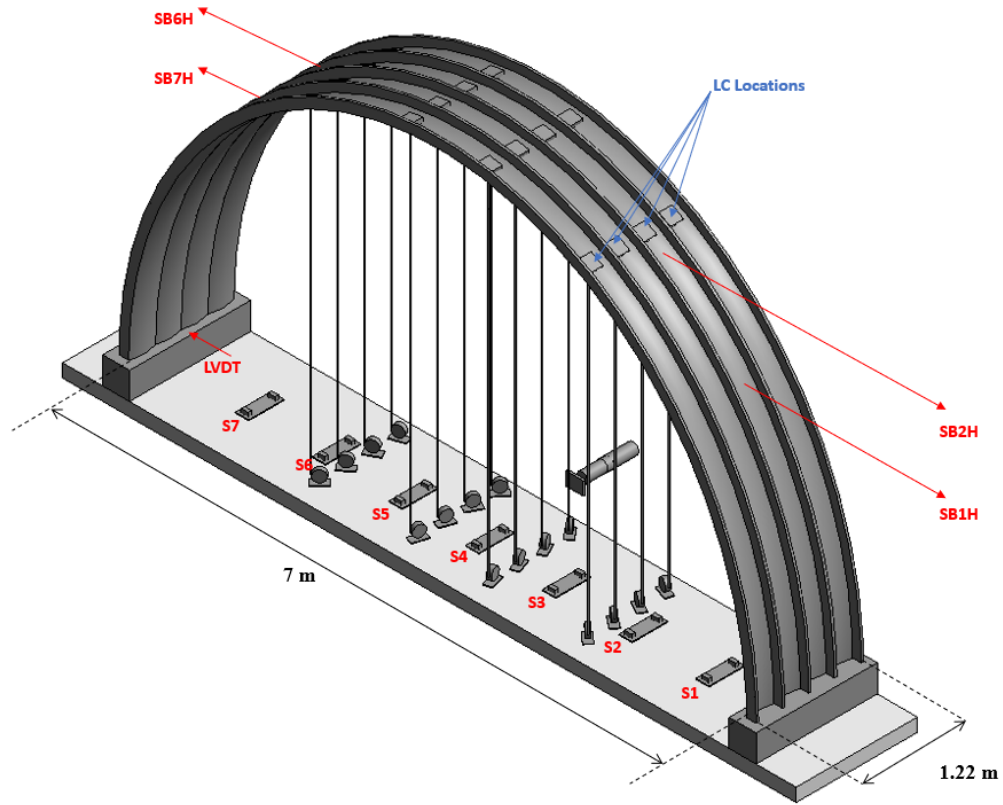


Figure B-3: Experimental Instrumentation & Loading Pattern Overview

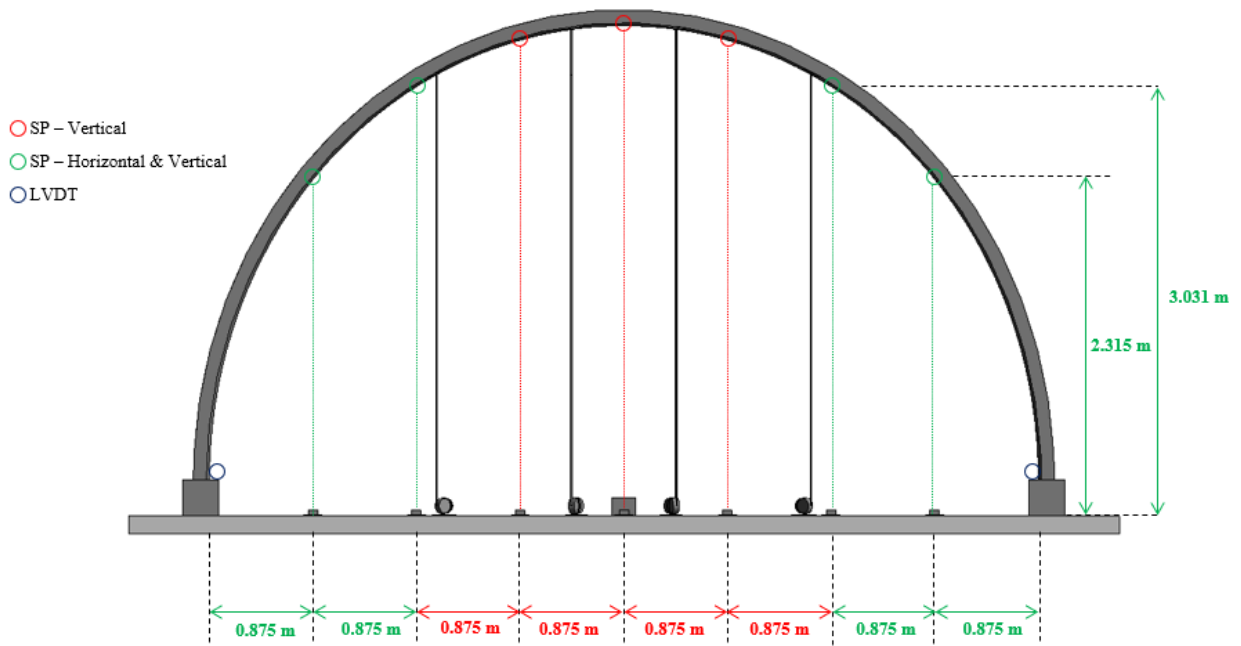


Figure B-4: Instrumentation Layout for Both Balanced and Unbalance Loading Pattern

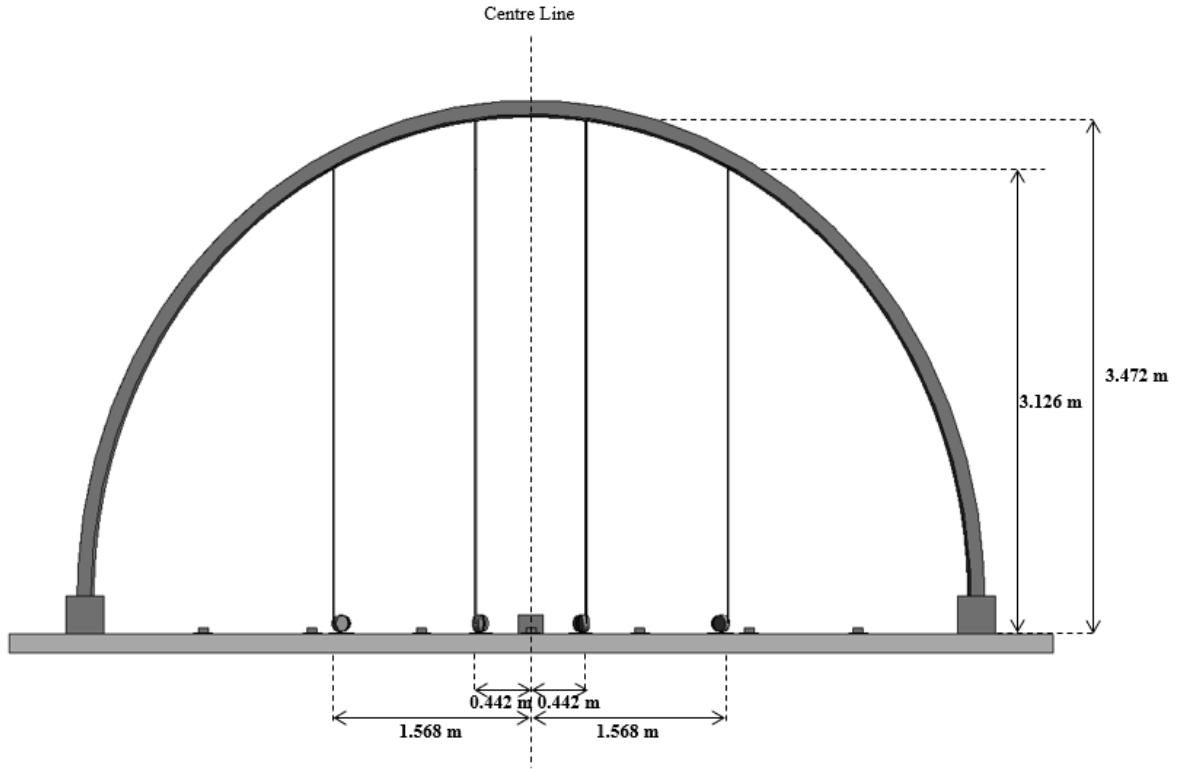


Figure B-5: Side View Loading Dimensions for Balanced Loading Pattern

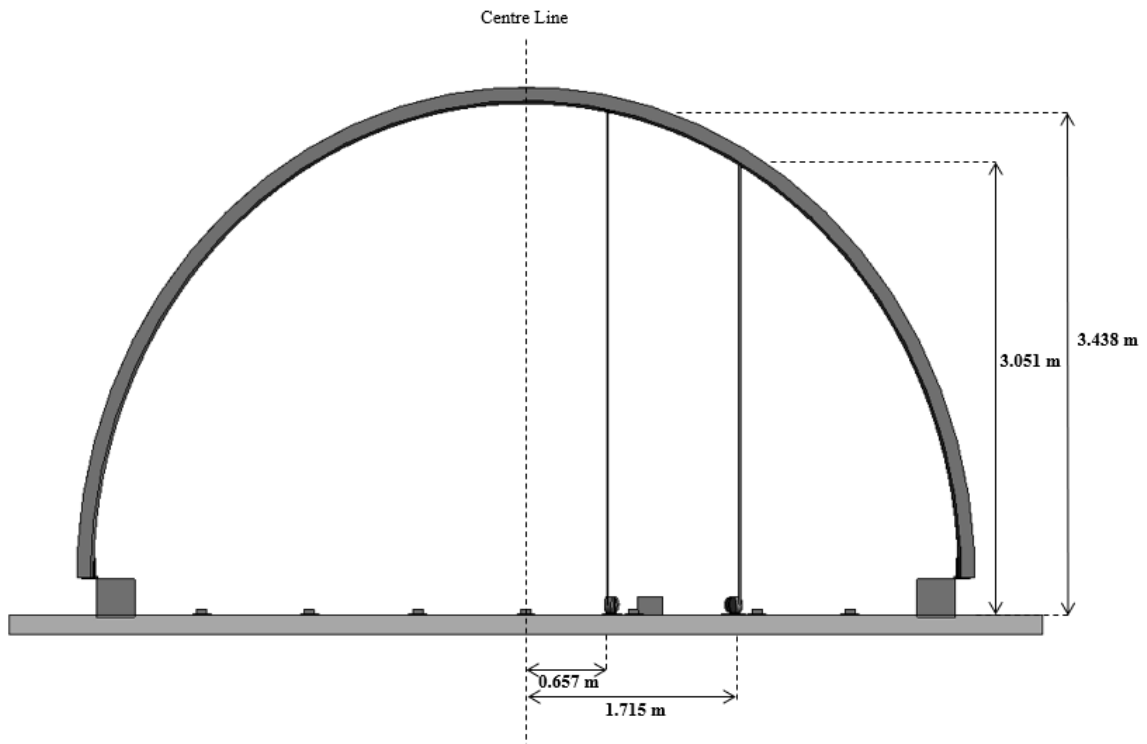


Figure B-6: Side View Dimensions for Unbalanced Loading Pattern

APPENDIX C - EXPERIMENTAL EQUIPMENT, SET-UP & RESULT IMAGES

The following figures presented in Appendix C consist of the experimental pictures and images for equipment used, full-scale experimental set-up and outcome of loading the specimens. This Appendix is meant to supplement the research paper to provide a better understanding and overview of the scale of the experimental results.



Figure C-1: M.I.C. ABM Trailer



Figure C-2: ABM Set-Up



Figure C-3: Steel Panel Forming Process



Figure C-4: Scale of 7m-Diameter Panels on Jobsite



Figure C-5: Seaming Machine



Figure C-6: Steel Rollers for Seaming Machine



Figure C-7: Beginning of Seaming Process



Figure C-8: Seaming Process



Figure C-9: Seamed K-Span



Figure C-10: 100 kN Actuator Set-up

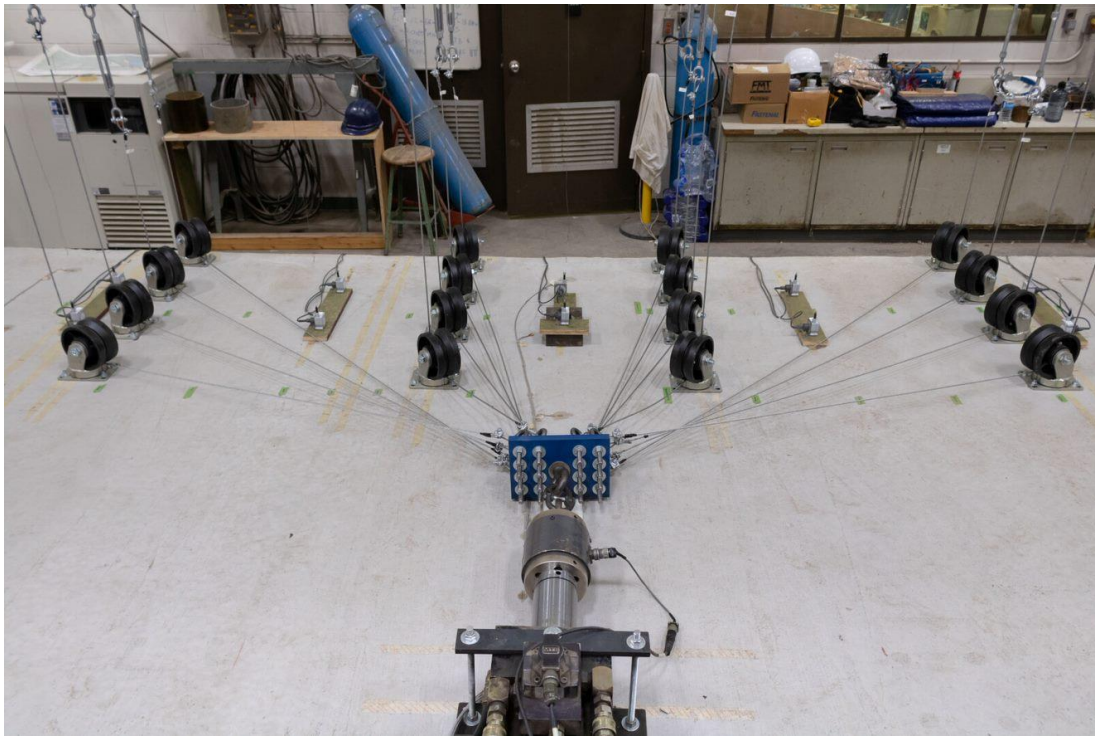


Figure C-11: Pulleys and Actuator Connection Configuration



Figure C-12: Pulleys Anchored to Concrete Slab



Figure C-13: Turnbuckles Used for Controlling Load on Cables

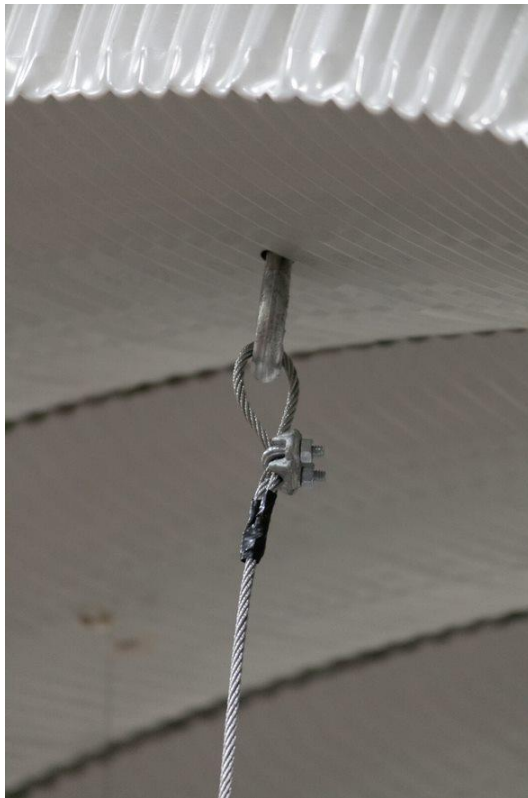


Figure C-14: K-Span Connections Between Eyebolts and Steel Cable

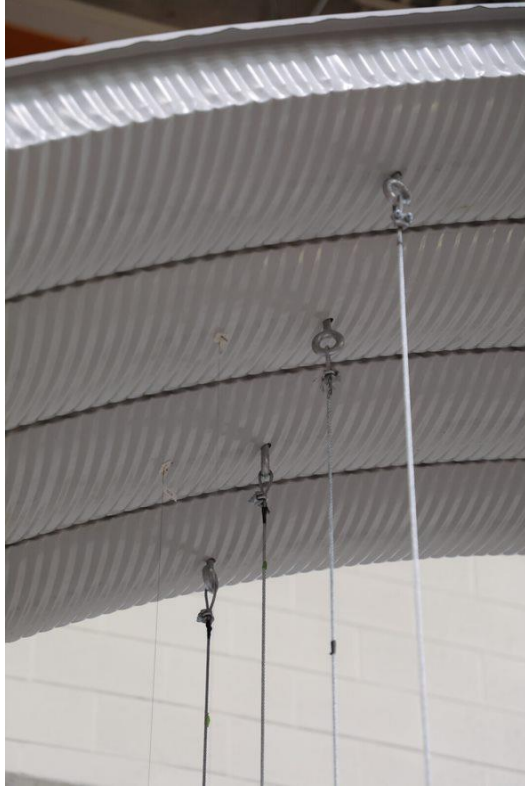


Figure C-15: One Row of Loading Points

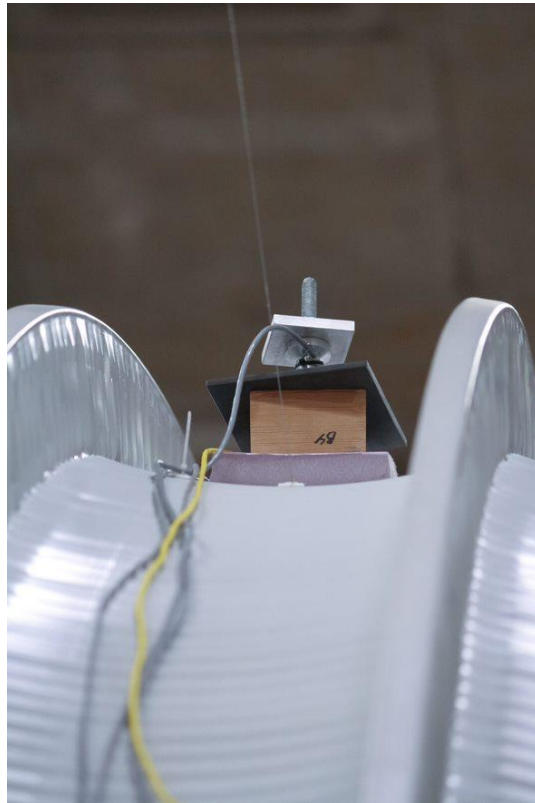


Figure C-16: Loading Point and Load Cell Assembly

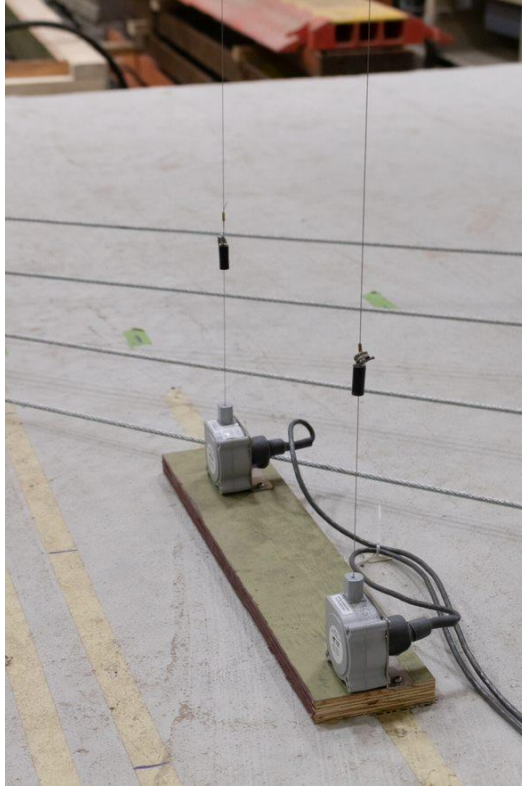


Figure C-17: Vertical Linear String Potentiometers

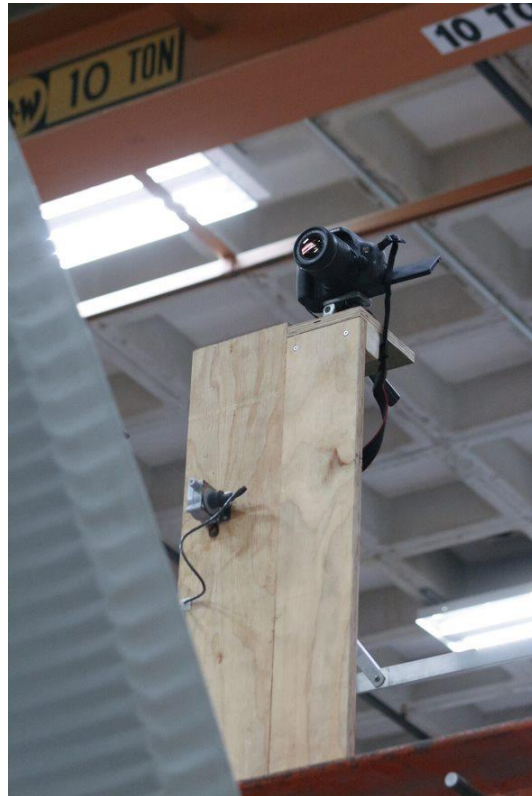


Figure C-18: Horizontal Linear String Potentiometer and Camera Set-Up

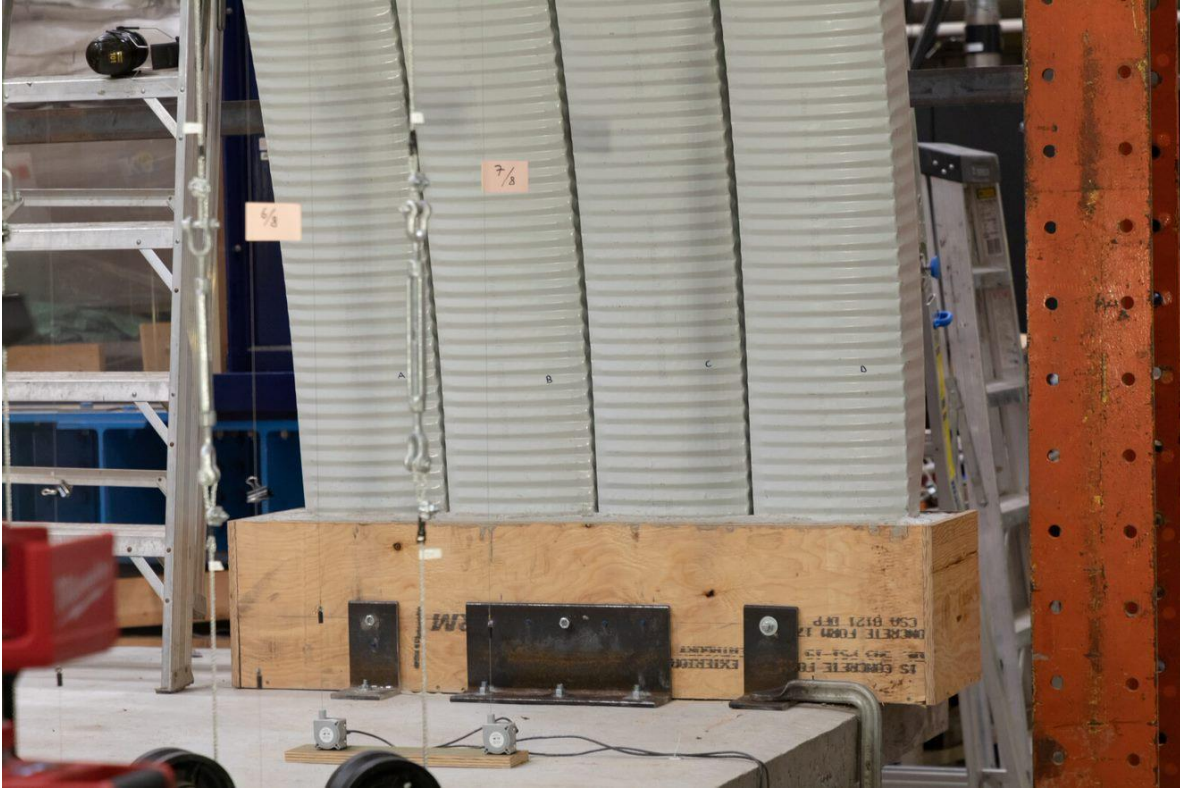


Figure C-19: Fixed Base Support 1



Figure C-20: Fixed Base Support 2



Figure C-21: Pinned Base Support 1



Figure C-22: Pinned Base Support 2



Figure C-23: Balanced Loading & Fixed Support Specimen Prior to Loading



Figure C-24: Balanced Loading & Fixed Support Specimen at Loading



Figure C-25: Balanced Loading & Fixed Support Specimen Localized Buckling near Supports

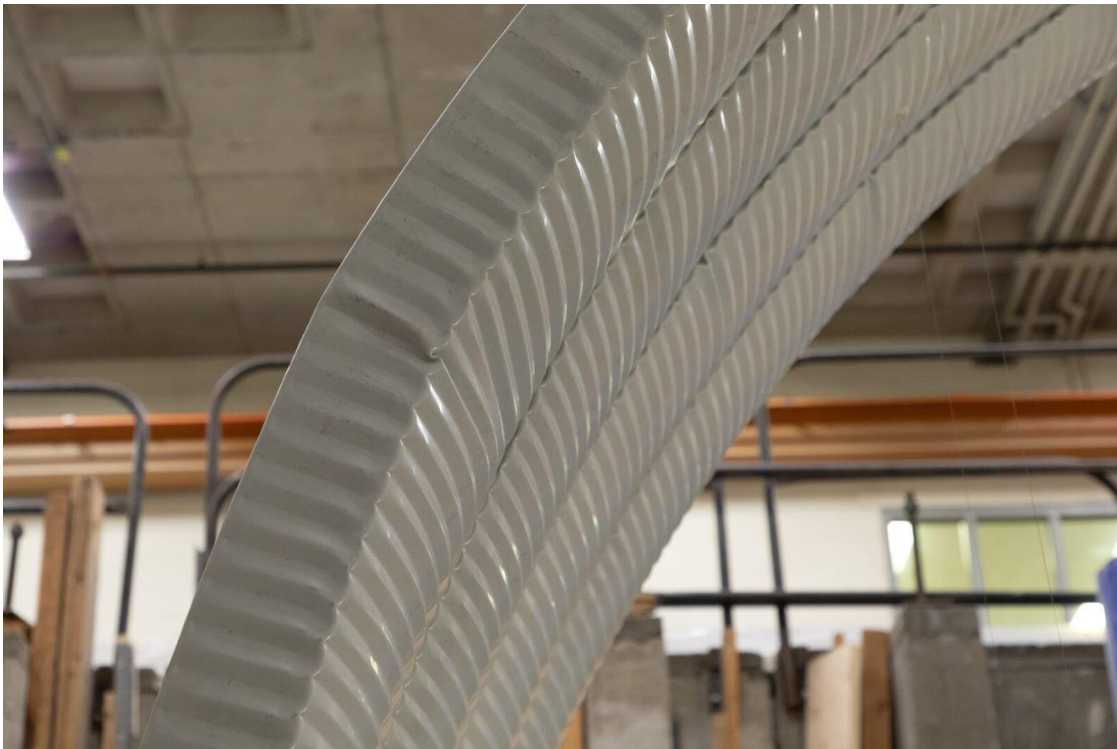


Figure C-26: Balanced Loading & Fixed Support Specimen Localized Crimping under Web



Figure C-27: Balanced Loading & Fixed Support Specimen Localized Crimping of Web from Back Side



Figure C-28: Balanced Loading & Fixed Support Specimen Localized Buckling near Supports

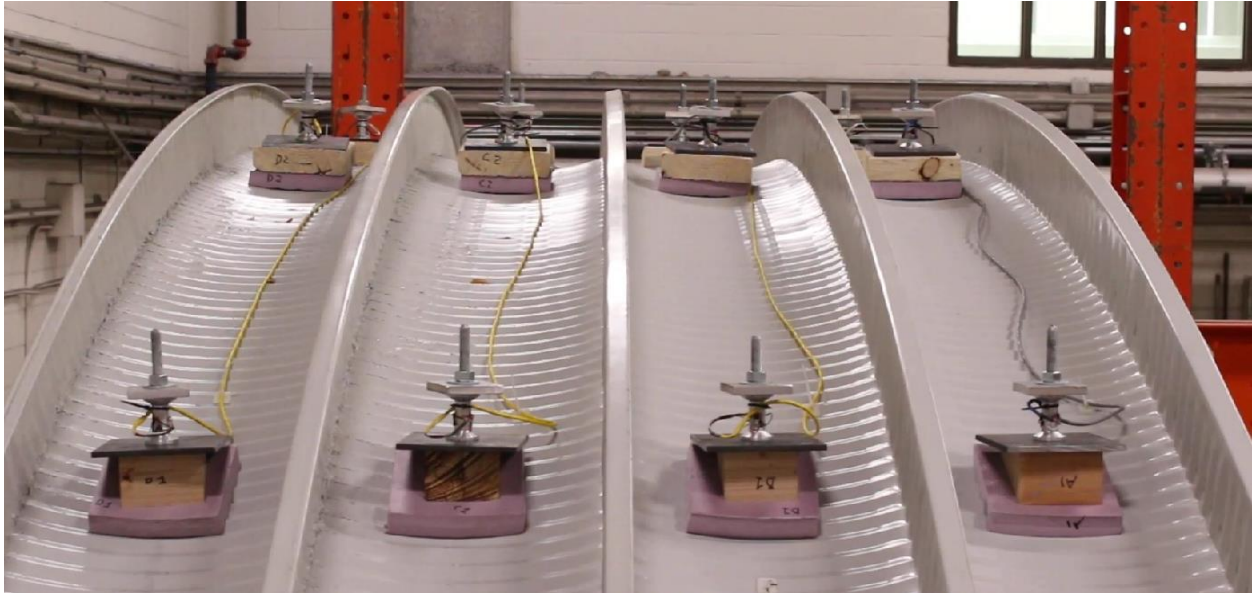


Figure C-29: Balanced Loading & Fixed Support Specimen Top View



Figure C-30: Balanced Loading & Fixed Support Specimen Localized Buckling of Seamed Lips

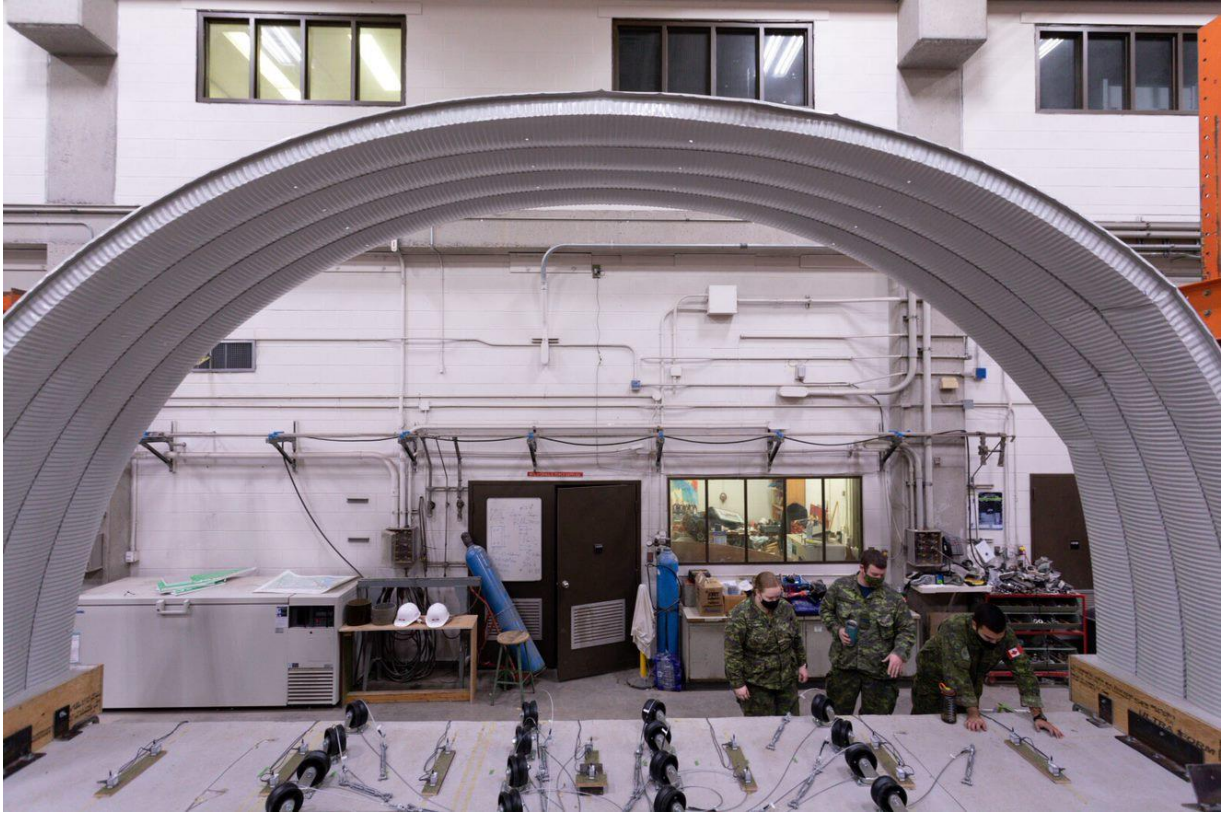


Figure C-31: Balanced Loading & Fixed Support Specimen Post Loading



Figure C-32: Balanced Loading & Pinned Support Specimen Prior to Loading

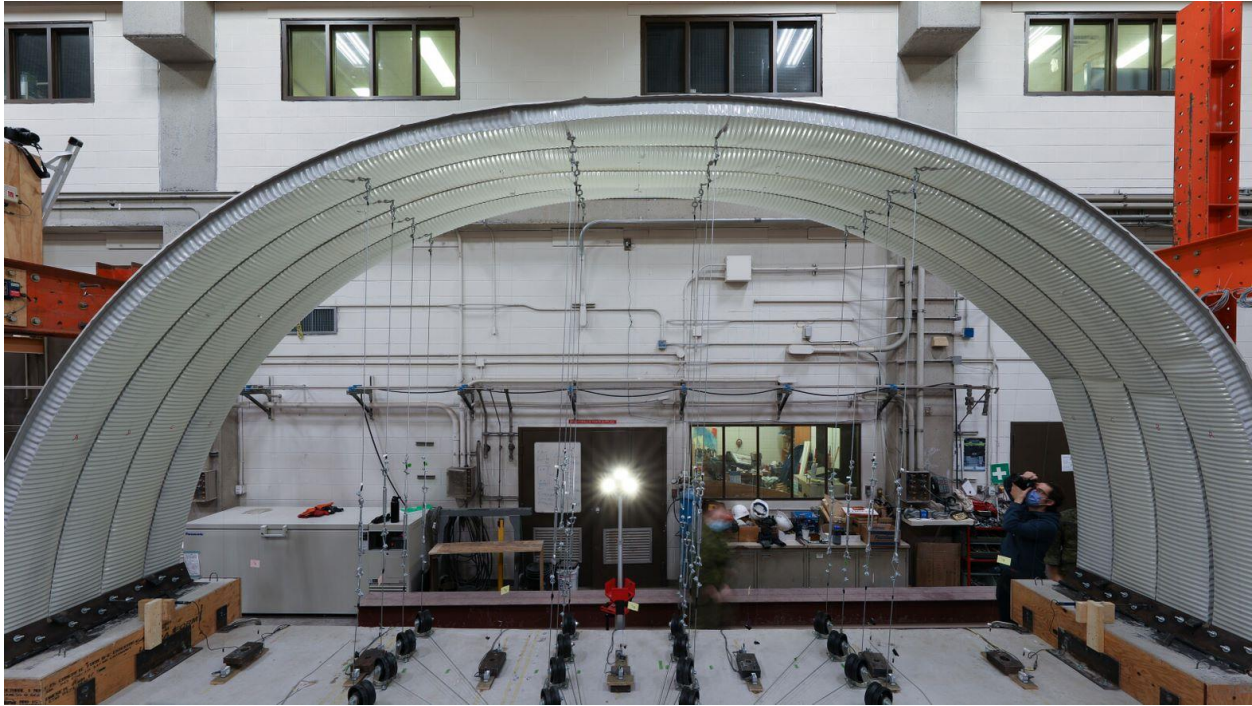


Figure C-33: Balanced Loading & Pinned Support Specimen during Loading



Figure C-34: Balanced Loading & Pinned Support Specimen Deformation Caused by Hinge Rotation 1

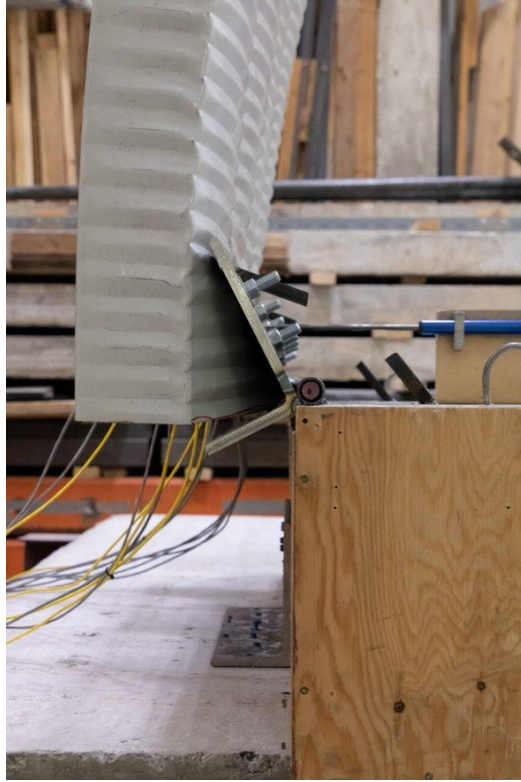


Figure C-35: Balanced Loading & Pinned Support Specimen Deformation Caused by Hinge Rotation 2



Figure C-36: Balanced Loading & Pinned Support Specimen Crimping of Webs



Figure C-37: Balanced Loading & Pinned Support Specimen Crimping of Webs Back Side

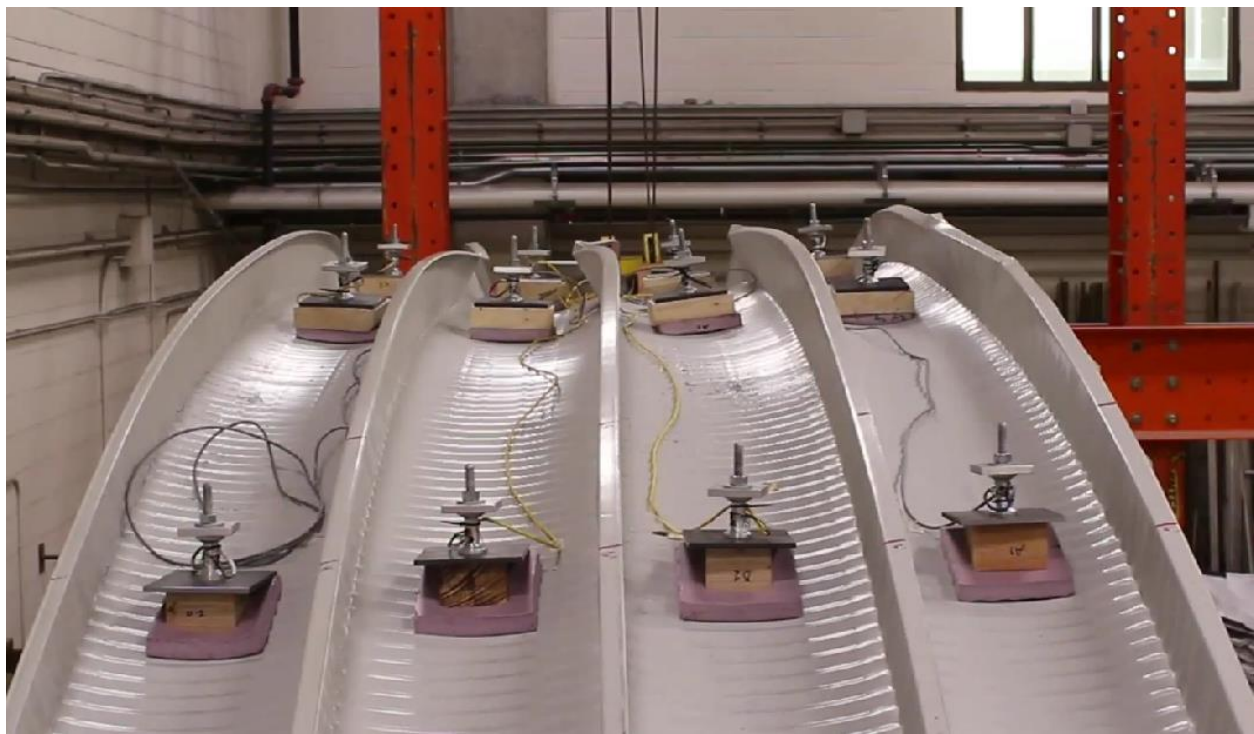


Figure C-38: Balanced Loading & Pinned Support Specimen Localized Buckling of Seamed Lips

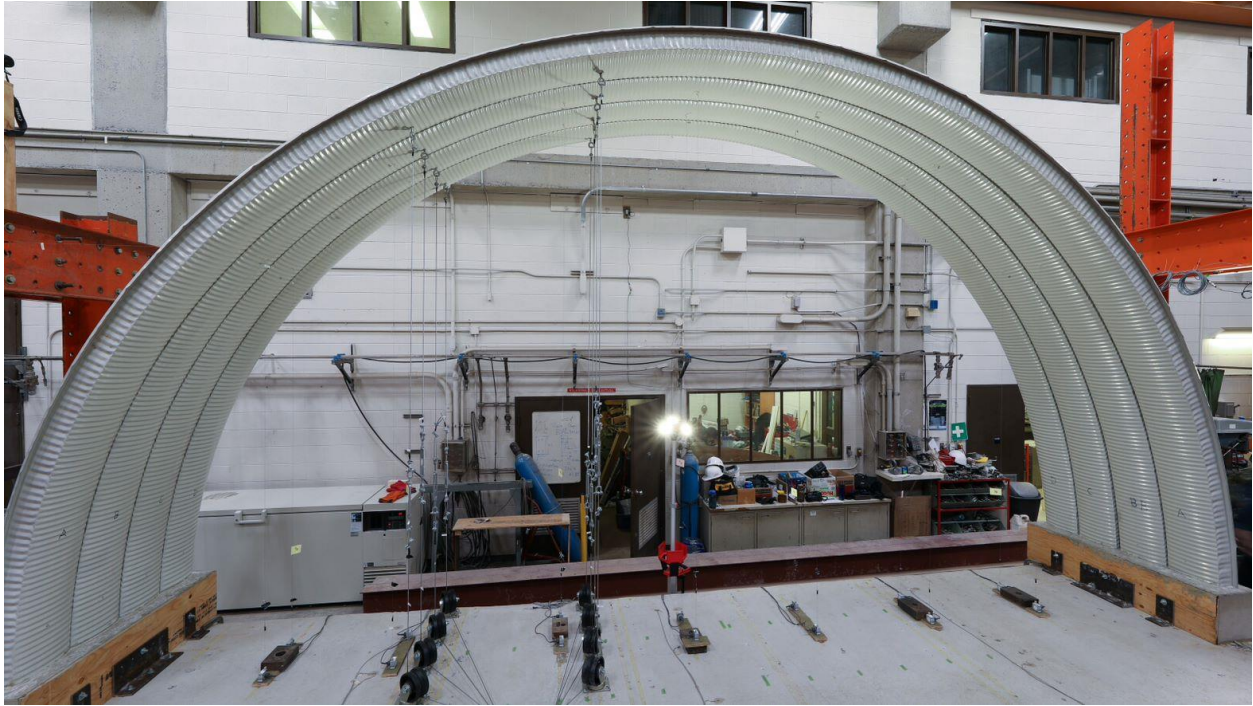


Figure C-39: Unbalanced Loading & Fixed Support Specimen Prior to Loading



Figure C-40: Unbalanced Loading & Fixed Support Specimen During Loading



Figure C-41: Unbalanced Loading & Fixed Support Specimen Localized Web Deformations 1



Figure C-42: Unbalanced Loading & Fixed Support Specimen Localized Web Deformations 2



Figure C-43: Unbalanced Loading & Fixed Support Specimen Buckling of the Seamed Lips

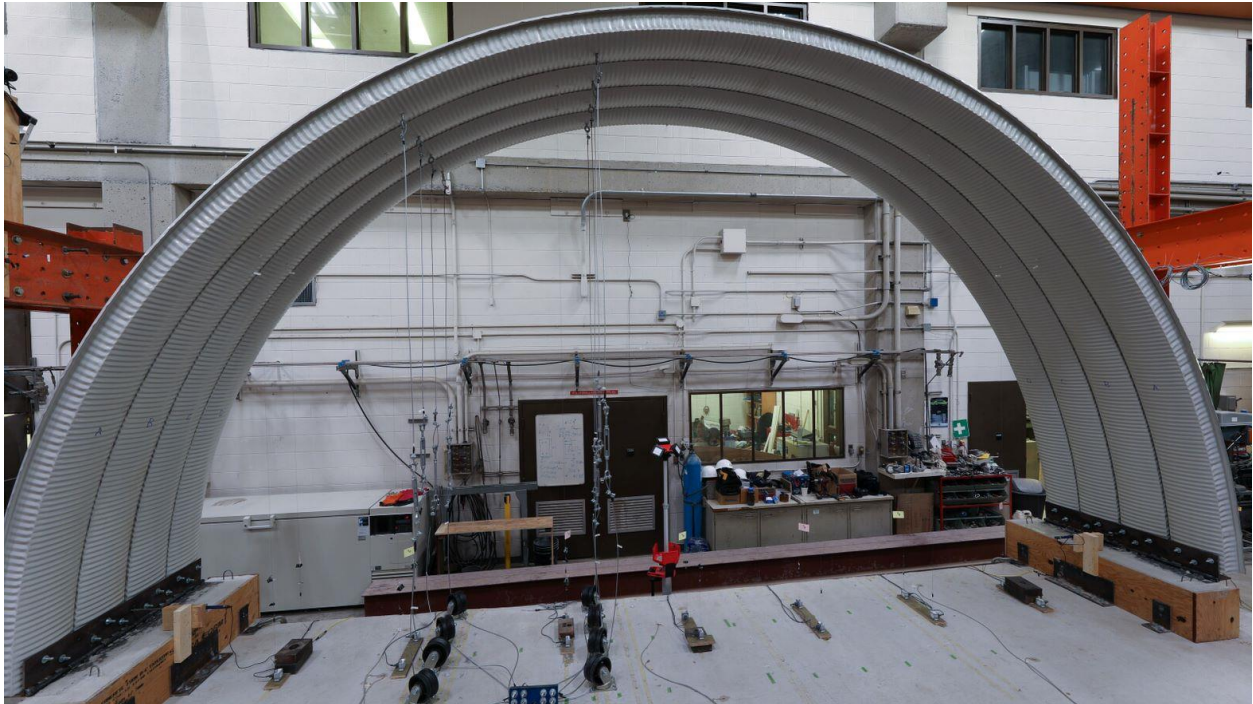


Figure C-44: Unbalanced Loading & Pinned Support Specimen Prior to Loading

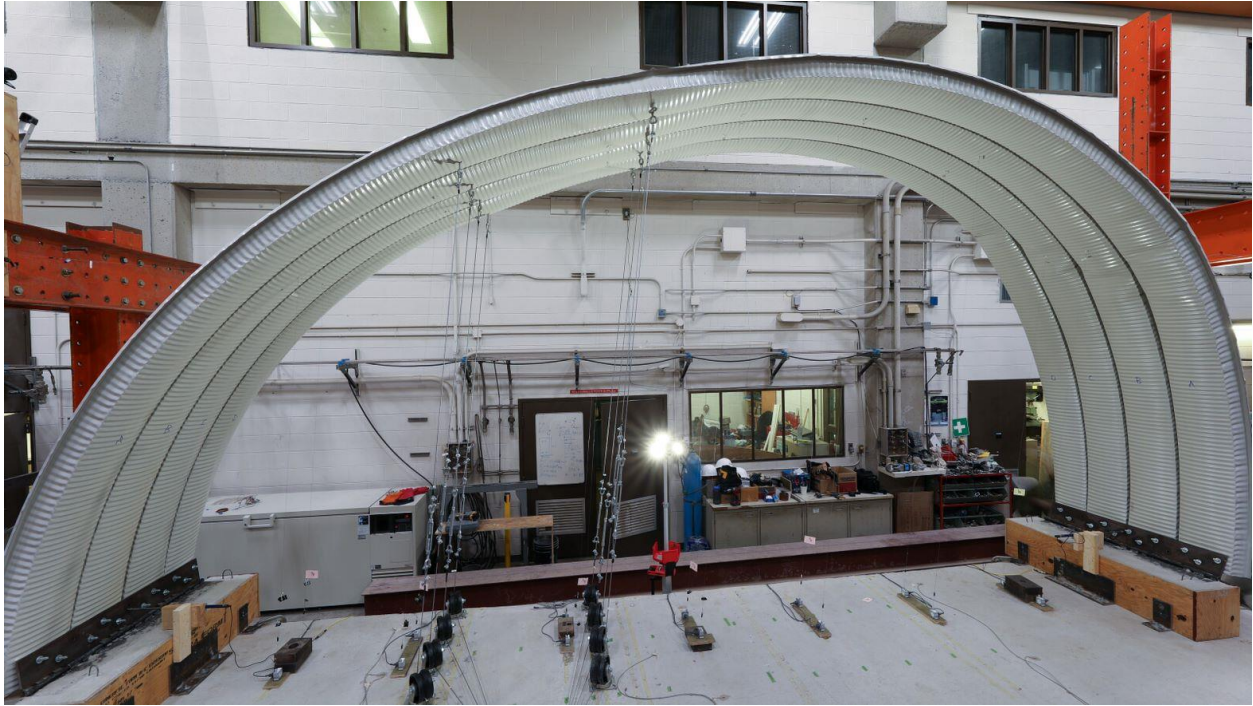


Figure C-45: Unbalanced Loading & Pinned Support Specimen During Loading



Figure C-46: Unbalanced Loading & Pinned Support Specimen Hinge Rotation Deformations



Figure C-47: Unbalanced Loading & Pinned Support Specimen Localized Web Crimping

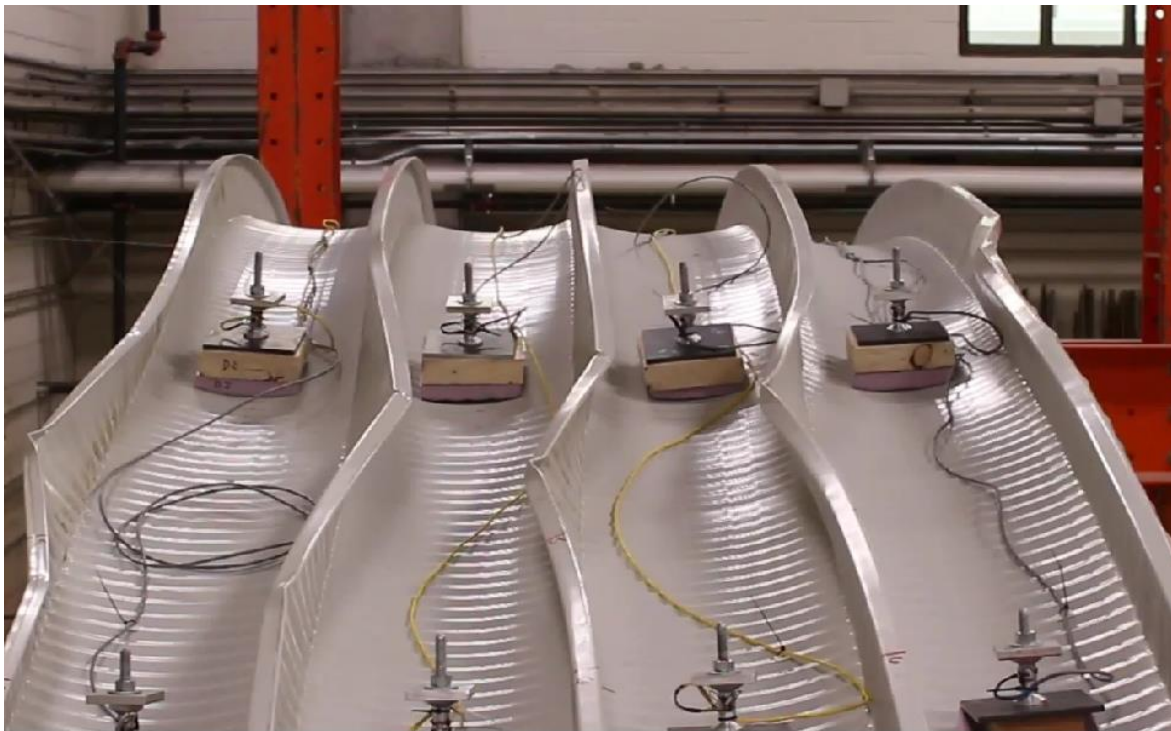


Figure C-48: Unbalanced Loading & Pinned Support Specimen Buckling of Seamed Lips